LINEAR SWEEP SQUARE WAVE VOLTAMMETRY

by

Matthew Stephen Krause, Jr.

A Dissertation Submitted to the Faculty of the

DEPARTMENT OF CHEMISTRY

In Partial Fulfillment of the Requirements
For the Degree of

DOCTOR OF PHILOSOPHY

In the Graduate College

THE UNIVERSITY OF ARIZONA

1 9 6 9

THE UNIVERSITY OF ARIZONA

GRADUATE COLLEGE

I hereby recommend that this dissertation prepared under my direction by Matthew Stephen Krause, Jr.

entitled LINEAR SWEEP SQUARE WAVE VOLTAMMETRY

be accepted as fulfilling the dissertation requirement of the degree of Doctor of Philosophy

Louis Ramaley — Dissertation Director — March 25, 1969 — Date

After inspection of the final copy of the dissertation, the following members of the Final Examination Committee concur in its approval and recommend its acceptance:*

Hunter Lenhard	March 25, 1969
George S. Wilson	March 26, 1969
John V. Rund	March 26, 1969
Robert D. Feltham	March 27, 1969

*This approval and acceptance is contingent on the candidate's adequate performance and defense of this dissertation at the final oral examination. The inclusion of this sheet bound into the library copy of the dissertation is evidence of satisfactory performance at the final examination.

STATEMENT BY AUTHOR

This dissertation has been submitted in partial fulfillment of requirements for an advanced degree at The University of Arizona and is deposited in the University Library to be made available to borrowers under rules of the Library.

Brief quotations from this dissertation are allowable without special permission, provided that accurate acknowledgment of source is made. Requests for permission for extended quotation from or reproduction of this manuscript in whole or in part may be granted by the copyright holder.

SIGNED: Matthew Stephen Krause Jr

ACKNOWLEDGMENT

The author is indebted to Dr. Louis Ramaley, the director of this dissertation, for his patience and assistance during the experimental work and in the preparation of this manuscript.

The author would also like to thank the faculty of the Department of Chemistry for his Dupont Teaching Fellowship in the Academic year 1967-1968 and the Burr-Brown Research Corporation for technical assistance and the loan of operational amplifiers, without which this work could not have been completed. The continued financial assistance of his parents and patience, compassion, and encouragement of his wife, Jan, are gratefully acknowledged.

TABLE OF CONTENTS

TABLE OF CONTENTS--Continued

LIST OF ILLUSTRATIONS

LIST OF ILLUSTRATIONS--Continued

LIST OF TABLES

LIST OF TABLES

ABSTRACT

The electroanalytical technique of linear sweep square voltammetry was investigated at the hanging mercury drop electrode. The time potential wave form consisted of a linear sum of a square wave of half period τ and a synchronized staircase voltage function of period 2τ. Sweep rates of 0.1 to 0.005V/sec were investigated.

The construction of a transistorized operational amplifier three-electrode potentiostat, along with the appropriate solid state timing and sampling circuits, is described.

A comparison of the observed currents as a function of the various operating parameters for the iron(III) oxalate showed excellent agreement with theoretical predictions. Detection limits and peak resolution were found to be comparable to that of square wave polarography. The technique was found to be a rapid, sensitive analytical tool. Current linearity of 1% was observed over a thousand-fold concentration range.

Application of this technique to anodic stripping analysis and trace surfactant analysis is reported. The behavior of cadmium(II) in N,N,N - trimethylethylenediammonium nitrate, a non-interacting pH=7 supporting electrolyte buffer, was investigated.

Attempts at trace fluoride analysis using this technique and the reduction of the zirconium alizarin-red-S complex are described, including the results obtained at platinum and graphite electrodes for this reduction.

CHAPTER I

INTRODUCTION

Electrochemical techniques have been used in the study or analysis of electroactive and surface active species. Perhaps the most widely used method is voltammetry in its various forms. In voltammetric techniques, the potential of a test electrode is varied in a controlled manner versus a reference electrode and the resultant current is measured as a function of this potential. The shape of the current voltage curve is characteristic of the species studied. The following discussion is intended only to be superficial and therefore the reader desiring greater detail is referred to the appropriate chapters in the books on electrochemical techniques by Meites (1) and Delahay (2).

The electrochemical cell, in the absence of a depolarizer, may be thought of in terms of its electrical analog:

where R_s is the solution resistance between the electrodes and C_{dl} is the double layer capacitance of the test electrode which is a function of the area of the electrode and its potential. In this diagram we assume that the size of the counter electrode is so great compared to the test electrode that its double layer capacitance may be neglected. In

the three-electrode potentiostat used in this work, R_s is the resistance from the test to the salt bridge of the reference electrode.

Direct current polarography is perhaps the most common of the voltammetric techniques. It is performed at a dropping mercury electrode (DME). The DME has the advantage of producing effectively a new electrode for each drop. Therefore it is reasonably free from surface contamination when compared to stationary electrodes. In dc polarography, a slowly changing potential is applied to the DME; the rate of change of this potential with time (v) is on the order of 0.1V/min, a rate so slow that the potential for each drop is almost constant. This slow potential scan rate allows the current required to charge the double layer to decay almost to zero at a time near the end of the drop life when its area is changing very slowly with time.

The detection limit of this method is limited to about 5×10^{-6}M by this residual charging current. The resolution of successive waves requires a minimum half wave potential, $E_{\frac{1}{2}}$, separation of 100 mV. Since the currents measured by this technique are additive, successive species may be analyzed by the difference in their diffusion currents; however, if a 100-fold excess of a more easily reduced species exists in solution, the reduction for the second species will be obscured. In order to provide a more useful signal, the first derivative of this polarogram is often recorded. This allows better resolution of overlapping peaks and detection of a less concentrated species in the presence of the more easily reduced high concentration species; however, the detection limit is not extended significantly.

The application of a small sinusoidal voltage (10 mV peak-to-peak) to this slowly changing dc potential is known to produce a current signal which is similar to the first derivative of the dc polarogram where the peak potential, E_p, occurs at the dc polarographic $E_{\frac{1}{2}}$ for reversible systems. The magnitude of the current signal is enhanced with respect to dc polarography; however, phase sensitive detection is necessary to separate the double layer charging current from the faradaic signal and the overall detection limit is not much greater than dc polarography.

Another form of voltammetry is the linear sweep cyclic technique in which a rapid, linear sweep voltage ($v = 0.1V/sec$ to $1000V/sec$) is applied to a stationary electrode or to a DME late in the drop life when its area is effectively constant. The current is again recorded as a function of potential.

In this method the reversible peak potential trails the $E_{\frac{1}{2}}$ by a fixed amount and the peak current is proportional to concentration. Information concerning the reverse electrode process is also obtained by observing the reverse sweep direction current. In this method the peak current, i_p, is proportional to $v^{\frac{1}{2}}$; however, the double layer current is proportional to v, and therefore the minimum concentration detectable is ultimately limited by the background current to about $10^{-6}M$. While measurement of the first reduced species is simple, the second species must be measured from an extrapolation of the first species' current. This limits the accuracy in multicomponent system analyses.

The use of a square wave voltage from a rotating commutator to generate a derivative signal has been used in conjunction with a galvanometer and a DME (3), but this method achieved little popularity as it did not eliminate the double layer current.

In 1952, Barker and Jenkins (4) proposed the technique of square wave polarography. Since the electrical analog for a cell in absence of a depolarizer is a simple series RC circuit, the response of a cell to a potential step is a rapidly decaying current. If the current were measured after the application of this potential step, for example, 0.5 msec, the current will have decayed to zero. Likewise, for a potential step in the opposite direction, a similar phenomenon will result. In the presence of a depolarizer the currents will not decay to zero due to diffusion to the electrode of the electroactive species.

Square wave polarography work is performed at a dropping mercury electrode, and only currents late in the drop life are recorded to minimize currents due to the expanding electrode surface. Furthermore, to avoid any dc component on the square wave current, the sweep potential is very slow; in trace analysis, for example, instead of a continuous sweep potential, the potential is advanced to a new value for each drop. This requirement of slow sweep rate in trace analysis yields scan rates of about one volt per hour. If the value of the peak-to-peak square wave voltage, ΔE, is sufficiently small, the current voltage curve recorded will be an accurate representation of the first derivative of the dc polarogram for a reversible system. This method is limited in application to solutions of low resistivity. The

detection limit of $5x10^{-8}$M suffers from a phenomenon called capillary response. Capillary response has been shown by Cooke, Kelley, and Fisher (5) to be caused by solution creeping into the tip of the capillary and producing a separation of the mercury column from the capillary wall. This solution in the capillary exhibits a longer time constant than the electrode solution interface, charges at a slower rate, and therefore produces a nonzero background current.

Attempts to eliminate this effect have not been totally successful (6, 7), and perhaps the best solution to this problem is the use of a stationary electrode not involving a capillary, for example, a hanging mercury drop electrode (HMDE) using a platinum contact to hold the drop. This stationary electrode would also avoid problems concerning the changing electrode area of a DME but would be sensitive to surface contamination.

Figure 1a offers representations of electrode response in square wave polarography both in the presence and absence of a depolarizer.

In 1961, Mann (8) applied Barker's (7) conclusion concerning electrode response to a potential step and devised the technique of staircase voltammetry. In this technique the potential of the test electrode is varied by a staircase voltage function, and the current is sampled at some finite time after this potential step when the current for the double layer has decayed to zero. Figure 1b demonstrates the resultant potential and current wave forms. In a later paper, Mann (9) demonstrated the ability to use staircase voltammetry at high sweep

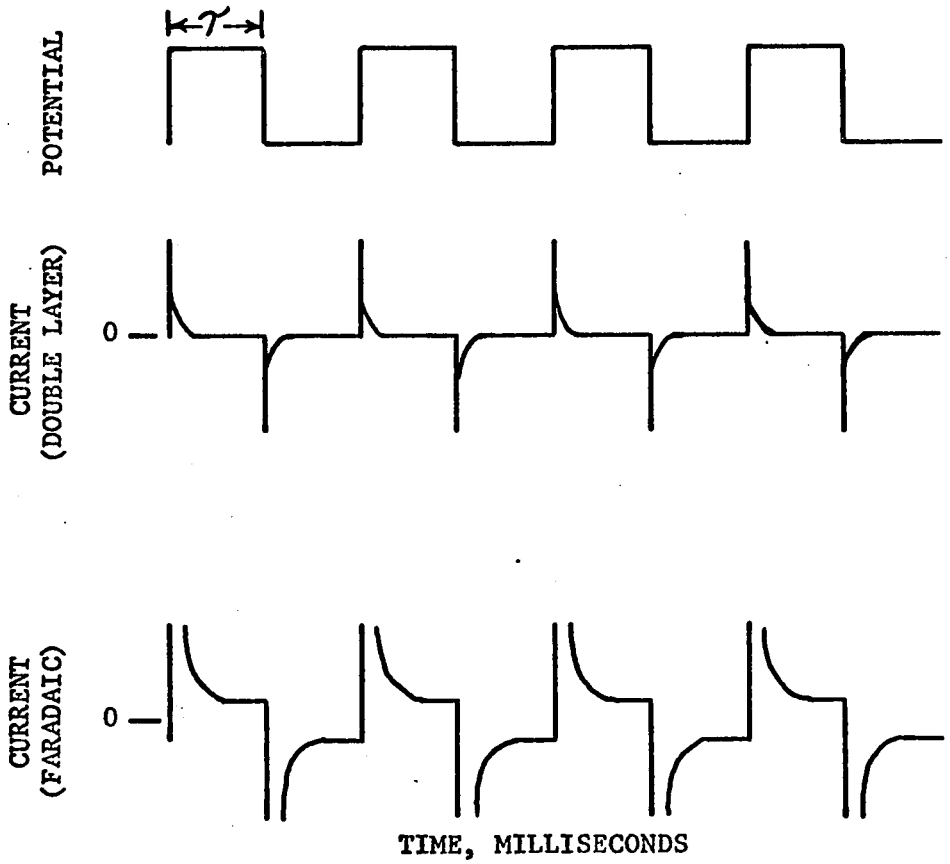

a. Potential and current versus time in square wave polarography.

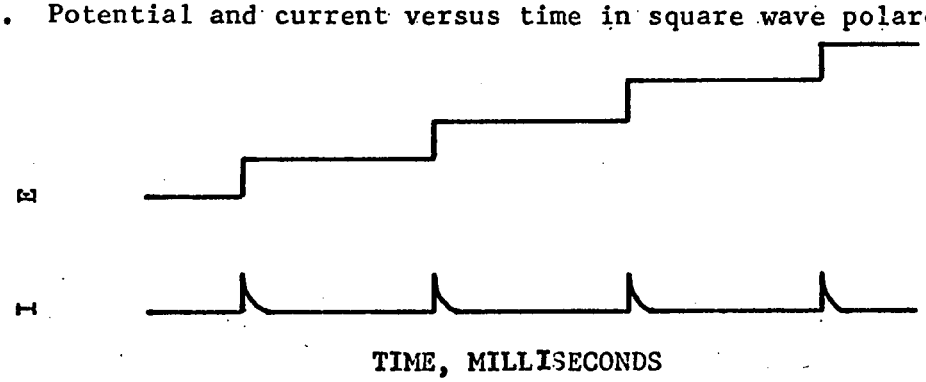

b. Potential and current versus time in staircase voltammetry.

Figure 1. Current and potential time curves.

rates while maintaining freedom from double layer current complications.

In 1962, Saito and Okamoto (10) reported the development of the technique of oscilloscopic square wave polarography. They superimposed a square wave voltage on a rapid dc potential scan and applied this technique to both inorganic and organic depolarizers (11). Their detection limit for inorganic systems is limited to only 10^{-5}M, probably by the magnitude of the charging current of the double layer under these potential scan conditions.

In view of these results, the logical extension of this work is a combination of a square wave voltage function of half period τ with a staircase potential function of period 2τ. This approach will allow rapid sweep rates without any tilting of the square wave. It should then be possible to complete square wave analysis in reasonable periods of time. The resultant potential wave form is presented in Figure 2. In this figure, the fraction of the square wave indicated by a or b represents the time during which the current sample and hold circuits A or B, respectively, are sampling the current flowing. The measure instant, t_m, is the time from the beginning of the square wave at which the appropriate sample and hold circuits switch to the hold mode. If the potential step function is smaller than ΔE, the current observed should be identical to that of square wave polarography.

While this technique will not disrupt the flatness of the square wave, it will produce an asymmetrical square wave. The resultant voltage function as produced in this work consisted of successive steps of $-\Delta E$ and $+\Delta E-E_{step}$ for sweeps in the cathodic direction, and $+\Delta E$ and

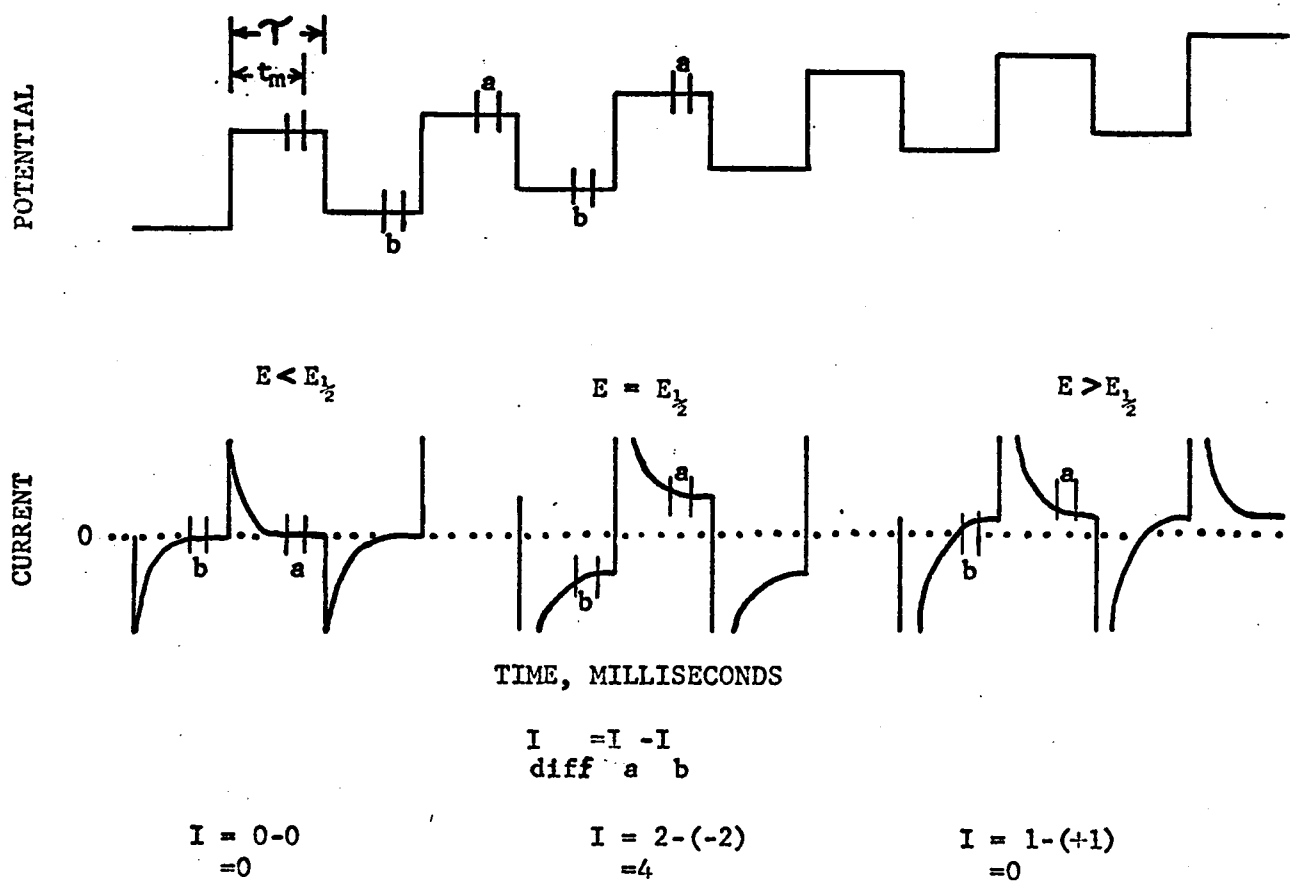

Figure 2. Potential versus time and current versus potential curves for linear sweep square wave voltammetry.

$-\Delta E+E_{step}$ for sweeps in the anodic direction. The wave form in Figure 2 is therefore an accurate, although exaggerated, representation of this effect. Because of the rapid sweep rates involved, it is necessary to use a stationary electrode and the HMDE was used for this study. The application of this potential wave form to a stationary electrode shall hereafter be referred to as linear sweep square wave voltammetry.

The instrument constructed is of three-electrode potentiostatic design. In 1959, Kelley, Fisher, and Jones (12) suggested the use of operational amplifiers in the construction of a three-electrode potentiostat. They demonstrated the use of this circuit in reduction of both IR drop and polarization of the reference electrode. The reduction of IR drop is accomplished as this circuit only considers the resistance from the salt bridge to the test electrode, a quantity which is controlled by electrode placement. This effect of resistance reduction in square wave voltammetry will also speed the charging of the electrode double layer.

In 1965, Buchanan and McCarten (13) reported the construction of a potentiostatic square wave polarograph utilizing vacuum tube operational amplifiers. They obtained a detection limit for cadmium(II) of about 2×10^{-6}M. This result does not compare favorably to that of Barker who obtained a detection limit of 10^{-7}M thirteen years earlier.

In square wave polarography and voltammetry the currents for the positive and negative square wave pulses are measured separately and their difference is recorded. The result (for slow sweep rates) is

that the output current signal is twice that for either half cycle. Figure 2 contains a representation of the currents as a function of potential as they are observed and recorded in square wave techniques. As was previously stated for trace analysis, Barker uses a potential step voltage sweep, one step per drop, and averages the current for a large number of square wave cycles. By this method, he suppresses the noise in his electronics and achieves his detection limits.

In the case of square wave voltammetry, however, the currents measured for successive positive and negative square wave periods correspond to different potentials versus the reference electrode and therefore cannot be signal averaged. The electronic circuits used must therefore be as free as possible from noise. The development of stable transistorized operational amplifiers made construction of this instrument possible.

CHAPTER II

STATEMENT OF THE PROBLEM

The purpose of this dissertation is the development of the electroanalytical technique of linear sweep square wave voltammetry, and the application of this technique to trace metal analysis. An expression relating current to the applied control potential will also be established.

CHAPTER III

INSTRUMENT AND ELECTROCHEMICAL CELL

The instrument utilized in this dissertation was constructed in a modular form from solid state operational amplifiers (Figure 3). The description of the circuits and of the requirements upon these amplifiers shall be considered from a block diagram approach.

Potentiostat

The ideal operational amplifier has infinite dc gain, a wide band width (a high unity gain crossover frequency and a rapid output slewing rate), minimal voltage and current drift and offset, low noise, a high input and common mode impedance, and a high common mode rejection ratio (CMRR). Since all of these qualities are not common to one practical device, the amplifiers must be chosen for the requirements placed upon them by their location in the instrument.

The critical part of this electrochemical instrument is the potentiostat. It consists of three amplifiers: a voltage follower, a control amplifier, and a current-to-voltage transducer (current follower).

The voltage follower serves as an impedance-matching device. It must have a high input impedance and a low output impedance. The input impedance of a voltage follower is equal to approximately twice the

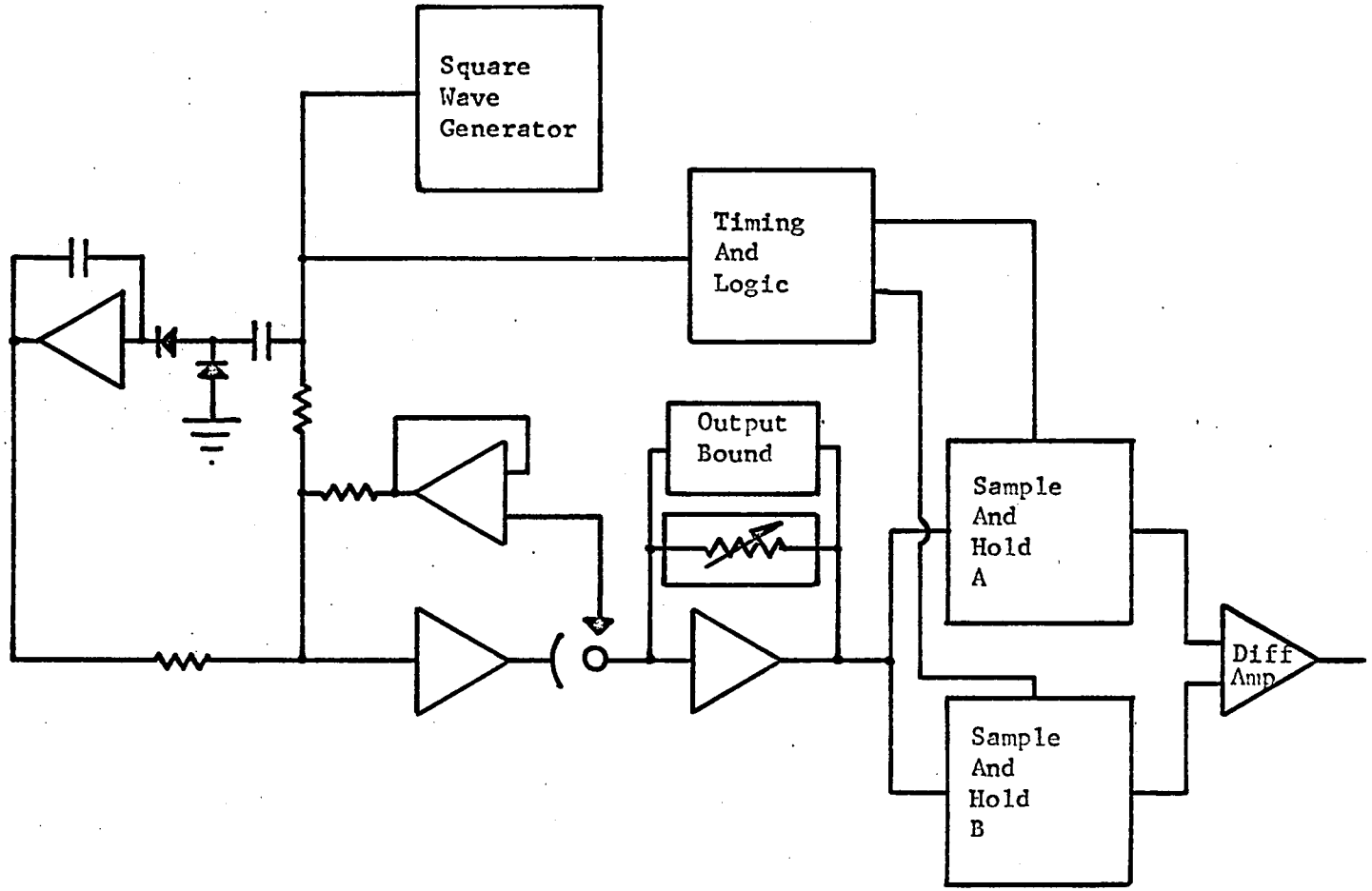

Figure 3. Block diagram of the instrument.

common mode input impedance. The output voltage is related to the input voltage by (14, p. 17)

$$E_o = E_i \left(\frac{1+1/CMRR}{1+1/A}\right) ;$$

hence, the CMRR and the gain, A, must be maximized. The amplifier chosen here is a Burr-Brown 3019 with a voltage gain of $10^{5.5}$, a CMRR of 10^4, and a common mode input impedance of 50M.

The control amplifier should also exhibit high gain and a wide band pass; however, more important perhaps is that it should be a low noise device. In the instrument constructed in this laboratory, the noise in this amplifier was the limiting factor for the entire system. Substitution of low noise amplifiers in various locations throughout the circuit showed little noise reduction provided that the amplifier previously used was one of good quality. However, the total system noise as determined at the output of the sample and hold circuits is strongly affected by the control amplifier, and therefore this amplifier must possess the best low noise specifications available. The amplifier chosen here is a Burr-Brown 3019 having an input noise of 0.4 μV, a figure ten times lower than most other amplifiers. This low noise is gained at the expense of slewing rate, 1.2V/μsec, versus ten or more for other amplifiers.

Since the only feedback element for this amplifier is the cell, occasional instability is encountered. This is eliminated by placing a small capacitor from the output to the inverting input. The size of this capacitor is important. As it increases, the system noise

decreases; however, the response time also decreases, and therefore the ability to charge the double layer is diminished. An observation of the output of this amplifier versus input signal showed that a capacitor of up to 0.001 μf could be tolerated without affecting the settling time of the amplifier.

The current follower amplifier serves as a current-to-voltage transducer. Its output is given by

$$E_o = I_{in} R_{feedback}$$

The major requirement is a low input offset current. The Burr-Brown 3013 used here has an input offset current of 2×10^{-11}A. In addition, it is a reasonably fast amplifier with a unity gain band width of 10M Hz and a 30V/μsec slewing rate. The noise level of this amplifier did not affect the output noise. Across the feedback resistor of the current follower is a bound circuit.

The output of all amplifiers is 20 mA, more than enough for most electrochemical requirements since typical faradaic currents are less than 0.1 mA. However, their outputs are limited to $\pm$ 10V. Since the desire to measure low currents with the current follower, for example, 10^{-8}A, requires a large feedback resistor, typically 1M, the output current is now limited to 10^{-7}A. As the double layer can be envisioned as a series resistor-capacitor (RC) network, the current due to a potential step across this network is

$$i = (E/R)e^{-t/RC}$$

At t = 0, when the square wave changes sign for a 50-mV square wave and

a cell resistance of 10 ohms, i = 0.05/10, about 5 mA. This current limits the value of the current follower feedback resistor to 2K. In order to allow for maximum current in the beginning of the square wave and maximum amplification thereafter, it is necessary to either switch the value appropriately or bound the output by a device that will allow full current output when the voltage output exceeds a certain value. Both methods were attempted. Preliminary work was done with a driven diode bridge (Figure 4a). When the device is in the conduct mode, its resistance, and hence the feedback resistance of the amplifier, is small, typically 200 ohms. When in the nonconducting mode, the diodes are back-biased and their resistance is now exceedingly high, typically 100M, and the feedback resistance of the amplifier is now the selected value. Using this network, the amplifier is raised to its high gain configuration only during the instant when the current is to be sampled. Another possible method is the use of back-to-back zener diodes (Figure 4b). These are devices having a high resistance until a characteristic potential is reached, at which point they conduct in the reverse biased mode. Unfortunately, these devices only have resistances of approximately 100K prior to conduction and therefore are of no use with large feedback resistors. Another possibility is the electrical equivalent of a zener diode, that is, a back-biased diode (Figure 4c). By using a battery of potential less than the output of the amplifier, that is, 8.4V, to bias the diode, it will be of very high resistance until the output of the amplifier exceeds that of the battery, at which point it

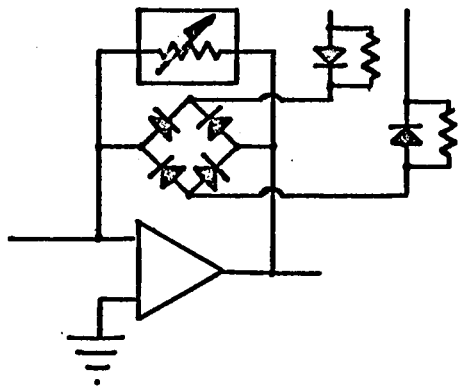

a.

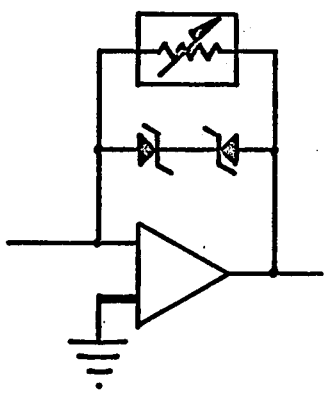

b.

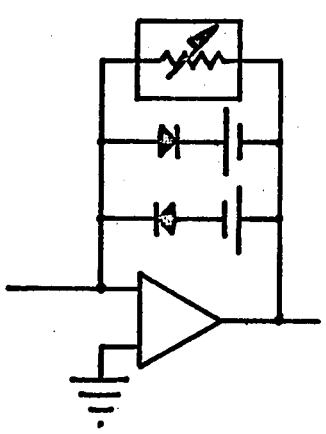

c.

Figure 4. Current follower output bound configurations.

will conduct and allow the amplifier to supply the necessary control current.

Both the driven diode gate and the back-biased diode network were used and performed well. However, the diode gate arrangement required a finite time for the amplifier to rise to its full output level, and owing to the simplicity of the battery diode network, it was the one of choice.

Later work with the instrument and attempts to use positive feedback to compensate for "IR" drop in the cell demonstrated that the amplifier behaved best with a fixed current follower feedback time constant. If this value was maintained at about 50 μsec, minimum overshoot was observed as the amplifier returned from the voltage bound and the settling time of the system was not impaired.

Sweep Generator

The voltage sweep function used in this work is produced by a staircase generator (Figure B-2, App.) similar to that diagrammed in Philbrick Researches Applications Manual (14, p. 72). The circuit consists of a network which differentiates the input square wave and feeds one polarity "spike" to the summing point of the amplifier and the other "spike" to ground. The amplifier integrates pulses of only one polarity and thus produces a staircase voltage function at its output. This circuit (Figure 3) provides a sweep potential in one direction. In order to perform cyclic voltammetry, it is necessary to switch the polarity of the pulses by switching diodes at some set potential and cause the staircase to reverse direction. This was

accomplished by feeding the output of the generator into a voltage comparator amplifier (14, p. 101), a variable fraction of whose output voltage is fed back into its positive input to provide a controllable amount of hysteresis. When the signal to the comparator amplifier, that is, the output of the staircase generator, exceeds a certain value, the output of the comparator amplifier switches rapidly to the opposite polarity. The output of the comparator is inverted and used to electrically switch the appropriate diode input network into the sweep circuit. Provision is made for the control of the initial sweep direction when the shorting switch above the staircase generator is released.

The amplitude of the input square wave is controlled by a variable potentiometer to allow for calibration of the sweep rate. Since the staircase amplifier functions as an integrator, it must be a low drift device of very low input offset current. Two possible types of amplifiers are usable here, a chopper stabilized operational amplifier or a Field Effect Transistor Input (FET) type. The stabilized amplifier tried was a Burr-Brown 1538A, having an input offset current of 30 pA. The device functioned well; however, the chopper was driven by the $\pm$ 15V power supply and produced a ripple upon the supply's output at the frequency of the chopper. This ripple appeared as noise on the output of the current follower amplifier. The use of a Burr-Brown 1556 (FET), with current offset of 50 pA, adds no extraneous noise to the system. The drift stability of the FET amplifier is sufficiently good (50 uV/day drift versus 5 uV/day stabilized) that, considering the noise, it is the better selection for this application. The voltage

comparator and inverter amplifiers used here are not critical and utility grade amplifiers, that is, Analog Device 105's, are used.

Sample and Hold

The output of the current follower is applied to the inputs of a matched pair of sample and hold circuits (Figure B-3). Each of these is locked to sample the current at a specific time on one polarity of the square wave and hold that value until the next sampling command is received. The circuit is a slightly modified version of the one in the Philbrick manual (14, p. 61). The diode gates (D10 through D13) employ Fairchild FD 300 diodes. Since the gate driving signals operate to either side of ground, they are used to completely control the gate condition. A 100-ohm potentiometer is placed between the diodes on the output side of the gate with the center tap connected to the input of the "holding" amplifier. This is used to balance the capacitive current spikes generated when the gate condition is changed. If this is not done, a few millivolt difference in the output during hold versus track modes is observed.

The size of the capacitor on the hold amplifier is selected to obtain a compromise between maximum hold stability (a large capacitance) and maximum tracking rate (small capacitance). A value of 0.01 μf is selected. Since the rate of charging of this capacitor is limited by the current output of the drive amplifiers, for example, 5 mA, this circuit should be able to change its output at a rate of 250V in 0.5 msec.

Another necessary modification is a pair of back-to-back zener diodes from the output of the driving amplifier to its negative input. Since the one millisecond overload recovery time of this device is generally longer than the sample times employed, it is necessary to use this circuit to prevent amplifier saturation during the "hold" mode when the feedback loop is open.

The amplifiers here should be high current (20 mA). This controls the slewing time of the circuit. The driving amplifier should be fast and differential, while the holding amplifier should have the characteristics of an accurate integrator.

The amplifiers chosen here are compromises due to financial limitations. The Analog Device 107 driving amplifier should have had more current ability (20 mA versus 5 mA) and the holding amplifier, an Analog Device 102, might better have been an FET to take advantage of the lower offset current (Analog Device--2nA) and thus alleviate the need of an input current adjustment on this amplifier.

An electronic switch (Burr-Brown 9580) was also tried. It replaced the driving amplifier and gate in the circuit (Figure B-3) and operated on a simple logic signal. The switch is a 20-mA output device and functions as well as the previous circuit. However, the magnitude of the capacitive current spike when the switch changes from track to hold is slightly greater. Since no advantage would be gained by a rewiring for this device, the previous circuit was used.

The outputs of the sample and hold circuits are fed to a differential amplifier or the differential inputs of a recorder. Since

the recorder available for this study (Mosley 2-S) does not have differential inputs, a Burr-Brown Model 1552 amplifier is used as a differential amplifier. The time constant of this amplifier was set at 0.01 sec to reduce noise. For trace analysis, a second unity gain inverting amplifier with a longer time constant, for example, 0.1 to 0.5 sec, is placed between the differential amplifier and the recorder to further "smooth" the noise. When this additional filtering inverter is used, the input signals to the differential amplifier are reversed to maintain the positive polarity of the current signal.

Square Wave Generator

A Wavetex Model 104 Function Generator is used. It is a solid state sine, triangular, and square wave generator. In the square wave mode, its specifications are:

Output Square Wave

10V peak-to-peak maximum symmetrical about ground

600 ohms output impedance

15 nsec rise time

0.1% tilt

1% frequency stability

In actual operation, all specifications are met or exceeded. The frequency stability is greater than stated and is measured as 0.2% versus the Hewlett-Packard Model 522B electronic counter. The rapid rise time is necessary to achieve efficient charging of the double layer.

Timing and Logic Circuits

The circuits (Figure 5) are assembled with solid state components and powered by regulated ± 15V power supplies (15). The circuits were assembled in a modular arrangement and will be discussed in that fashion. Because of the high output impedance of the square wave generator, its output is fed into a simple emitter-follower amplifier to avoid undue load on the generator.

Synchronization and Delay Logic. The square wave output is differentiated and amplified (Figure B-4). Since the emitter and collector of this transistor are 180° out of phase, the positive spikes from both locations are summed and amplified. The output of this amplifier is a spike of one polarity occurring for each change in polarity of the square wave.

Delay and Measuring Monostables. These spikes are fed to a series pair of monostable multivibrators (Figure B-4). Variable resistance is used for fine adjustment of pulse width and the possibility of additional capacitance is available for coarse adjustment. The first monostable generates the delay for the tracking circuits after the change of square wave polarity. This delay signal is then fed to the second variable monostable which generates the sample signal for the sample and hold circuits. A pulse of controlled duration is now produced at a certain time period after each square wave.

Sample and Hold Logic. Since one track and hold follows the positive square wave and one follows the negative square wave, a logic network is necessary to differentiate between the pulses previously

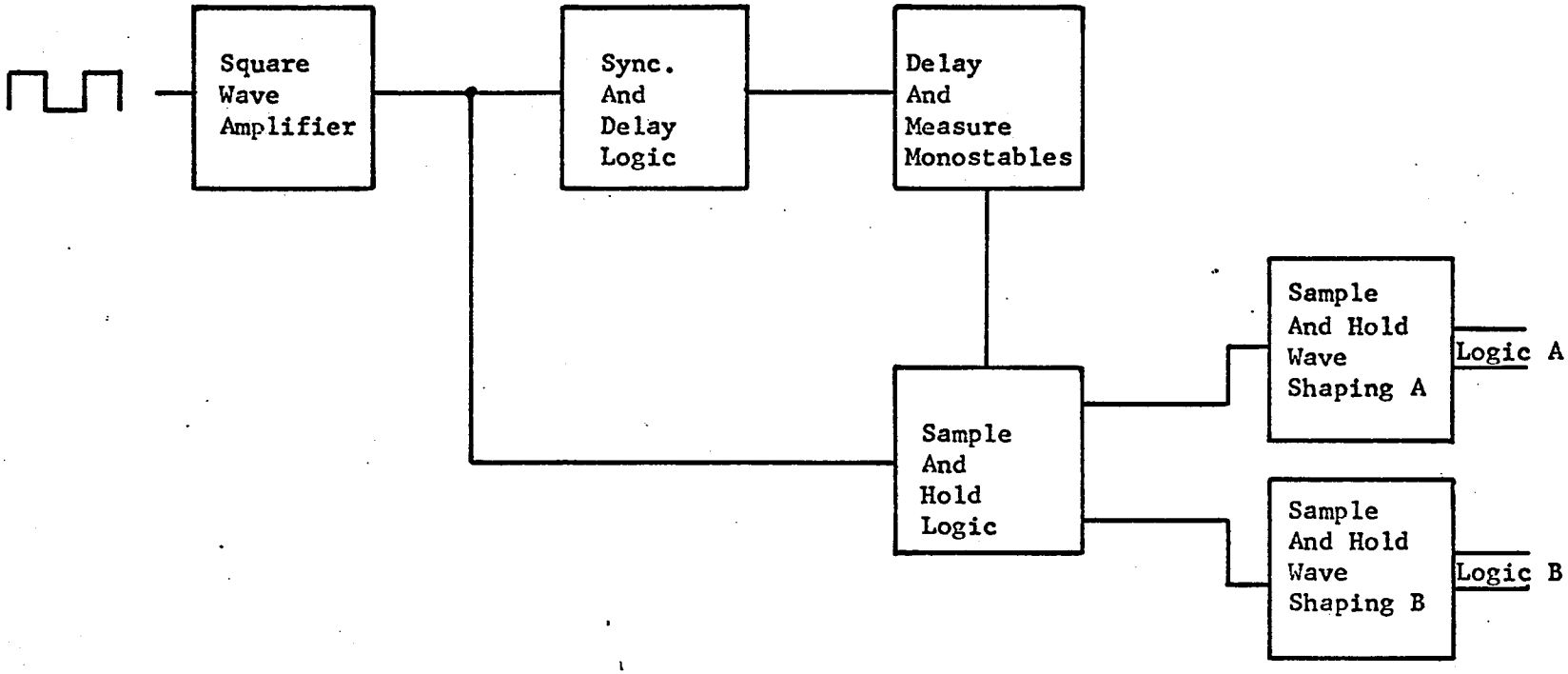

Figure 5. Block diagram of timing circuits.

generated. Two AND gates were constructed (Figure B-5). One produces a positive pulse when both the monostable and square wave are positive.

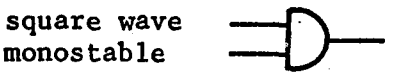

The second inverts the monostable and produces a negative pulse when both are negative.

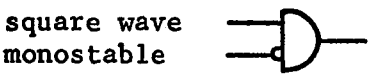

These signals are amplified and fed to matched wave shaping circuits (Figure B-6) which produce the required pair of signals for each sample and hold circuit.

Solid state components are used throughout so as to minimize noise. Each amplifier has separate power supply leads coming from a terminal point connected to the Philbrick PR-300R power supply by #14 wire. Each amplifier is decoupled at its power supply inputs by 250 μf capacitors to ground. Each ground lead in the chassis runs to a central ground location. All external signal grounds run directly to this ground and then to the building ground or water pipe.

The potentiostat, sweep generator, and sample and hold circuits are on a separate relay rack from all sources of 60 Hz signal, that is, the power supplies, timing circuits, and square wave generator. Attempts at electrostatic and magnetic shielding of the amplifiers were unnecessary. The wiring for the amplifiers is entirely enclosed in aluminum electrostatic shielding.

Electronic Operation Check

The summing points of the amplifiers are adjusted to 0.0 mV. The input of the follower is grounded and its output adjusted to 0.0 mV. The input current to the summing points of the sample and hold circuits is adjusted for no drift in the output during the hold mode.

The electrochemical cell can be simulated by a series RC circuit. In this work, the area of the electrode is typically $6 \times 10^{-2} cm^2$. The double layer capacitance is typically 16 $\mu f\ cm^{-2}$ and the cell resistance (reference to test electrode) is about 25 ohms. To simulate these conditions, a 12-ohm resistor is placed from the output of the control amplifier to the voltage follower. A 27-ohm resistor is placed in series with a 1 uf capacitor from the voltage follower to the current follower. This circuit yields an RC time constant of 27 μsec. The current flowing in this network in response to a change in potential of E is

$$i = E/Re^{-t/RC}$$

and

$$t = (RC/0.4343)\ \log E/R - RC/0.4343\ \log i$$

Therefore a plot of t versus log i will have a slope of -RC/0.4343.

Preliminary work with this network indicates that the magnitude of the current flowing at a time after the change in square wave sign is proportional to the magnitude of the square wave decaying to zero for the absence of a square wave. In order to maximize the accuracy of these measurements, a large square wave of 0.5V is used. To avoid

possible rise-time problems in the current follower, the feedback resistor is limited to 10K, and 6.8V zener bounds are placed across this amplifier.

Figure 6 represents the reduction of the data for the current flowing through the cell simulator as recorded from the outputs of the sample and hold circuits. Two slopes are observed from the data. The first slope gives an RC of 25 μsec versus 27 μsec theoretical while the second slope is 385 μsec. The two apparent slopes are also characteristic of similar data obtained in an actual electrochemical system. Since square wave voltammetry depends on a rapid decay of the double layer current, attempts were made to improve the charging rate at times greater than 0.2 msec.

A possible source of error was the sample and hold circuitry; however, comparison of their output with the current curves as measured on the Tektronix Model 502A oscilloscope indicated that they present an accurate representation of the current level.

The next possibility was that the amplifiers (1 MHz unity gain band pass) used in the polarograph were too slow to control the system with sufficient accuracy. The control amplifier and voltage and current followers were exchanged for 10 MHz amplifiers. The amplifiers used were Burr-Brown 3013 amplifiers as control and voltage follower amplifiers and a Burr-Brown 1538A stabilized amplifier as the current follower. The behavior of this system was the same (within experimental error) as that previously obtained (Figure 6).

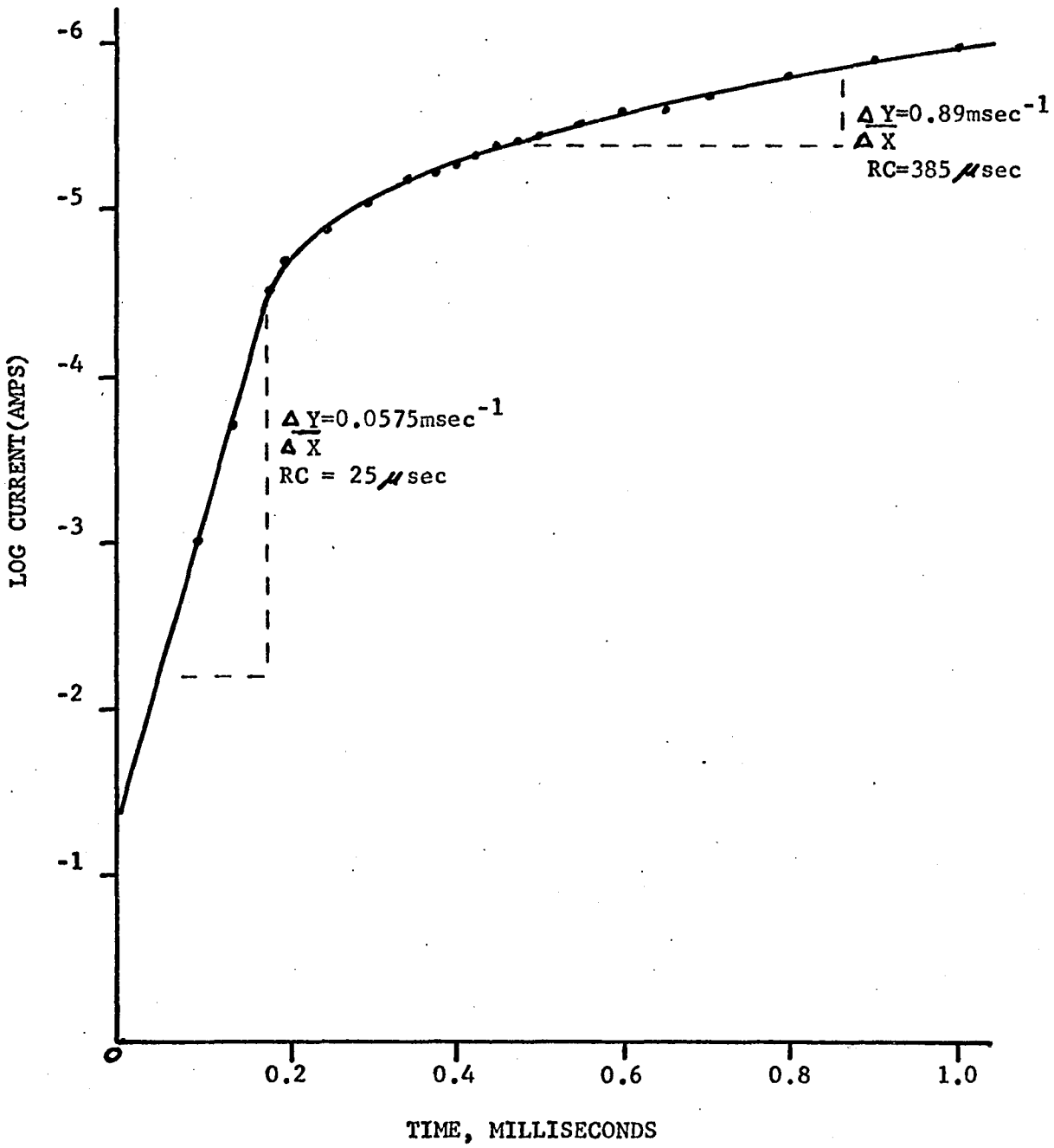

Figure 6. Current measured as a function of time in simulated cell in response to a square wave voltage.

Another possible problem source was the square wave applied to the circuit. If it exhibited any tilt, the charging current would not decay to zero. A circuit was constructed which produced a square wave having a tilt less than 0.01% (Figure 7). The data were again unchanged.

A final attempt was made by changing the size of the capacitor over the control amplifier. Reduction below the current value of 0.001 μf did not improve the response and only served to increase the current noise. Use of values below 0.001 μf resulted in oscillation during the later attempts in square wave spiking.

Consultation with the amplifier manufacturer did not provide any suggestions to improve the behavior of the instrument. The behavior as observed is the same for the three bound circuits previously described (Figure 4), with the exception of the driven diode gate (Figure 4a) which experienced tracking difficulty at extremely short times due to rise-time limitation of the current measuring amplifier. Since no solution to this difficulty became apparent, work on electrochemical systems was begun.

Square Wave Spiking

Before beginning work on a reversible electrochemical system, iron oxalate, the limitations imposed by the background current at high current gain were investigated.

Solutions of 10^{-6}M cadmium(II) in 0.1M and 0.5M potassium nitrate were investigated. The background observed at a high current gain is characteristic of the double layer capacitance curve for

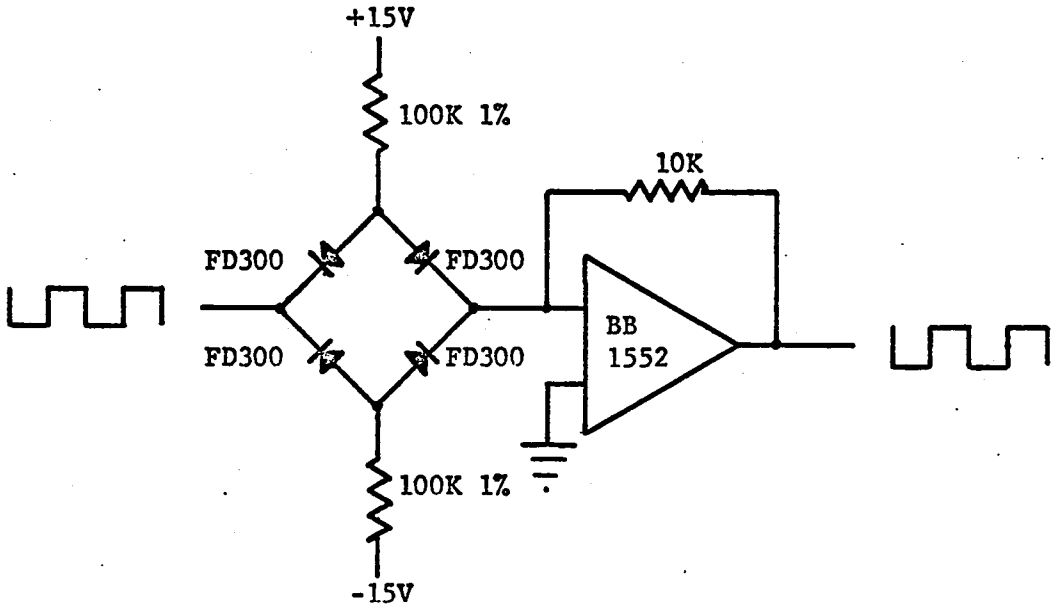

Figure 7. Square wave shaping circuit.

potassium nitrate at a mercury electrode and almost obscured the faradaic signal. In work on staircase sweep voltammetry, Vyaselev (16) suggests the use of an exponential spike on the leading edge of the step. This spike reduced the background by apparently speeding the charging of the double layer. Attempts to apply this spike to the square wave were made. A variable capacitor was placed in parallel with the square wave input resistor. The background was improved; however, the size of the capacitor had to be varied with supporting electrolyte concentration and drop size. The potentiostat became a bit unstable and the output of the current-measuring amplifier oscillated slightly on coming out of bound when the capacitor was of sufficient size to improve the background. Also, a reduction of 20% in the faradaic current was observed at high depolarizer concentration. The spiking was abandoned.

Positive Feedback

Positive feedback is used by many authors (17, 18, 19, 20) to correct the control potential for the current flowing through the cell. The traditional method feeds a small amount of the output of the current follower back to the control amplifier. Because of the bound network used in this work on the current follower, the amount of feedback during the period of amplifier bound will not represent the required amount.

If a resistor, for example, 47 ohms, is placed between the output of the control amplifier and the counter electrode, and a differential amplifier is used to measure the potential across this resistor,

the output of this amplifier (Figure 8) is proportional to the current flowing through the cell. This output is fed through a potentiometer so that a variable amount of the output may be fed back into the control amplifier through an appropriate input resistor, for example, 10K. The time constant of this amplifier must be maintained reasonably high, 300 μsec, to prevent oscillation of the system. This network was successful in suppressing the double layer background and was used during the work with current versus concentration. It exhibited only a minimal suppression of the faradaic signal of about 1%.

The 47-ohm resistor used in the work was placed in the position used in capacitive load isolation with operational amplifiers. Runs of background current in the presence and absence of this resistor indicate that the amplifiers are better able to charge the double layer capacity when this resistor further isolates the capacitance from the control amplifier.

Electrochemical Cell

The cell used in this work was made of borosilicate glass (Figure 9). A female joint on one side is provided for the entry of the reference electrode. An isolation compartment is provided between the reference electrode and the cell to prevent the salt bridge polymer from entering the test electrode compartment. The isolation compartment can be replaced with a comparable device differing in that it replaces the frit in the cell with a Luggin capillary. A Teflon stopcock is provided in the bottom of the cell for the changing of solutions and a medium frit is placed in the cell near the bottom to allow deaeration

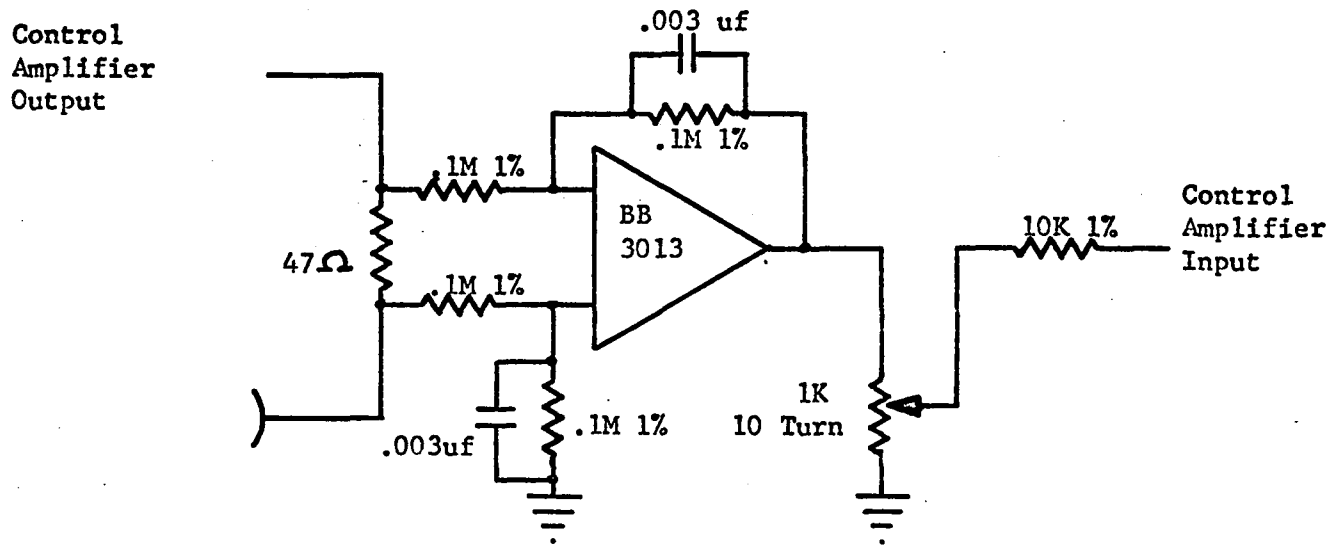

Figure 8. Positive feedback circuit.

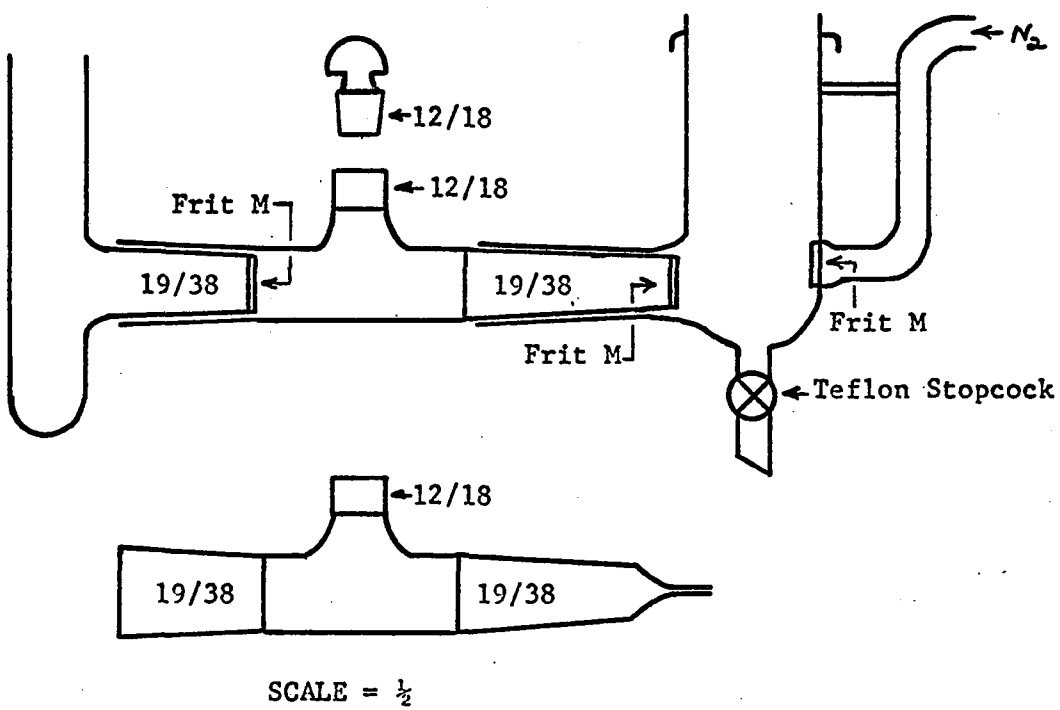

Figure 9. Electrochemical cell.

with nitrogen bubbling. The top of the cell is cut flat and not polished. A Teflon sheet is used as a cell top. It is grooved to prevent sliding on the top of the cell and is held down by rubber bands attached to glass hooks on the side of the cell. The top has appropriate holes for the test electrode, concentric counter electrode, Teflon spoon, dropping mercury electrode (DME), and an inlet to pass nitrogen over the solution during measurements. A Teflon spoon on a Teflon rod is used to collect the drops and hang them on the test electrode. The reference electrode used is a Saturated Calomel Electrode (SCE).

Test Electrode

The test electrode is a Hanging Mercury Drop Electrode (HMDE) (21, 22, 23). It is of standard construction made by sealing 0.025-inch diameter platinum wire in 4-mm o.d. soft glass tubing. The end of the seal is drawn out to a fine point to reduce shielding of the drop by the glass. The electrode was amalgamated according to the method of Ramaley, Brubaker, and Enke (24).

The platinum-glass seal must be of high quality. Any failures of this seal will expose some unamalgamated platinum to solution. This will produce capacitive dispersion at the test electrode which will appear as a greater than theoretical time constant for the electrode and a high background current, and also as hydrogen evolution.

The condition of this seal must be frequently observed. Cleaning of the electrode and mechanical jarring during use may cause small cracks to appear in a previously excellent seal.

Since the mercury drop used in this work has to make contact with the amalgamated platinum, the electrode area is less than the area of the drop determined on the basis of the drop's mass, assuming a perfect sphere. In order to accurately determine this difference and therefore to know the correct area of the drop, the double layer capacitance of the electrode was measured. D. C. Grahame (25) has made extensive studies of the characteristics of the electrode double layer. He has compiled values for the differential capacitance of a mercury electrode in 0.1M potassium chloride. By selecting a potential where the capacitance was only a slight function of potential and biasing the electrode to that potential, it was possible to measure the capacity of the electrode and therefore determine its area from Grahame's data.

An impedance bridge was constructed (Figure 10). The Wavetex Function Generator was used in the sine wave mode and drove the bridge through an isolation transformer, Gertsch Model ST 100. R_B was a 100-ohm Electro-Scieftific Industries 0.002% resistor. R_A and R_S were General Radio Model 1432X decade resistors. The Detector, D, was a General Radio Type 1232A tuned amplifier and null detector. C_S was a Heath Kit Model 1N-21, 1.0% decade capacitor calibrated to 0.1% by use of a General Radio Model 716-C Capacitance Bridge. The Leeds and Northrup Students' Potentiometer Model 7651, which was used to bias the test electrode, was isolated from the bridge ac by a 200-henry coil and was calibrated versus a standard Weston cell. The above described cell was used except that the counter electrode used here was a large cylindrical platinum screen which surrounded the entire inside of the cell.

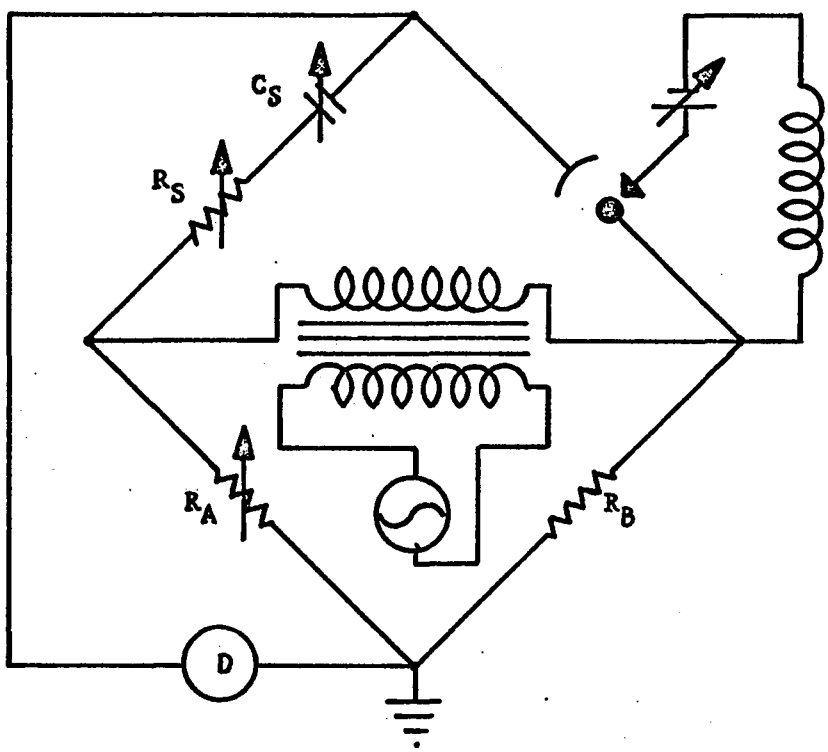

Figure 10. Electrochemical impedance bridge.

When the bridge is in balance, the values of the cell resistance and capacitance are:

$$R_C = (R_B/R_A)R_S$$

$$C_C = (R_A/R_B)C_S$$

On the basis of Grahame's data, the best results should be obtained at -1.15V versus SCE. At this potential, the variation of the differential capacitance with potential is minimal. The value of the differential capacitance at this potential is 16.04 μf cm^{-2}. Measurements were carried out in 0.1002N potassium chloride at 25°C and 1.0 KHz. Since at this potential the amplitude of the sine wave has little effect on the value of the differential capacitance, a 40 mV (peak-to-peak) sine wave was used to facilitate bridge balancing.

The first attempts at measuring the capacitance of the electrode exhibited a large degree of scatter in the values obtained. It was noted that the mass of ten drops collected from the DME was greater after the oxygen was purged from solution. This indicated that the presence of a depolarizer, for example, oxygen, affected the potential at which the unbiased DME would drop, and since the interfacial tension between mercury and water is a function of potential, the depolarizer would affect the mass of the drops. To avoid this problem, a variable battery bias was placed between the SCE and the DME. By use of this bias, the potential of the DME and therefore the mass of the drops could be controlled. This bias was arranged such that it was easily disconnected from the SCE so as not to interfere with the

electrochemical measurements. The bias was used in the collection of all subsequent drops. The potential selected was varied to suit the individual electrochemical system. The reproducibility in the drop masses improved from 4% deviation unbiased to less than 0.5% for the DME with controlled potential.

If a spherical shape is assumed, the area of a mercury drop can be related to the mass of the electrode by

$$A = 0.8510(\text{mass})^{2/3}\ \text{cm}^2\text{gm}^{-2/3}$$

For the electrodes prepared, the "mass" area was always more than the area determined by capacitance measurements. In the case of the electrode used, this difference measured $1.4\text{x}10^{-3}\text{cm}^2$. Measurements were then made on the amalgamated platinum contact alone. To do this, a drop was hung, scraped off with the spoon (to remove excess mercury), and then the bridge balanced. This method gave numbers with less scatter and averaged an area of $1.6\text{x}10^{-3}\text{cm}^2$. The diameter of the platinum wire at the contact was determined to be between 0.04 and 0.05 cm with a Bausch and Lomb Calibrated Eyepiece. The area calculated is $1.59\text{x}10^{-3}\text{cm}^2$, assuming 0.0225 cm to be an average radius. The numbers are reasonably consistent and indicate that the difference between the "mass" and capacitive area is the area of contact.

CHAPTER IV

THEORY

To a first approximation, the currents observed in linear sweep square wave voltammetry as a function of the operating parameters should be the same as those in square wave polarography. The major differences between the behavior of the two techniques is a result of two factors. First, in square wave polarography as in all polarographic techniques, the rate of change of the dc potential as a function of time is so slow that the potential may be considered constant. In the commercial instruments, the sweep potential is a step function with a period of one to several seconds. This slow potential sweep allows Barker, Faircloth, and Gardner (26) to consider the interfacial depolarizer concentration to be determined by the dc potential with only a small oscillation about this average value resulting from depolarizer response to the small amplitude square wave potential. The second is that as a result of the method of potential sweep used in this work, a linear sum of staircase and square wave voltage functions, the resultant square wave will be unsymmetrical in shape.

In basic forms the derivations of current voltage equations resulting from the square wave voltage as derived by Kambara (27) and Barker et al. (26) are similar. In both cases the authors attempt to calculate the flux of the depolarizer at the electrode as a function of the alternation of potential at this surface.

The flux at the surface is obtained from the solution of Fick's equations for linear diffusion

$$\partial C_{ox}/\partial t = D_o(\partial^2 C_{ox}/\partial x^2)$$

$$\partial C_{red}/\partial t = D_r(\partial^2 C_{red}/\partial x^2)$$

Semi-infinite diffusion to a planar electrode is assumed. The electrochemical reaction is assumed to be completely reversible. This is an important criterion if the concentration at the interface is to be accurately related to the potential. For a reversible reaction the interfacial concentration will instantaneously adjust with changes in the applied potential.

The boundary conditions upon the diffusion equations are:

$$t = 0 \qquad 0 \leq x \leq \infty \qquad C_{ox} = C^*_{ox} \qquad C_{red} = C^*_{red} = 0$$

$$t > 0 \qquad x \longrightarrow \infty \qquad C_{ox} \longrightarrow C^*_{ox} \qquad C_{red} \longrightarrow 0$$

where

x = distance from the electrode

C^* = bulk solution depolarizer concentration

C_0, C_1, C_2, etc. = interfacial oxidized depolarizer concentration

C_{ox} = oxidized form concentration = $f(x,t)$

C_{red} = reduced form concentration = $f(x,t)$

The potential is considered a discontinuous function of time and is described by

$$E(t) = E_0 \text{ for } t \leq 0$$

$$E_1 \text{ for } 0 < t < \tau$$

$$E_2 \text{ for } \tau < t < 2\tau$$

$$E_m \text{ for } (m-1)\tau < t < m\tau$$

where 2τ is the period of the square wave. The potential can be related to the concentration through the Ilkovic-modified Nernst equation

$$E = E_{\frac{1}{2}} + RT/nF \ln C_{ox}/C^*_{ox} - C_{ox}$$

and

$$C_0 = C^*_{ox} P/(1 + P)$$

where

$$P = \exp(E - E_{\frac{1}{2}})nF/RT$$

and

$$E_{\frac{1}{2}} = E^o + \frac{RT}{2nF} \ln \frac{D_r}{D_o}$$

The solutions to the equations may be obtained by comparison to the solutions obtained for the analogous problems in heat conduction (28). By utilization of the principle of superposition (29), the concentration expression may be broken into parts, each part corresponding to a half period of the square wave.

The solution thus obtained for the concentration of depolarizer at the electrode is (30)

$$C_{ox}(x,t) = C^*_{ox} + (C_1 - C^*_{ox})\text{erfc } x/kt$$

where

$$\text{erf}\lambda = \frac{2}{\pi^{\frac{1}{2}}} \int_0^{\lambda} \exp(-z^2)\, dz$$

$$\text{erfc}\,\lambda = 1 - \text{erf}\,\lambda$$

C_1 = interfacial concentration at potential E_1

for a change from potential E_0 where no electrochemical reactions occur to E_1. The next step is a return to a new potential E_2 where the concentration is again changed and yields

$$C_{ox}(x,t) = C^*_{ox} + (C_1 - C^*_{ox})\text{erfc}\ x/kt + (C_2 - C_1)\text{erfc}\ x/k(t - \tau)$$

The third half period will yield

$$C_{ox}(x,t) = C^*_{ox} + (C_1 - C^*_{ox})\text{erfc}\ x/kt + (C_2 - C_1)\text{erfc}\ x/k(t - \tau)$$

$$+ (C_3 - C_2)\text{erfc}\ x/k(t - 2\tau)$$

and in the general form

$$C_{ox}(x,t) = C^*_{ox} + (C_1 - C^*_{ox})\text{erfc}\ x/kt$$

$$+ \sum_{m=1}^{m} (C_{m+1} - C_m)\text{erfc}\ x/k(t - m\tau)$$

This is the equation in its most general form. The values of C_1, C_2, C_3, ... C_m can be calculated from the previous potential relating equations and the resultant series summed by a computer.

The flux, q, in solution of a depolarizer may be related to its concentration, $C_{ox}(x,t)$ by

$$q(x,t) = D_o \frac{\partial C_{ox}(x,t)}{\partial x}$$

where $\partial C_{ox}(x,t)/\partial x$ may be obtained from

$$\frac{d\ erf[\lambda(u)]}{du} = \frac{2}{\pi^{\frac{1}{2}}} \exp\left\{-[\lambda(u)]^2 \frac{d\lambda(u)}{du}\right\}$$

The resultant derivative expression for the flux when evaluated at $x = 0$ may then be related to the current for a plane electrode of area A, by

$$i = nFAq(0,t)$$

In the case of square wave polarography, the concentrations $C_{(2m+1)}$ are all equal to C_1 and C_{2m} are equal to C_2, the resultant series is now

$$C_{ox}(x,t) = C^*_{ox} + (C_1 - C^*_{ox})\text{erfc } x/kt + \sum_{m=1}^{\infty} (-1)^m (C_1 - C_2)\text{erfc } x/k(t - m\tau)$$

Barker's derivation assumed the dc flux then is established at some time past and therefore an average concentration condition already exists at the interface at $t = 0$. If C^*_{ox} can therefore be equated to C_2, then $C_1 - C_2$ may be considered to be ΔC, and if one considers $t = 0$ as the instant that the square wave was first applied, one obtains

$$C_{ox}(x,t) = C^*_{ox} + \sum_{m=0}^{\infty} \Delta C(-1)^m \text{erfc } x/k(t - m\tau)$$

and

$$q = \pm \Delta C(D_o/\pi t)^{\frac{1}{2}} \sum_{m=0}^{\infty} (-1)^m/(t - \tau m)^{\frac{1}{2}}$$

This describes the flux due to either the plus or minus concentration variation.

Since in square wave polarography both oscillations are sampled and then measured differentially, that is, $q = (+q) - (-q)$, the resultant flux measured is

$$q = 2\Delta C\,(D_o/\pi)^{\frac{1}{2}} \sum_{m=0}^{\infty} (-1)^m/(t - m\gamma)^{\frac{1}{2}}$$

This equation predicts the flux as a result of an infinite number of oscillations; in practice, however, only a finite number have occurred. Barker states that this presents no problem as the early concentration oscillations add little to the current at the time it is measured.

In linear sweep square wave voltammetry, the average dc potential of the electrode does not remain constant. However, if the potential sweep step is significantly smaller than the applied square wave voltage, the dc potential may be considered constant for a short period of time. For a square wave of 200 Hz and a sweep rate of 0.04V/sec, five square wave cycles will occur in the time required for the potential to sweep 1 mV.

The problem is to demonstrate at what point the differential flux for a finite number of cycles (q_F) converges sufficiently close to that observed for an infinite number (q_∞).

Rewriting the flux expression as

$$q_F = k \sum_{m=0}^{i-1} \frac{(-1)^{i-m-1}}{(i-1+B-m)^{\frac{1}{2}}} - \left[-k \sum_{m=0}^{i} \frac{(-1)^{i-m}}{(i+B-m)^{\frac{1}{2}}} \right]$$

where

$$k = \Delta C\,(D_o/\pi\tau)^{\frac{1}{2}}$$

$$t = (i + B)\tau$$

i = number of half cycles that have occurred since t = 0

B = the fraction of the square wave period where the current is sampled,

one may write the flux for a finite number of cycles

$$q_F = k[1/(4 + B)^{\frac{1}{2}} - 1/(3 + B)^{\frac{1}{2}} + 1/(2 + B)^{\frac{1}{2}} - 1/(1 + B)^{\frac{1}{2}} + 1/B^{\frac{1}{2}}]$$

$$- \; -k[-1/(5 + B)^{\frac{1}{2}} + 1/(4 + B)^{\frac{1}{2}} - 1/(3 + B)^{\frac{1}{2}} + 1/(2 + B)^{\frac{1}{2}}$$

$$- 1/(1 + B)^{\frac{1}{2}} + 1/B^{\frac{1}{2}}]$$

This equation is for the completion of three square wave cycles, with the term $-1/(5 + B)^{\frac{1}{2}}$ having occurred furthest in the past. This may be generalized in the form

$$q_F = 2k \sum_{m=0}^{i-1} \frac{(-1)^m}{(m + B)^{\frac{1}{2}}} + k \frac{(-1)^i}{(i + B)^{\frac{1}{2}}}$$

and clearly as

$$m \rightarrow \infty$$

$$q_F \rightarrow q_\infty = 2k \sum_{m=0}^{\infty} (-1)^m/(m + B)^{\frac{1}{2}}$$

It is possible to evaluate q_F and q_∞ at some B to compare the rate and degree of convergence of q_F to q_∞. Since B = 0.6 is a value used in later sweep rate work, it shall be used for this comparison.

At B = 0.6

$$q_{\infty} = 2k(0.83916)$$

$$= 1.6783\ k$$

# square wave cycles	q_F/k	$[(q_F - q_{\infty})/q_{\infty}]100$
1	1.7913	6.7
2	1.71409	2.1
3	1.697	1.112
4	1.6902	0.707
5	1.68665	0.495
6	1.68466	0.377

On the basis of these calculations, the differential current recorded at the end of five square wave cycles is within 0.5% of the value for an infinite number of cycles. Therefore, it seems reasonably justified that q_{∞} will provide a sufficiently accurate representation of the square wave flux in sweep square wave voltammetry.

To evaluate the concentration flux at the electrode-solution interface with respect to the square wave potential, the expression

$$C_0 = C^*_{ox}\ P/(1 + P)$$

is differentiated with respect to potential and yields

$$dC_0/dE = nF/RT\ C^*_{ox}\ P/(1 + P)^2$$

As stated by Barker two conditions must be considered. In the case where the square wave ΔE is much smaller than RT/nF, we may write

$$\Delta C = nF/RT\ C^*_{ox}\ P/(1 + P)^2\ \Delta E \qquad (I)$$

as the square wave component of the flux will not be sufficient to perturb the average dc component.

In the case where the alternating component is significant in size, we may write

$$\Delta C = C^*_{ox}\left[\frac{\exp(E - E_{\frac{1}{2}} + \frac{\Delta E}{2})\frac{nF}{RT}}{1 + \exp(E - E_{\frac{1}{2}} + \frac{\Delta E}{2}\ \frac{nF}{RT}} - \frac{\exp(E - E_{\frac{1}{2}} - \frac{\Delta E}{2})\frac{nF}{RT}}{1 + \exp(E - E_{\frac{1}{2}} - \frac{\Delta E}{2})\frac{nF}{RT}}\right] \quad \text{(II)}$$

The second form of ΔC is perfectly general and is the form to be used in the computer evaluation of the current function. Since $i = AnFq$, the equations can be combined into the equations for the current as a function of potential. The general equation, hereafter referred to as equation (III), is

$$i = 2nF\ C^*_{ox}\ A\left[\frac{P\exp\frac{\Delta EnF}{2RT}}{1 + P\exp\frac{\Delta EnF}{2RT}} - \frac{P\exp\frac{-\Delta EnF}{2RT}}{1 + P\exp\frac{-\Delta EnF}{2RT}}\right](D_o/\pi\tau)^{\frac{1}{2}}\sum_{m=0}^{\infty}\frac{(-1)^m}{(m+B)^{\frac{1}{2}}} \quad \text{(III)}$$

and the more limited form, hereafter known as equation (IV),

$$i = 2\frac{n^2F^2}{RT}\ A\ C^*_{ox}\ \frac{P}{(1+P)^2}\ \Delta E\ (D_o/\pi\tau)^{\frac{1}{2}}\ \sum_{m=0}^{\infty}\ \frac{(-1)^m}{(m+B)^{\frac{1}{2}}} \quad \text{(IV)}$$

It should be noted that these equations are the product of two terms. The one term common to both is a concentration, time, and electrode area dependent term,

$$2nAF\ C^*_{ox}\ (D_o/\pi\tau)^{\frac{1}{2}}\ \sum_{m=0}^{\infty}\ \frac{(-1)^m}{(m+B)^{\frac{1}{2}}}$$

The other term in the equation is the potential-containing variable and

its form is determined by the square wave size and the number of electrons involved in the reaction.

The deviation from linear diffusion will present a minimal error in square wave voltammetry. The current flowing at a spherical electrode may be considered to be the sum of two terms. The first term represents the current flowing to a planar electrode, while the second term corrects the current for the sphericity of the electrode. Thus:

$$i_{spherical} = nFAD_o^{\frac{1}{2}} C_{ox}^* \frac{1}{(\pi t)^{\frac{1}{2}}} + nFAD_o C_{ox}^* r_e^{-1} \quad (2, p. 61)$$

where r_e is the radius of the test electrode, and if the first term is much greater than the second, then the diffusion to the electrode may be considered to be linear; that is,

if

$$nFAD_o^{\frac{1}{2}} C_{ox}^* (\pi t)^{-\frac{1}{2}} \gg nFAD_o C_{ox}^* r_e^{-1}$$

or

$$r_e \gg (\pi t D_o)^{\frac{1}{2}}$$

then

$$i_{spherical} = i_{planar}$$

where t (or $B\tau$ in the case of linear sweep square wave voltammetry) is the time at which the current is measured. For B = 1.0, $\tau = 10^{-2}$sec (50 Hz), and $D_o = 10^{-5}cm^2sec^{-1}$, r_e must be greater than $5.6x10^{-4}$cm.

Typical electrode areas encountered in this work are greater than $6x10^{-2}cm^2$ and thus r_e is greater than $7x10^{-2}$cm. Therefore, the sphericity of the electrode will contribute little to the current measured, and the electrode will behave as though it were planar. The

assumption of semi-infinite diffusion presents a greater limitation for the use of the above equations.

These equations will be followed for an electrochemical system for which both the reduced and oxidized forms are soluble in solution. The case where the reduced form is soluble in the electrode violates the boundary condition of semi-infinite diffusion, as the mercury drop which constitutes the electrode is of finite volume and therefore cannot be infinite in dimension along the diffusion axis. In this case, there will be concentration of reduced form in the electrode greater than that expected for semi-infinite diffusion, and the currents measured will be greater than those calculated by the above equations.

CHAPTER V

EXPERIMENTAL VERIFICATION OF THEORY

In order to test the validity of the above equations, experiments were performed on a reversible electrochemical couple, for which both the reduced and oxidized forms are soluble in solution. The systems investigated were chromium(III) cyanide, titanium(IV) thiocyanate, and iron(III) oxalate. All fulfill the above requirements; however, the cyanide and thiocyanate ions depolarize the mercury electrode until just before the beginning of the couple's reduction peak. This would yield an undesirable background current and might interfere with the accurate measurement of the peak current. Since the background for the oxalate medium lacked these undesirable features, the iron oxalate couple was chosen for the studies.

Effect of IR Drop

In order to optimize the signal to noise ratio (S/N), a solution 1×10^{-2}M in iron(III) and 0.5M potassium oxalate was used. Work with 10^{-3}M iron solution indicated that a free ligand excess of 0.25M was sufficient to assure reversibility. However, the current observed for the 10^{-2}M iron solution was not the expected ten times that of 10^{-3}M iron.

Under the conditions of a 10 mV, 100 Hz square wave with B = 0.05, A = 6.00×10^{-2}cm^2

[Fe(III)]	i	$W_{\frac{1}{2}}$
1.019×10^{-2}M	6.07×10^{-4}A	114 mV
1.019×10^{-3}M	1.038×10^{-4}A	90 mV

Two things are obvious from these data: first, the current is not linear with concentration, and secondly, that the half peak width, a quantity which is responsive to n and the reversibility ($W_{\frac{1}{2}}$ = 90.4 mV for a reversible reduction where n = 1) would tend to indicate a slightly irreversible behavior for the higher iron concentration. Increasing the oxalate concentration to 1.0M tended to increase the current and decrease the $W_{\frac{1}{2}}$. The same effect was, however, observed by maintaining the oxalate at 0.5M and adding potassium nitrate to raise the ionic strength, μ, to the level of 1.0M potassium oxalate. The literature on this couple (31, 32) states that both the pH of 6 and free ligand excess of 0.25M used are sufficient to maintain the reversibility of the couple because under these conditions the iron oxalate complex does not undergo a change in oxalate coordination number upon reduction. The improvement in the system's behavior may then be related to solution resistance since increasing ionic strength decreases the resistance of the solution. It is therefore possible that the difficulties with the iron solution may be related to IR drop in solution.

In a three electrode potentiostatic instrument, the IR drop error in the control potential is generated in the resistance between the test electrode and the tip of the reference electrode by the current flowing through the cell. The magnitude of this resistance may

be determined for a concentrically surrounded spherical electrode by

$$R_s = \frac{\rho}{4} (1/r_e - 1/r)$$

where

R_s = solution resistance between test and reference electrode

ρ = specific resistivity of the solution

r_e = radius of test electrode

r = distance from the tip of reference electrode to the center of the test electrode.

On the basis of conductivity measurements, ρ for 0.5M potassium oxalate was determined to be 15 ohm-cm. By using a cell with a Luggin capillary reference electrode in which the distance between the test and reference electrodes could be varied, it should be possible to reduce the IR drop and verify if this is the difficulty.

IR drop has the property of reducing the effective potential applied to the test electrode, that is,

$$E_{applied} - IR_s = E_{test}$$

In dc polarography it will have the effect of diminishing the slope of the polarographic wave and will shift the $E_{\frac{1}{2}}$ to more negative potentials; however, the diffusion current, if measured sufficiently along the plateau, will be unchanged.

In square wave voltammetric techniques, IR drop will have the effect of reducing the size of the square wave potential and will therefore diminish the square wave flux component, but it will not disturb the reduction peak potential, E_p.

As was previously shown, the current output of a square wave polarograph is a function of both a positive and a negative concentration flux. In the case where ΔE is sufficiently greater than the sweep rate, the current measured is actually twice the current flowing in the cell at any instant of time. The magnitude of the IR drop will then be equal to one-half of the product of the measured current and the R_s.

For the electrode in question, assuming that it is a perfect sphere without the contact area correction, the mass area is $6.16 \times 10^{-2} cm^2$ and $r_e = 7.02 \times 10^{-2} cm$.

Inspection of the data in Table 1 shows that as the distance between the reference and test electrode is decreased, the peak current increases and the peak width decreases. The current almost achieves the correct value for a distance of 0.05 cm.

It was observed that as the solution resistance is changed, the IR drop maintains a reasonably constant value of about 4.6 mV. Attempts to rationalize this behavior failed.

In runs upon solutions of iron concentration of 1×10^{-2} to $5 \times 10^{-2} M$ at a B = 0.1, 100 Hz, and 10 mV square wave, the various peak currents rise to a high value and then level off, yielding a peak with an almost flat top. The potential at the middle of this distorted peak is still equal to $E_{\frac{1}{2}}$ within experimental error. The individual sample and hold amplifiers offer increasingly distorted outputs with rising concentration. The maximum current for the anodic sample and hold approaches more anodic potentials while the cathodic sample and hold's current maximum approaches more negative potentials. This distortion

Table 1. Peak Current Dependence on Solution Resistance.

Data for 1.019×10^{-2} M Iron 0.5M potassium oxalate pH = 6 B = 0.05 10 mV, 100 Hz square wave

i_p (amp)	$W_{\frac{1}{2}}$ (mV)	E_p(SCE)	r(cm)	R_s(ohm)	$\frac{i_p \cdot R_s}{2}$
6.07×10^{-4}	114	-0.242	1.0	15.8	4.77×10^{-3}
6.40 "	113	-0.242	0.77	15.4	4.93 "
6.77 "	110	-0.244	0.37	13.7	4.64 "
7.83 "	103	-0.244	0.22	11.5	4.54 "
9.14 "	93	-0.244	0.17	9.94	4.54 "
9.70 "	90	-0.246	0.12	7.00	3.40 "

is what possibly prevented the rationalization of the constant IR drop effect previously mentioned.

Utilization of the positive feedback circuit allowed the high concentration solutions to approach theoretical current levels. This amount of positive feedback created a high noise level in the instrument.

At low levels of IR drop ($IR < 2$ mV), it is possible to correct the currents obtained on the basis of the amount of square wave amplitude reduction, and obtain currents approximately equal to those expected in the absence of IR drop. This confirms the fact that the behavior of the iron solutions at high concentration is the result of IR drop.

These observations indicate that it is necessary to either limit the depolarizer concentration, that is, under these conditions $[Fe(III)] < 5 \times 10^{-3} M$, or use a Luggin capillary. While a Luggin capillary is useful in reducing IR drop, the maximum IR drop occurs within about 2 mm of the drop surface. While this distance provides little difficulty with either a DME or most stationary electrodes, the HMDE with its requirement of a spoon for drop hanging would provide difficulties concerning the tip of the capillary and repositioning of the electrode after drop attachment.

Also, the arm of the capillary must be filled with the solution of interest to avoid concentration gradients at the electrode, and unless the oxygen is removed from the capillary, the oxygen would continue to diffuse into the test solution almost at the immediate drop surface.

The final consideration concerning the Luggin capillary rests in the fact that by reducing R_s it would reduce RC for the test electrode and thereby improve the background at high current amplification. In actual operation, the Luggin capillary reduced the background current by 2.5×10^{-8}A; however, it increased the system noise from 2.0×10^{-8}A to 4×10^{-8}A. To achieve this noise level, the Luggin capillary reference electrode had to be electrostatically shielded, and have a shielded wire connecting it to the voltage follower of the potentiostat.

The standard reference cell, that is, the one in which the tip of the reference electrode is 1 cm from the test electrode, performed equally well whether shielded or not but was also improved by shielding its connection to the follower as was the Luggin. Electrostatic shielding of the reference electrodes provided a problem in that the shield had to extend over ground glass joints of the cell through which electrolyte solution crept. If this creeping solution contacted the shield, it shorted out the potentiostat and caused erratic behavior.

Evaluation of these factors led to the conclusion that in the limited size cell which is used, and under the conditions of trace analysis, the advantages gained by a Luggin capillary when using an HMDE are far outweighed by the difficulties encountered. Therefore, in subsequent work a cell where the reference electrode was about 1 cm from the test electrode was used.

Current Dependence on Sweep Rate

Equations derived for linear sweep square wave voltammetry predict that the current observed should be independent of sweep rate.

However, the assumption used in reaching this conclusion is that the square wave amplitude is significantly greater than the potential step which generates the sweep rate.

Because of the method used in sweep generation, the square wave is distorted from perfect symmetry. The behavior of the staircase generator must be considered again. The falling portion of the square wave will feed a negative current spike into the summing point of the staircase generator. The output of this amplifier will go positive to produce an equal and opposite current spike at the summing point. Therefore, at the control amplifier, a negative square wave will be summed with a positive staircase step. For the positive square wave direction, there will be no response from the staircase generator when it is in this sweep direction mode. Therefore, one cycle of the square wave will be diminished by the amount of the potential step, and for a 10 mV square wave and a 1 mV step there is a square wave of successive -10 mV and +9 mV steps. Under these conditions the square wave flux may now be considered as being the result of a 9.5 mV square wave.

In order to verify this conclusion, the current for 1.045×10^{-3}M iron in 0.5M potassium oxalate, pH = 6, B = 0.6, A = $6.74 \times 10^{-2} cm^2$, 200 Hz square wave was investigated at sweep rates of 0.1, 0.04, 0.02, 0.01, and 0.005V/sec and for square wave amplitudes of 2.5, 5, 10, and 20 mV.

The sweep rate is calibrated by varying the input square wave to the staircase generator with the 2.5K input potentiometer. The output of the staircase generator is fed to an electronic switch

(Figure 11) which produces a pulse at its output going from -5 to +5V when the input to the switch is +5.00V. The output of this electronic switch is fed to a second pole on the sweep generator shorting switch. This pole is open when the sweep switch is closed. Hence when the sweep is started, this pole closes and the output of the electronic switch is fed to the trigger circuits of the Hewlett-Packard #522B electronic counter now in the time measure mode. When the sweep generator exceeds 5.000V, the electronic switch sends a stop pulse to the counter and the time for a 5V sweep is recorded. The staircase input potentiometer is adjusted such that a 5V sweep requires 50.0 seconds.

The data obtained for the current as a function of the sweep rate are presented in Table 2. It can be seen that for all square wave values the current increases as the sweep rate decreases and that the magnitude of this change diminishes for increasing square wave size.

There are two methods by which the currents can be adjusted for sweep rate variation. In both methods, the magnitude of the sweep potential step must be considered. For a 200 Hz square wave, the step sizes as a function of sweep rate are

Sweep Rate V/sec	Step Size mV
0.10	0.5
0.04	0.2
0.02	0.1
0.01	0.05
0.005	0.025

The first method considers the current observed to have been simply the

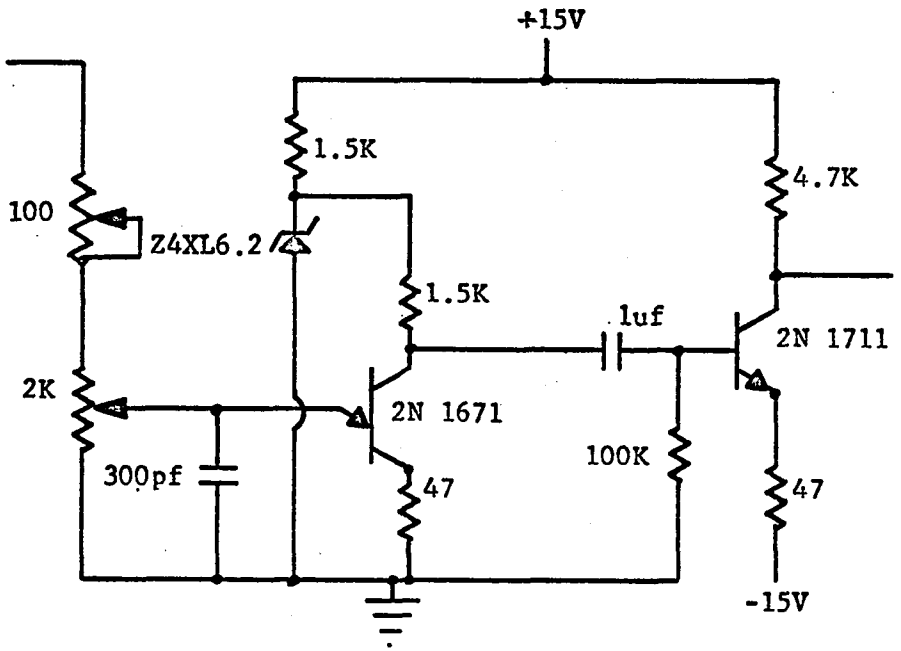

Figure 11. Electronic switch.

Table 2. Peak Current Dependence on Sweep Rate.

1.045×10^{-3} M Fe^{+3} 0.5M potassium oxalate pH = 6 200 Hz B = 0.6 A = 6.74×10^{-2} cm^2 24°C

	Sweep rate	i(measured) (amp)	i(measured) corrected for sweep rate current	i(measured) corrected for square wave distortion
2.5 mV	0.1V/sec	7.30×10^{-6}	8.04×10^{-6}	8.11×10^{-6}
	0.04	7.71 "	8.01 "	8.03 "
	0.02	7.89 "	8.03 "	8.05 "
	0.01	7.96 "	8.04 "	8.04 "
	0.005	8.02 "	8.06 "	8.07 "
5 mV	0.10	1.52×10^{-5}	1.59×10^{-5}	1.60×10^{-5}
	0.04	1.56 "	1.59 "	1.59 "
	0.02	1.57 "	1.58 "	1.59 "
	0.01	1.585 "	1.59 "	1.59 "
	0.005	1.59 "	1.59 "	1.60 "

Table 2.--Continued

	Sweep rate	i(measured) (amp)	i(measured) corrected for sweep rate current	i(measured) corrected for square wave distortion
10 mV	0.1V/sec	3.14×10^{-5}	3.21×10^{-5}	3.21×10^{-5}
	0.04	3.14 "	3.17 "	3.17 "
	0.02	3.15 "	3.16 "	3.17 "
	0.01	3.15 "	3.16 "	3.16 "
	0.005	3.18 "	3.18 "	3.18 "
20 mV	0.1	6.17×10^{-5}	6.24×10^{-5}	6.25×10^{-5}
	0.04	6.21 "	6.24 "	6.24 "
	0.02	6.21 "	6.22 "	6.23 "
	0.01	6.25 "	6.26 "	6.26 "
	0.005	6.28 "	6.28 "	6.28 "

current that would have been observed in the absence of potential sweep plus the current that results from the potential sweep.

The potential sweep goes positive when the square wave goes negative, and since the instrument is set up to record the current from the positive square wave as positive and to invert the current of the negative portion and therefore record it as positive, the instrument will invert the current signal due to sweep and therefore subtract it from the square wave current component.

Operating the instrument without a square wave component (a condition that is not staircase voltammetry), the following currents are recorded: B = 0.6, 200 Hz, 1.045×10^{-3}M iron, 0.5M potassium oxalate, pH = 6, A = $6.74 \times 10^{-2} cm^2$.

Sweep Rate	Step Size	Current	i/Step Size
0.1V/sec	0.5 mV	-7.4×10^{-7}A	1.5×10^{-3}
0.04	0.2	-3.0×10^{-7}A	1.5×10^{-3}
0.02	0.1	-1.4×10^{-7}A	1.4×10^{-3}
0.01	0.05	-0.8×10^{-7}A	1.6×10^{-3}
0.005	0.025	-0.4×10^{-7}A	1.6×10^{-3}

These data indicate that the current produced appears to be directly related to the size of the step. If this current were due to a linear sweep voltammetry effect, it should follow a $v^{\frac{1}{2}}$ dependence which it does not. This current may also be considered as being the product of a square wave of two grossly different components; the positive component is the size of the step and the negative component is zero.

This would yield a square wave of average amplitude of one-half the step size. If the currents resulting at sweep rates of 0.1V/sec and 0.01V/sec are compared to that for a 2.5 mV square wave, there is a reasonable consistency in the values of $i/\Delta E_{average}$.

Sweep Rate	Step Size	$\Delta E_{average}$	$i/\Delta E_{average}$
0.1V/sec	0.5 mV	0.25 mV	-3.0×10^{-3}
0.01	0.05	0.025	-3.2×10^{-3}
--	--	2.5	3.2×10^{-3}

Therefore, since this current due to the sweep rate is subtracted from the current due to the square wave, if appropriate amounts of current are added to the measured value, the resultant currents should be constant; that is,

$$i_{corrected} = k = i_{measured\ with\ square\ wave} + i_{measured\ without\ square\ wave}$$

The second method of correcting the measured currents for sweep rate is merely to multiply the current measured by a factor which will correct the data for square wave distortion. As an example, consider the 2.5 mV square wave. At a sweep rate of 0.1V/sec, it is composed of two different square wave sizes; the positive square wave component is 2.5 mV while the negative component is -2.5 + 0.5 or 2.0 mV. The average square wave amplitude is 2.25 mV and the current correction factor is 2.5/2.25 = 1.111. The factors thus calculated are tabulated in Table 3. Inspection of this table confirms the expected conclusion that the currents observed at slow sweep rates and large values of ΔE

Table 3. Peak Current Correction Factors for Sweep Rate.

Sweep rate (200 Hz)	Δ E 2.5 (mV)	ΔE 5.0 (mV)	Δ E 10 (mV)	Δ E 20 (mV)
0.10V/sec	1.111	1.053	1.026	1.013
0.04	1.042	1.020	1.010	1.005
0.02	1.020	1.010	1.005	1.003
0.01	1.010	1.005	1.003	1.001
0.005	1.006	1.003	1.002	1.0001

are reasonably undistorted from the values expected for the extremely slow sweep rates of square wave polarography, that is, 1V per 10 minutes to 1V per hour.

Table 2 contains the currents as measured, as corrected for sweep current, and as corrected for square wave distortion. Both methods of correction yield results which are equally independent of sweep rate within the 1% accuracy of these measurements.

The method of correcting the data by compensating for square wave distortion does not require current measurement and will be independent of the time dependent factors in the square wave polarographic equations. It will therefore be the method of choice for correction of currents for sweep rate if and when this correction is necessary.

Current Dependence on B

The dependence of the current upon the fraction B of the square wave at which the current is measured was investigated. A plot of current versus B is presented in Figure 12. As predicted in equations derived earlier

$$\frac{i}{\sum_{m=0}^{\infty} \frac{(-1)^m}{(m + B)^{\frac{1}{2}}}}$$

should be a constant. Values of this summation have been calculated for B of 0.05 to 1 at 0.05 intervals and are presented in Table 4. Table 5 presents the results of this study. Each point is the average of three runs.

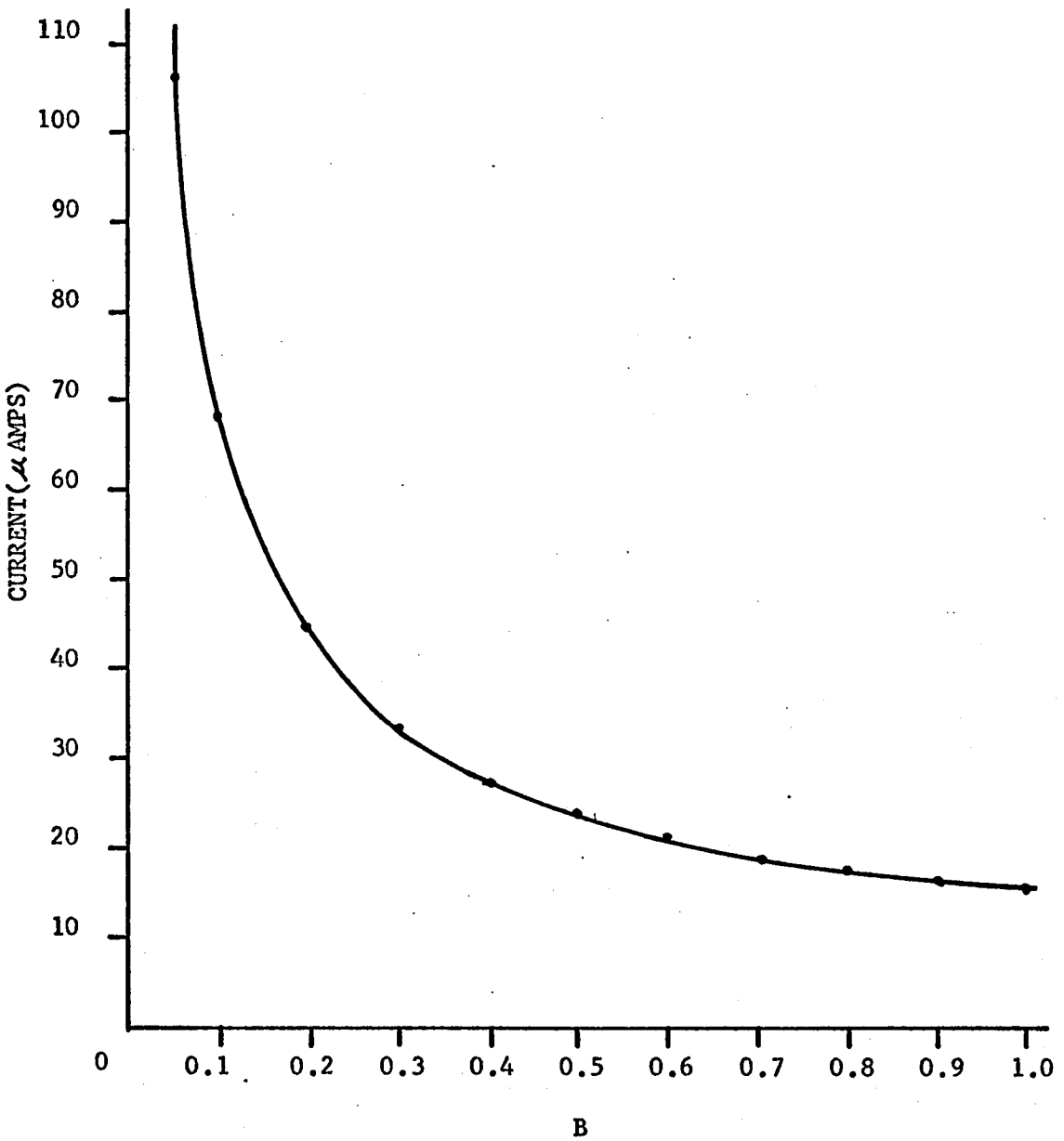

Figure 12. Current versus B.

Table 4. Evaluation of $\sum_{m=0}^{\infty} \frac{(-1)^m}{(m+B)^{\frac{1}{2}}}$ at Various B.

B	$\sum_{m=0}^{\infty} \frac{(-1)^m}{(m+B)^{\frac{1}{2}}}$
0.05	3.88
0.10	2.59
0.15	2.03
0.20	1.70
0.25	1.47
0.30	1.31
0.35	1.19
0.40	1.09
0.45	1.01
0.50	0.944
0.55	0.888
0.60	0.839
0.65	0.797
0.70	0.760
0.75	0.727
0.80	0.697
0.85	0.671
0.90	0.647
0.95	0.625
1.00	0.605

Table 5. Peak Current Dependence on B.

1.045×10^{-3} M Fe^{+3} 0.5M potassium oxalate pH = 6 25°C $A = 6.04 \times 10^{-2}$ cm^2

100 Hz, 10 mV square wave 0.02V/sec sweep rate τ = 5 msec

Measure instant $(B\tau)$ msec	B	E_p (SCE)	$W_{\frac{1}{2}}$ (mV)	Peak current (amp)	$\frac{i_p}{\sum_{m=0}^{\infty} \frac{(-1)^m}{(m+B)^{\frac{1}{2}}}}$
0.25	0.05	-0.245	90	10.65×10^{-5}	2.74
0.50	0.10	-0.245	90	6.85 "	2.65
1.00	0.20	-0.244	90	4.43 "	2.60
1.50	0.30	-0.245	91	3.38 "	2.54
2.00	0.40	-0.245	90	2.73 "	2.51
2.50	0.50	-0.246	90	2.41 "	2.45
3.00	0.60	-0.245	89	2.11 "	2.52
3.50	0.70	-0.245	90	1.93 "	2.54
4.00	0.80	-0.246	89	1.76 "	2.52
4.50	0.90	-0.245	90	1.63 "	2.52
5.00	1.00	-0.244	90	1.52 "	2.51

The data in this table exhibit good agreement with theory until between 1.5 and 1.0 msec measure instant ($B\tau = t_m$). At this point there is some deviation from the theoretical behavior in the direction of higher currents. Figure 13 represents an attempt to reduce the current reading with respect to a $t^{-\frac{1}{2}}(0 < t < \tau)$ dependence. A $t^{-\frac{1}{2}}$ dependence of current is experienced at electrodes in response to a potential step and therefore this might be a better model for the current dependence than the summation involving B. The final column in Table 5 indicates only an 8% deviation versus theory in the worst case; a comparable reduction of current as a function of $t^{-\frac{1}{2}}$ (not shown) deviated by 60%. Therefore, as long as the instant at which the current is sampled is greater than 1 msec, the derived equation will provide an accurate representation of the current.

Current Dependence on Square Wave Period

The final time dependent part of the square wave equation was investigated. The current is predicted to follow a $\tau^{-\frac{1}{2}}$ dependence where τ is the square wave half period. Preliminary work was done at a B of 0.5. However, under this condition, when τ was equal to 2.0 msec, the measure instant was 1 msec and at this point, as previously noted in the case of i versus B studies, $i/\tau^{-\frac{1}{2}}$ deviated to higher values from a previously constant value.

In order to avoid this problem and to extend the region over which the behavior of current with τ could be observed without complications, B was increased to 0.9.

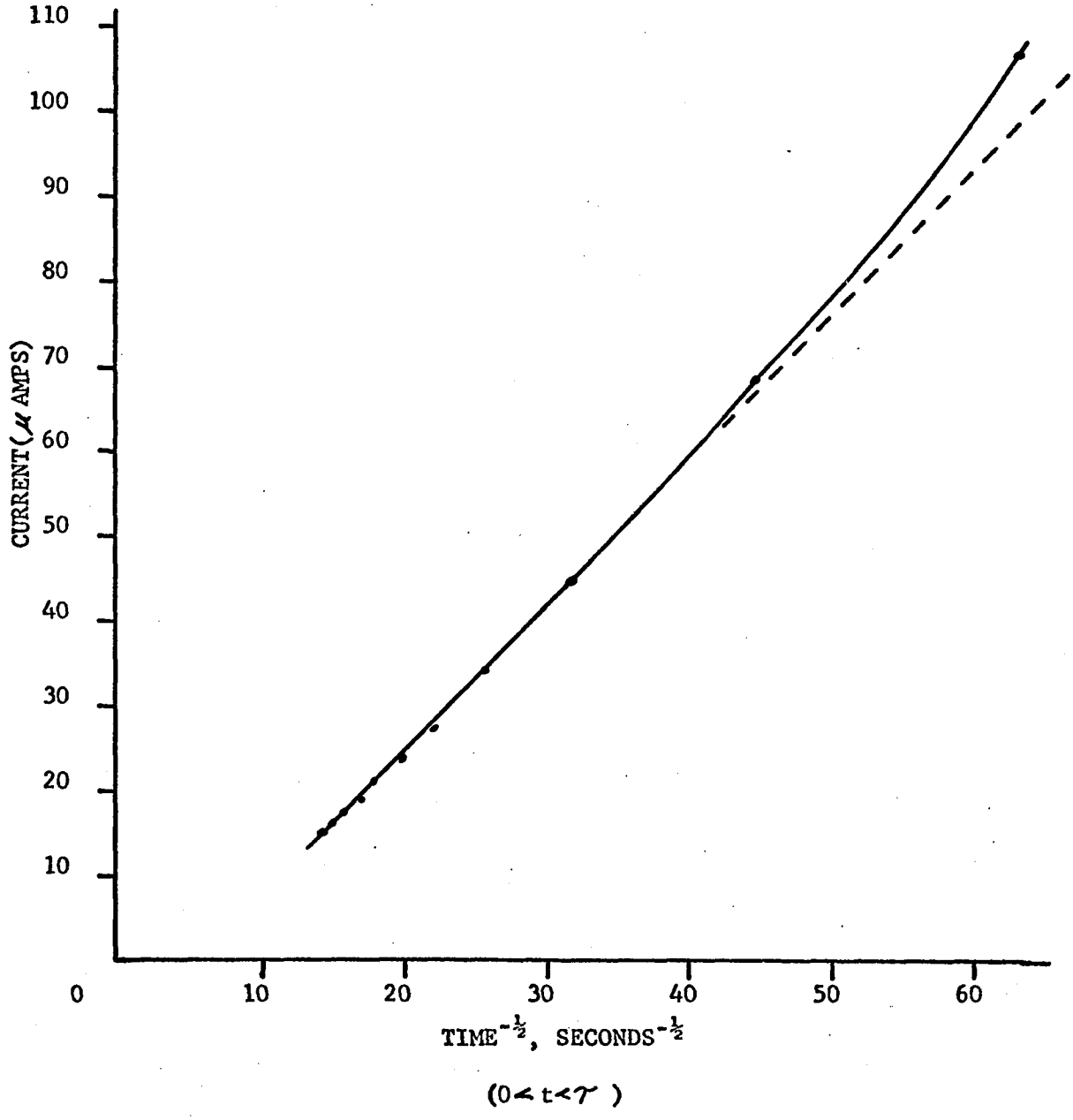

Figure 13. Current versus $t^{-\frac{1}{2}}$.

In these measurements the sweep rate was maintained constant by adjusting the staircase generator's input potentiometer. In Table 6, $i_{corrected}$ is the current corrected as previously described for decrease in the square wave size due to sweep rate. Theory predicts that the current divided by $\gamma^{-\frac{1}{2}}$ should be a constant. Inspection of the final column in Table 6 where these values are listed shows that again excellent agreement with theory is exhibited until the measure instant becomes less than 1 msec; at this point the constant again deviates to high values.

Current Dependence on Square Wave Size

The two equations, (III) and (IV), derived for square wave polarography differ only in the term which is related to the change in interfacial depolarizer with concentration. Of two equations for ΔC_{ox}, equation (I),

$$\Delta C_{ox} = \frac{nF}{RT} C^*_{ox} \Delta E \frac{P}{(1 + P)^2}$$

was said to be valid only as long as RT/nF (25.7 mV at 25°C for n=1) was greater than ΔE. The second equation, (II),

$$C_{ox} = C^*_{ox} \left[\frac{P\exp(\Delta EnF/2RT)}{1 + P\exp(\Delta EnF/2RT)} - \frac{P\exp(-\Delta Enf/2RT)}{1 + P\exp(-\Delta EnF/2RT)} \right]$$

is considered applicable for all values of ΔE. These two equations yield two results which are important. One quantity is the value of these expressions at the peak current, that is, when P = 1, which is a function of ΔE and n. The second quantity is the half peak width, $W_{\frac{1}{2}}$,

Table 6. Peak Current Dependence on τ.

1.045×10^{-3} M Fe^{+3}	0.5M potassium oxalate		pH = 6	B = 0.9
	0.02V/sec sweep rate		10 mV square wave	
τ (msec)	$\tau^{-\frac{1}{2}}$	i (amp)	$i_{corrected}$ (amp) for sweep rate	$\frac{i_{corr}}{\tau^{\frac{1}{2}}}$
5.0	1.414×10	1.54×10^{-5}	1.555×10^{-5}	1.10×10^{-6}
4.5	1.49 "	1.62 "	1.633 "	1.096 "
4.0	1.58 "	1.74 "	1.75 "	1.107 "
3.5	1.69 "	1.87 "	1.88 "	1.111 "
3.0	1.825 "	2.02 "	2.024 "	1.109 "
2.5	2.00 "	2.18 "	2.18 "	1.109 "
2.0	2.235 "	2.50 "	2.50 "	1.118 "
1.5	2.58 "	2.89 "	2.89 "	1.12 "
1.3	2.775 "	3.13 "	3.13 "	1.128 "
1.2	2.885 "	3.24 "	3.24 "	1.123 "
1.1	3.015 "	3.40 "	3.40 "	1.128 "
1.0	3.165 "	3.62 "	3.62 "	1.144 "
0.9	3.33 "	3.85 "	3.85 "	1.153 "
0.8	3.54 "	4.09 "	4.09 "	1.155 "
0.6	4.08 "	4.80 "	4.80 "	1.176 "

a quantity which equation (I) predicts to be only a function of n, while equation (II) predicts to be a function of both ΔE and n.

It is possible to solve these equations in a fashion that will yield a value of $W_{\frac{1}{2}}$. For equation (I), the following values are obtained at 25°C:

n	$W_{\frac{1}{2}}$
1	90.4 mV
2	45.2
3	30.1

Equation (II) is more cumbersome and since only a system where n = 1 was studied, the values of $W_{\frac{1}{2}}$ were obtained only as a function of ΔE. For n = 1 at 25°C,

ΔE	$W_{\frac{1}{2}}$
10 mV	90.90 mV
20	91.93
50	99.06

Table 7 exhibits the results of variation of ΔE. The $W_{\frac{1}{2}}$ is clearly a function of ΔE and does follow within experimental error the behavior predicted on the basis of equation (II).

Equations (I) and (II) may also be evaluated at P = 1 to yield a quantity $k' = \Delta C_{ox\ peak}/C^*_{ox}$ which is proportional to the peak current $i_p/k' = \text{constant}$. The two solutions are derived respectively from equations (I) and (II).

$$k'_I = \frac{nF}{4RT}\ \Delta E \qquad (V)$$

$$k'_{II} = \frac{\exp(\Delta EnF/2RT) - 1}{\exp(\Delta EnF/2RT) + 1} \qquad (VI)$$

Table 7. Peak Current and $W_{\frac{1}{2}}$ Dependence on $\Delta E(n=1)$.

100 Hz	B = 0.5	1.045×10^{-3} M Fe^{+3}	0.5M potassium oxalate	pH = 6
	25°C	0.04V/sec	A = $6.01 \times 10^{-2} cm^2$	
ΔE (mV)	E_p (SCE)	$W_{\frac{1}{2}}$ (mV)	i (amp)	$i_{corrected}$ for sweep rate
2.5	-0.245	90.4	5.30×10^{-6}	5.76×10^{-6}
5.0	-0.245	90.4	1.08×10^{-5}	1.12×10^{-5}
10.0	-0.245	90.5	2.22×10^{-5}	2.265×10^{-5}
20.0	-0.244	92.0	4.44×10^{-5}	4.485×10^{-5}
50.0	-0.244	98.0	1.050×10^{-4}	1.054×10^{-4}

Calculated values of equations (V) and (VI) are contained in Table 8 with the additional representation of the percentage error between the peak currents as predicted by the two equations (I) and (II) considering equation (VI) to be correct due to its more general nature.

$$\% \text{ error} = \left[\frac{\frac{nF\Delta E}{4RT}}{\frac{\exp \frac{\Delta EnF}{2RT} - 1}{\exp \frac{\Delta EnF}{2RT} + 1}} - 1 \right] \times 100$$

These values indicate that for about a 1% accuracy between equations (I) and (II), ΔE should be less than 0.5 RT/nF.

Table 9 contains values for i_{peak}/k' where k' is obtained from both (V) and (VI). The peak currents are corrected for sweep rate as was previously described. The behavior of peak current with respect to ΔE as predicted by equation (II), that is, $i_{p\ corrected}/k'_{II}$, is again seen to be the more general. The observations are within experimental error of the predictions on the basis of (II) and at values of $\Delta E < 0.5$ RT/nF (12 mV). The currents as predicted by both (I) and (II) are indistinguishable.

Current Dependence on Electrode Area

The dependence of the current upon the area of the drop was investigated for electrodes consisting of one, two, and three drops from the DME. Under the following conditions, 1.045×10^{-3}M iron(III) in 0.5M potassium oxalate, pH = 6, 100 Hz, B = 0.5, 0.01V/sec, with the mass of ten drops equal to 0.06475g, the currents measured are

Table 8. Peak Current Factors as a Function of n and ΔE.

	ΔE (mV)				
	2.5	5.0	10	20	50
n = 1					
(V)	0.02433	0.04866	0.09738	0.1947	0.4868
(VI)	0.02433	0.04863	0.09703	0.1923	0.4517
% error	-	0.06	0.4	1.38	8
n = 2					
(V)	0.04866	0.09738	0.1947	0.3895	0.9734
(VI)	0.04863	0.09703	0.1923	0.3709	0.7502
% error	0.06	0.4	1.3	5	29
n = 3					
(V)	0.07299	0.1461	0.2921	0.5842	1.461
(VI)	0.07287	0.1451	0.2840	0.5257	0.8978
% error	0.16	0.71	2.8	11.0	62

Table 9. Peak Current Dependence on ΔE Compared to Theory.

100 Hz	B = 0.6	1.045×10^{-3}M Fe^{+3}	0.5M potassium oxalate		pH = 6
	25°C	0.04V/sec	A = $6.01 \times 10^{-2} cm^2$		
ΔE (mV)	i_{corr}(amp)	(V)	$i_{corr}/(V)$	(VI)	$i_{corr}/(VI)$
2.5	5.76×10^{-6}	0.02433	237	0.02433	237
5	1.125×10^{-5}	0.04866	231	0.04863	231
10	2.265×10^{-5}	0.09738	233	0.09703	233
20	4.485×10^{-5}	0.1947	230	0.1923	233
50	1.054×10^{-4}	0.4868	216	0.4517	233

Number of Drops	Mass Area	Current
3	$6.15\times10^{-2}cm^2$	$2.37\times10^{-5}A$
2	$4.69\times10^{-2}cm^2$	$1.77\times10^{-5}A$
1	$2.96\times10^{-2}cm^2$	$1.10\times10^{-5}A$

A plot of the mass area versus current is linear within 1%. The intercept at zero current is $2.0\times10^{-3}cm^2$. This value compares favorably with the previous measurements of the drop contact area of $1.6\times10^{-3}cm^2$. During later work with thallium in a potassium nitrate medium, this experiment was repeated. The intercept was $1.2\times10^{-3}cm^2$. Therefore this graphical method can yield an estimate of the electrode area accurate to about 1%.

Current Dependence on Concentration of Depolarizer

In square wave polarography, as in most electrochemical techniques, the current measured, whether peak or diffusion, is proportional to concentration. Attempts were made to study the limits of linearity of current with concentration for the iron oxalate couple. Preliminary observations of the oxalate medium at high current gain exhibited peaks at -0.261 (SCE) and -0.56 (SCE). Since both peaks had $W_{\frac{1}{2}}$ of about 48 mV, they were tentatively identified as being copper(II) and lead(II) (1, p. 644).

	$E_{\frac{1}{2}}$	$E_{3/4}-E_{\frac{1}{4}}$	
Cu(II)	-0.272	-0.28	1M potassium oxalate pH 5 → 10
Pb(II)	-0.581	-0.28	1M potassium oxalate pH 7.5 → 10.5

The slight discrepancy between E_p and $E_{\frac{1}{2}}$ is probably due to a

difference in supporting electrolyte conditions. The peaks also exhibited peak current enhancement in cyclic work due to anodic stripping. Since the lead wave was of no immediate interest, only the copper peak was further considered, as the copper would interfere with accurate measurement of the iron current.

On the basis of a standard addition method of analysis, the copper level in 0.5M potassium oxalate was determined to be about 2×10^{-6}M. Potassium oxalate can be prepared at a higher degree of purity than is available as an analytical reagent grade. However, the method is complicated and the yields are too small to conveniently produce sufficient quantities of supporting electrolyte needed for this study. Furthermore, the oxalate background has a pronounced bend in the vicinity of the iron peak which would make accurate measurement of the peak current difficult. For these reasons the iron oxalate system was abandoned.

The thallium(I) nitrate system was then considered. Potassium nitrate (Mallinckrodt AR grade) has been found to be the cleanest reagent readily available in the laboratory. Attempts at extracting metals from an unbuffered 1.0M potassium nitrate solution produced no noticeable color change in the dithizone-carbon tetrachloride layer. Under comparable conditions, "AR" potassium chloride will rapidly color the organic phase pink due to the heavy metals extracted. The measured lead level was about 1×10^{-8}M in a solution of 0.5M potassium nitrate. The favorable background and availability of potassium nitrate combined

with the reversible behavior of thallium(I) in this medium resulted in its selection as the system for this study.

It is necessary at this time to consider the methods available to accurately measure the peak currents for the reductions of interest and to separate from these measurements the current that is a result of the background.

A nonzero background current at high current gain may be attributed to a number of factors: 1) a nonideal double layer charging rate due to electronics, 2) an imperfect electrode in which some platinum is exposed to solution, 3) residual oxygen in solution, and 4) trace metallic impurities in the supporting electrolyte.

Of these factors, the oxygen in solution may be removed by standard polarographic techniques, while the remaining factors should merely contribute to a constant nonlinear and nonzero background. This problem is one often encountered in high sensitivity electrochemical techniques. Kaplan and Sorokovskaya (34) have considered this problem in detail when it is encountered in applied square wave polarography. The solution to this problem as proposed here is basically similar to Kaplan's. Figure 14 displays a representation of the type of currents in question. There are two methods by which the background and faradaic currents may be separated. One method is a hill and valley approach where a line is drawn connecting two points to either side of E_p and the current is measured from this line to i_p. The assumption that the background follows this line is often poor, and the "measured" faradaic current may be greater than the true value (this example) or

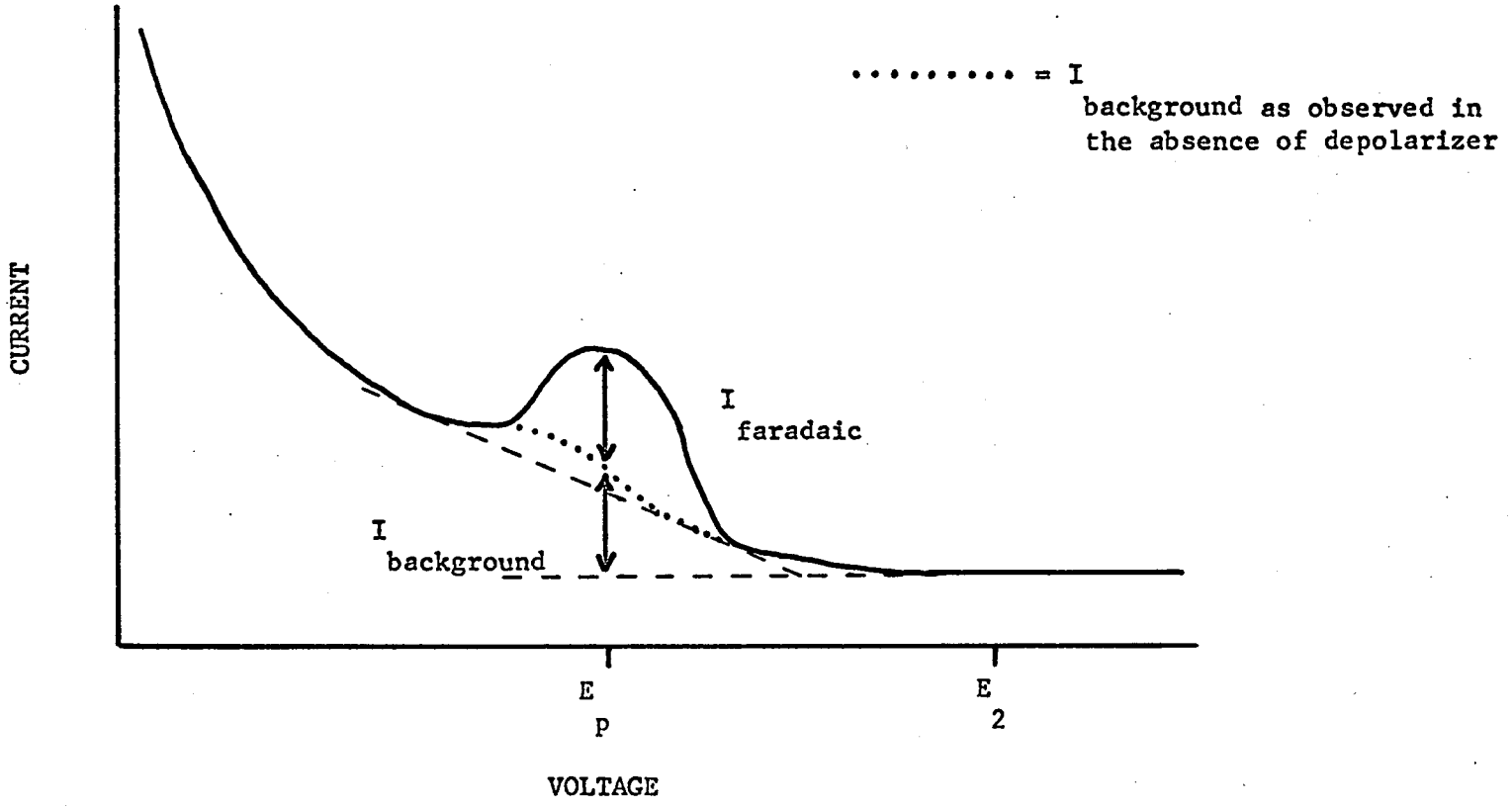

Figure 14. Measurement of faradaic currents.

less than the true value if the peak of interest is between two large peaks. The second method which is used in this study is similar to that of Kaplan. A second reference potential, E_2, is selected, where the background is either zero or linear. The current is then measured at E_p from a straight line through the current at E_2. The currents thus measured are plotted as a function of concentration, and the current at zero concentration is the background current. The background current thus obtained is subtracted from the currents measured to yield faradaic current. The background current thus measured is equal to current similarly measured for supporting electrolyte alone.

A series of solutions from 5×10^{-7}M to 5×10^{-4}M thallium was prepared in 0.5M potassium nitrate. These solutions were prepared in 500-ml quantities and stored in 500-ml Nalgene bottles. The bottles were cleaned with alcoholic potassium hydroxide to remove any residual organics from the bottles which might be surface active. The solutions were prepared three times. Each time they were allowed to equilibrate in the bottles for one day with occasional shaking, and then discarded until the third solution which was then retained.

Beginning with the most dilute solution, the cell was filled with the solution of interest, nitrogen was bubbled through for five minutes, the solution was discarded, the process repeated, and then the cell was filled; nitrogen passed through solution for 15 minutes. At this time the flow of nitrogen was changed to flow over the solution and the solution was analyzed four times, with fresh drop electrodes, the first run being discarded. The positive feedback circuit was

adjusted to yield the best background signal for the most dilute solution.

Since E_p for thallium(I) nitrate is -0.465 (SCE), the drops from the DME had to be collected at a potential where no reduction of the thallium would result; otherwise a slight concentration of thallium in the electrode would result due to amalgam formation. This effect would destroy the precision attainable. The DME was therefore biased to -0.20V (SCE).

Since each set of runs consumed the better part of a day, the solutions were run on three separate days. In order to normalize the data of one day to the next, the faradaic currents measured are divided by the electrode areas and therefore converted into current densities. The background currents were determined by a plot of current versus concentration for the four most dilute solutions extrapolated to zero concentration. Also, a least squares analysis was done upon these same points to determine the intercept.

Tables 10, 11, and 12 contain the results of this study. The final column in each table is the current density divided by concentration, a quantity which should be independent of concentration. A measure of the linearity of current versus concentration would be the standard deviation of these constants and this is also included.

Table 13 contains the current density-concentration constants from each day which are averaged together for each concentration. The standard deviation of these averages is thus reported.

Table 10. Current Density Dependence on Concentration, 8-19-68.

$A = 6.76 \times 10^{-2} cm^2$

Concentration [Tl(I)]	i_p (amp)	$i_{corr.}$	Current density (amp cm^{-2})	Current density / Concentration
5.00×10^{-7}	3.53×10^{-8}	2.93×10^{-8}	4.328×10^{-7}	0.8656
1.25×10^{-6}	7.90×10^{-8}	7.30×10^{-8}	1.078×10^{-6}	0.8624
2.50×10^{-6}	1.54×10^{-7}	1.49×10^{-7}	2.201×10^{-6}	0.8804
5.00×10^{-6}	3.07×10^{-7}	3.01×10^{-7}	4.446×10^{-6}	0.8892
1.25×10^{-5}	7.50×10^{-7}	7.44×10^{-7}	1.099×10^{-5}	0.8792
2.50×10^{-5}	1.49×10^{-6}	1.48×10^{-6}	2.186×10^{-5}	0.8744
5.00×10^{-5}	2.98×10^{-6}	2.97×10^{-6}	4.387×10^{-5}	0.8774
1.25×10^{-4}	7.34×10^{-6}	7.33×10^{-6}	1.083×10^{-4}	0.8664
2.50×10^{-4}	1.460×10^{-5}	1.46×10^{-5}	2.156×10^{-4}	0.8624
5.00×10^{-4}	2.905×10^{-5}	2.91×10^{-5}	4.298×10^{-4}	0.8596

Mean 0.872 ± 0.0097 (amp $cm^{-2} mole^{-1}$)

$\pm 1.1\%$

Table 11. Current Density Dependence on Concentration, 8-20-68.

Concentration [Tl(I)]	i_p (amp)	$i_{corr.}$	Current density (amp cm^{-2})	Current density / Concentration
		$A = 6.72 \times 10^{-2} cm^2$		
5.00×10^{-7}	3.75×10^{-8}	2.95×10^{-8}	4.390×10^{-7}	0.8778
1.25×10^{-6}	8.10×10^{-8}	7.30×10^{-8}	1.086×10^{-6}	0.8690
2.50×10^{-6}	1.52×10^{-7}	1.44×10^{-7}	2.143×10^{-6}	0.8572
5.00×10^{-6}	3.03×10^{-7}	2.95×10^{-7}	4.390×10^{-6}	0.8778
1.25×10^{-5}	7.47×10^{-7}	7.39×10^{-7}	1.099×10^{-5}	0.8797
2.50×10^{-5}	1.467×10^{-6}	1.459×10^{-6}	2.171×10^{-5}	0.8684
5.00×10^{-5}	2.93×10^{-6}	2.92×10^{-6}	4.345×10^{-5}	0.8690
1.25×10^{-4}	7.27×10^{-6}	7.26×10^{-6}	1.080×10^{-4}	0.8642
2.50×10^{-4}	1.448×10^{-5}	1.447×10^{-5}	2.153×10^{-4}	0.8612
5.00×10^{-4}	2.90×10^{-5}	2.90×10^{-5}	4.315×10^{-4}	0.8630
	Mean 0.869 ± 0.0096 (amp cm^{-2} $mole^{-1}$)			
	$\pm 1.1\%$			

Table 12. Current Density Dependence on Concentration, 8-21-68.

$A = 6.74 \times 10^{-2} cm^2$

Concentration [Tl(I)]	i_p (amp)	$i_{corr.}$	Current density (amp cm^{-2})	Current density / Concentration
5.00×10^{-7}	3.72×10^{-8}	2.92×10^{-8}	4.332×10^{-7}	0.8664
1.25×10^{-6}	8.21×10^{-8}	7.41×10^{-8}	1.099×10^{-6}	0.8795
2.50×10^{-6}	1.52×10^{-7}	1.44×10^{-7}	2.137×10^{-6}	0.8546
5.00×10^{-6}	3.04×10^{-7}	2.96×10^{-7}	4.392×10^{-6}	0.8784
1.25×10^{-5}	7.495×10^{-7}	7.42×10^{-7}	1.101×10^{-5}	0.8808
2.50×10^{-5}	1.507×10^{-6}	1.50×10^{-6}	2.226×10^{-5}	0.8904
5.00×10^{-5}	2.962×10^{-6}	2.954×10^{-6}	4.383×10^{-5}	0.8766
1.25×10^{-4}	7.32×10^{-6}	7.31×10^{-6}	1.085×10^{-4}	0.8680
2.50×10^{-4}	1.45×10^{-5}	1.45×10^{-5}	2.151×10^{-4}	0.8604
5.00×10^{-4}	2.906×10^{-5}	2.905×10^{-5}	4.310×10^{-4}	0.8620

Mean 0.872 ± 0.0111 (amp cm^{-2} $mole^{-1}$)

$\pm 1.3\%$

Table 13. Average Current Density Dependence on Concentration.

Concentration [Tl(I)]	8-19	8-20	8-21	Average constant
5.00×10^{-7}	0.8656	0.8778	0.8664	0.8699
1.25×10^{-6}	0.8624	0.8690	0.8795	0.8703
2.50×10^{-6}	0.8804	0.8572	0.8546	0.8641
5.00×10^{-6}	0.8892	0.8778	0.8784	0.8818
1.25×10^{-5}	0.8792	0.8797	0.8808	0.8799
2.50×10^{-5}	0.8744	0.8684	0.8904	0.8777
5.00×10^{-5}	0.8774	0.8690	0.8766	0.8734
1.25×10^{-4}	0.8664	0.8642	0.8680	0.8662
2.50×10^{-4}	0.8624	0.8612	0.8604	0.8614
5.00×10^{-4}	0.8596	0.8630	0.8620	0.8615
	Mean 0.8706 ± 0.0074 (amp cm^{-2} $mole^{-1}$)			
	$\pm 0.849\%$			

Since each day's work represents only one run of each solution, the average of the three runs is really only three determinations of the same solutions. If this is true, then the standard deviation of the average of the three days should be better than any single day's run.

These runs were made at ΔE = 10 mV, 191 Hz, 0.02V/sec, B = 0.6. A higher frequency, about 200 Hz, was chosen to reduce noise due to square wave interaction with the recorder's chopper frequency of 60 cps. In these runs, the background currents at the peak potential were determined by the two methods as

Date	Graphical	Least Squares Intercept
8-19-68	0.60×10^{-8}A	0.602×10^{-8}A
8-20-68	0.80×10^{-8}A	0.901×10^{-8}A
8-21-68	0.80×10^{-8}A	0.910×10^{-8}A

The data of 8-19-68 are unchanged on the basis of background determination. However, for 8-20-68, we obtain

Graphical background 0.80×10^{-8}A

mean = 0.869 ± 0.0096

$\pm 1.1\%$

Least squares background 0.901×10^{-8}A

mean = 0.863 ± 0.0095

$\pm 1.1\%$

Likewise, for 8-21-68, we obtain

Graphical background 0.80×10^{-8} A

mean = 0.872 ± 0.0111

$\pm$ 1.3%

Least squares background 0.910×10^{-8} A

mean = 0.866 ± 0.0148

$\pm$ 1.7%

Finally, upon comparison of the deviation of the three-day current density concentration constants for the two methods, one obtains

Graphical

0.8706 ± 0.0074 (amp cm^{-2} $mole^{-1}$)

$\pm$ 0.849%

Least squares

0.8760 ± 0.0097 (amp cm^{-2} $mole^{-1}$)

$\pm$ 1.1%

The data for the graphical extrapolation appear to give better results. This is probably caused by bias on the part of the operator. In drawing the graph, a best fit is sought and if a point lies off this line it does not influence the line drawn. The method of least squares weighs all points equally and will be affected by this errant point.

Summary of Theoretical Predictions Versus Experimental Observations

In the case of a one-electron reversible reduction, it has been shown that of the two equations which describe the current in linear sweep square wave voltammetry, equation (III) was found to be generally

applicable. The second form, equation (IV), was shown to be valid to 1% as long as $\Delta E < 0.5RT/nF$. The predicted current dependence upon and B was found accurate to about 1% until the measure instant became less than about 1 msec after the beginning of the square wave.

The current observed was a function of concentration over three orders of magnitude to an accuracy of 1%.

A plot of current versus drop size can yield the value of the electrode contact area, and therefore can be used to determine the actual electrode area from the mass area to about 1% accuracy. The voltage sweep rate dependence was seen to be predictable merely on the basis of square wave size distortion and can therefore be compensated for.

Finally, the current predicted by equations (III) and (IV) can be compared to that measured. For the conditions 1.045×10^{-3}M iron in 0.5M potassium oxalate, 25°C, B = 0.6, 10 mV square wave, 200 Hz, $A = 6.72 \times 10^{-2} cm^2$, $D = 6.31 \times 10^{-6} cm^2\ sec^{-1}$ (35), evaluation of these equations yields

(III) 3.125×10^{-5}A

(IV) 3.138×10^{-5}A

Under these conditions, the current measured when corrected for sweep rate is 3.18×10^{-5}A. Therefore, the equations predict the current measured to a 1.6% accuracy.

CHAPTER VI

DETECTION LIMITS AND MULTICOMPONENT ANALYSES

To test the utility of linear sweep square wave voltammetry for trace analysis, the detection limits for representative reversible systems, thallium(I), cadmium(II), and indium(III), for quasi-reversible titanium(IV) in 1M tartaric acid, and for irreversible chromium(III) in 1M potassium chloride were obtained. The detection limit is defined as the concentration of depolarizer for which the peak-to-peak signal plus noise level is twice the peak-to-peak noise level (S/N=2). The detection limit was determined for two cases. One was for a ΔE = 50 mV and a one-million-ohm feedback resistor on the current follower. The other was for a ΔE = 10 mV and a one-million-ohm feedback resistor multiplied times five by a resistive current divider on the current follower. The behavior of the current follower is less ideal with the one-million ohms times five network due probably to amplifier rise time limitations.

In the detection limit work, a 200 Hz square wave was used to optimize the S/N, by reducing the interactions between the recorder's chopper and the square wave. The faradaic currents were distinguished from the background current by the method previously described.

The sweep rates were reduced to 0.02V/sec to allow additional noise filtration in the form of along time constant amplifier and recorder.

The noise level was determined on the basis of the peak-to-peak variation of the background signal in the vicinity of the peak. Any sudden spikes (building voltage surges) which were nonrandom were discarded from this average. Two noise levels were observed on the background, depending on the time of the experiment. These different levels reflect the level of activity within the chemistry building. These levels were:

ΔE = 50 mV		Current Follower Feedback 1M
High Noise	1.5×10^{-8} A	
Low Noise	1.2×10^{-8} A	
ΔE = 10 mV		Current Follower Feedback 1Mx5
High Noise	7.2×10^{-9} A	
Low Noise	2.8×10^{-9} A	

All detection limits will be normalized to these noise levels. The degree of positive feedback was adjusted to optimize the background. The solutions used in the detection limit work are prepared in the same method as was done for the current versus concentration studies except in smaller volumes.

Thallium(I) Detection Limit

The detection limit for thallium was obtained in an ammonium acetate medium. Work at high current gain in potassium nitrate indicated that although the lead level in this supporting electrolyte was low, approximately 10^{-8}M, its reduction potential was sufficiently close to that of thallium as to interfere with measurement of the

thallium reduction current. Ammonium acetate was investigated as a supporting electrolyte. The background current of this medium was found to be a function of pH. At pH> 5.6 the background is flat over the region from -0.3V to -0.8V versus SCE. At lower pH, for example 5, there appeared two peaks, one at -4.5V, the other at -0.6V which could be tentatively assigned to a weak acetic acid interaction (adsorption) with the electrode. The medium selected for the thallium was unbuffered ammonium acetate 1.0M. The only difficulty with this electrolyte is a tendency to develop very fine nitrogen bubbles during deaeration, which often caused it to froth out of the cell. E_p for thallium in this medium is -0.48V (SCE). For 200 Hz, B = 0.6, A = $6.78 \times 10^{-2} cm^2$, the results obtained were:

Concentration [Tl(I)]	i_p (amp) (ΔE = 10 mV)	i_p (amp) (ΔE_p = 50 mV)
5.00×10^{-8}	3.4×10^{-9}	1.4×10^{-8}
7.50×10^{-8}	4.9×10^{-9}	2.1×10^{-8}
1.25×10^{-7}	7.2×10^{-9}	2.84×10^{-8}
2.5×10^{-7}	1.44×10^{-8}	5.69×10^{-8}
5.0×10^{-7}	2.81×10^{-8}	11.5×10^{-8}

A graph of current versus concentration was linear within the error imposed upon the measurements by the noise level. The detection limits obtained from this graph were:

Square wave		Noise	S/N=2	Detection Limit Concentration
10 mV	High	7.2×10^{-9} A	1.44×10^{-8} A	2.6×10^{-7} M
	Low	2.8×10^{-9} A	5.6×10^{-9} A	1.04×10^{-7} M
50 mV	High	2.5×10^{-8} A	5.0×10^{-8} A	2.2×10^{-7} M
	Low	1.2×10^{-8} A	2.4×10^{-8} A	1.08×10^{-7} M

The detection limits for the 50 mV and 10 mV methods are about the same. However, the instrument functions better electronically with the larger ΔE and therefore produces more favorable backgrounds.

Cadmium(II) Detection Limit

Cadmium(II) was used as an example of a reversible reduction where n = 2. Since potassium nitrate is free of cadmium and the lead peak is sufficiently resolved, it was again used as the supporting electrolyte. The results obtained for 200 Hz, B = 0.6, 0.02V/sec, 0.5M potassium nitrate, A = $6.80 \times 10^{-2} cm^2$, 25°C were:

Concentration [Cd(II)]	i_p (amp) (ΔE_p = 50 mV)	i_p (amp) (ΔE_p = 10 mV)
5.24×10^{-8}	2.8×10^{-8}	7.5×10^{-9}
1.048×10^{-7}	5.40×10^{-8}	1.45×10^{-8}
2.096×10^{-7}	1.18×10^{-7}	3.07×10^{-8}
5.24×10^{-7}	2.80×10^{-7}	7.60×10^{-8}

The currents observed are again linear with concentration with current equal to zero at zero concentration. From the plot of current versus concentration the detection limits obtained are:

Square Wave		Noise	S/N = 2	Detection Limit Concentration
50 mV	High	2.5×10^{-8}A	5×10^{-8}A	9.5×10^{-8}M
	Low	1.2×10^{-8}A	2.4×10^{-8}A	4.6×10^{-8}M
10 mV	High	7.2×10^{-8}A	1.44×10^{-8}A	1×10^{-7}M
	Low	2.8×10^{-8}A	5.6×10^{-9}A	4×10^{-8}M

Indium(III) Detection Limit

Indium(III) was selected as the electrochemical system for which n = 3. It is also illustrative of the importance of reversibility to maximize current at a given concentration. Breyer and Bauer (36) list indium(III) as reversible in chloride and acetate media. However, work in this laboratory was unable to confirm the reversibility in the chloride medium. Preliminary work was done with chloride medium, varying the chloride concentration and maintaining a constant ionic strength with potassium nitrate. Using a system of 6.68×10^{-6}M indium(III) with B = 0.6, 200 Hz, 10 mV, 0.02V/sec, pH = 3, A = 6.69×10^{-2}cm^2, the results obtained were:

$[Cl^-]$	$[NO_3^-]$	E_p (SCE)	i_p (amp)	$W_{\frac{1}{2}}$ (mV)
0.05	0.40	-0.562	2.0×10^{-7}	36.5
0.10	0.35	-0.573	4.3×10^{-7}	36.0
0.20	0.25	-0.596	7.5×10^{-7}	34.5
0.30	0.15	-0.596	1.025×10^{-6}	34.0
0.45	0	-0.606	1.16×10^{-6}	33.5

These results were not encouraging as the peak current was too dependent upon chloride concentration. Therefore, a study was made of indium(III) in acetate medium. An acetate concentration of 0.5M was found to be sufficient to insure reversibility. The pH was also found to influence the reversibility. If pH was greater than 6, hydrolysis of the indium would result and the peak current would diminish. At pH of less than 5, the reversibility again is diminished. This lower pH limit varies as the acetate concentration changes; it seemed that the

minimum value of the pH was controlled by a maximum allowable acetic acid concentration in solution. Since 0.5M ammonium acetate has a low conductivity, 0.5M ammonium nitrate was added to the supporting electrolyte to reduce the resistivity. The supporting electrolyte used was 0.5M ammonium acetate and 0.5M ammonium nitrate.

The behavior of indium(III) was studied in this medium from pH = 6 to pH = 5.6 for 6.68×10^{-5}M indium (III) in 0.5M ammonium acetate, 0.5M ammonium nitrate, with 10 mV, B = 0.6, 200 Hz, 0.02V/sec, 25°C, A = $6.71 \times 10^{-2} cm^2$. In this pH range, the results were E_p =-0.650, $i_p = 1.48 \times 10^{-6}$A, and $W_{\frac{1}{2}}$ = 32.5 mV.

Since the solution tended to froth more at low pH, the subsequent solutions were adjusted to pH = 5.8. It can be noted at this time that the acetate medium gives a smaller $W_{\frac{1}{2}}$ and a greater i_p than the chloride medium. Markovac and Lovrecek (37) have studied the kinetics of the indium-chloride system and have found it to suffer from kinetic complications at high current densities. It is therefore possible that the reduction kinetics in a chloride medium are not entirely suitable for square wave polarography.

A series of solutions of indium(III) acetate at a pH of 5.8 were analyzed, in the same method as the thallium(I) and cadmium(II). For 0.5M ammonium acetate, 0.5M ammonium nitrate, B = 0.6, 200 Hz, 0.02V/sec, A = $6.69 \times 10^{-2} cm^2$, the following results were obtained:

Concentration [In(III)]	i_p (amp) (ΔE = 10 mV)	i_p (amp) (ΔE = 50 mV)
3.34×10^{-8}	6.4×10^{-9}	2.8×10^{-8}
6.68×10^{-8}	1.35×10^{-8}	5.2×10^{-8}
1.336×10^{-7}	2.94×10^{-8}	1.03×10^{-7}
3.34×10^{-7}	7.40×10^{-8}	2.57×10^{-7}

The currents are again linear with concentration, and a graph of current versus concentration intersects the origin within experimental error. The detection limits from this graph are:

Square Wave	Noise		S/N = 2	Detection Limit Concentration
10 mV	High	7.2×10^{-9} A	1.44×10^{-8} A	6.8×10^{-8} M
	Low	2.8×10^{-9} A	5.6×10^{-9} A	2.8×10^{-8} M
50 mV	High	2.5×10^{-8} A	5×10^{-8} A	6.4×10^{-8} M
	Low	1.2×10^{-8} A	2.4×10^{-8} A	2.5×10^{-8} M

Quasi-reversible Reduction (n=1) Detection Limit

As an example of a quasi-reversible system where n = 1, titanium(IV/III) in 1M d-tartaric acid was studied. Randles and Somerton (38) have determined the equilibrium rate constant for this reduction to be 9×10^{-3} cm sec^{-1}. This can be thus compared to the result obtained for the iron oxalate couple where $k_e > 1$ cm sec^{-1}. In cyclic square wave voltammetry, two peak potentials are observed; $E_{p\ cathodic} = -0.510$ and $E_{p\ anodic} = -0.495$. The $W_{\frac{1}{2}}$ for this system increases with decreasing B, with the cathodic sweep direction peak achieving a minimum value

of 120 mV (versus 90 mV if reversible) for a 10 mV square wave at a B of 1.0.

The supporting electrolyte used, d-tartaric acid (Eastman), was found to be of higher quality than Mallinckrodt "AR" d-tartaric acid. Both electrolytes when dissolved at 4M concentrations were noticeably yellow; treatment with activated charcoal produced a colorless solution.

The Eastman d-tartaric acid after treatment with charcoal exhibited a significantly lower degree of faradaic current suppression due to adsorption of the tartaric acid or some impurity therein. Due to this adsorption the drops were collected and the solution immediately analyzed. By this method, faradaic currents obtained for successive runs were reproducible to better than 1%.

Despite the one molar concentration of the tartaric acid, this supporting electrolyte has the highest specific resistivity, 1M tartaric acid = 97 ohm-cm, of any medium used in this study for trace analysis, for example, 0.5M potassium nitrate = 22 ohm-cm. Addition of another inert supporting electrolyte to the 1M tartaric acid to reduce this resistance was not tried as it was felt that this might affect the solution ionic strength and thereby invalidate the reduction rate constant.

This high resistivity prohibited the use of the 1M x 5 feedback network on the current follower with the 10 mV square wave; however, the 50 mV square wave which required only a 1M feedback resistor remained operative. The 10 mV detection limit is therefore extrapolated

from a higher concentration than the detection limit and does not constitute an observed quantity. For 200 Hz, B = 0.6, A = $6.62 \times 10^{-2} cm^2$, 25°C, 0.02V/sec, the following results were obtained:

Concentration [Ti(IV)]	$i_{measured}$ (ΔE = 50 mV)	$i_{corrected}$ (ΔE = 50 mV)	$i_{measured}$ (ΔE = 10 mV)
3.42×10^{-6}	7.3×10^{-8}A	4.9×10^{-8}A	not measured
6.83×10^{-6}	1.27×10^{-7}A	1.03×10^{-7}A	1.85×10^{-8}A
1.37×10^{-5}	2.13×10^{-7}A	1.89×10^{-7}A	3.84×10^{-8}A
3.42×10^{-5}	5.01×10^{-7}A	4.77×10^{-7}A	8.98×10^{-8}A

The plot of i versus concentration for the 50 mV date did not have a zero intercept and was therefore corrected for this error, while the 10 mV data did intercept zero.

Both plots were linear with concentration within experimental error. From the corrected plots of current versus concentration, the following detection limits were obtained for 200 Hz, B = 0.6, 25°C, 0.02V/sec, A = $6.62 \times 10^{-2} cm^2$:

Square Wave		Noise	S/N = 2	Detection Limit Concentration
50 mV	High	2.5×10^{-8}A	5×10^{-8}A	3.4×10^{-6}M
	Low	1.2×10^{-8}A	2.4×10^{-8}A	1.8×10^{-6}M
10 mV	High	7.2×10^{-9}A	1.44×10^{-8}A	3.8×10^{-6}M
	Low	2.8×10^{-9}A	5.6×10^{-9}	1.48×10^{-6}M

Irreversible Reduction (n=1) Detection Limit

As an example of an irreversible electrochemical couple, chromium(III) in 1M potassium chloride at pH less than 3.0 was chosen.

The equilibrium rate constant (38) for this reduction is k_e = $1x10^{-5}$cm sec^{-1}. The cyclic square wave voltammetry of the system exhibited two peaks (Figure 15a); for B = 0.6, 200 Hz, 10 mV square wave, 0.04V/sec, $E_{p\ cathodic}$ =-1.05V (SCE), $W_{\frac{1}{2}}$ is 210 mV, and $E_{p\ anodic}$ = -0.51V (SCE), $W_{\frac{1}{2}}$ is 140 mV. Since the two peaks are completely resolved, an attempt was made to calculate the transfer coefficients for the two electrode processes which constitute this couple. Barker et al. (26) have derived equations for a completely irreversible reduction in square wave polarography which yield the result that

$$W_{\frac{1}{2}\ red} = k/\alpha_r\ n$$

where

α_r = transfer coefficient for the reduction

k = constant dependent upon measurement parametersΔE, B, etc.

Since

β_{ox} = transfer coefficient for the oxidation and

$\alpha_r + \beta_{ox} = 1$

$W_{\frac{1}{2}ox} = k/(1 - \alpha)\ n$

The transfer coefficients should in principle be calculable from the two half peak widths. Combining the equations yields:

$$\alpha_r = \frac{W_{\frac{1}{2}\ ox}}{W_{\frac{1}{2}\ red} + W_{\frac{1}{2}\ ox}}$$

and therefore

$\alpha_r = 0.40$ and $\beta_{ox} = 0.60$

Figure 15. Chromium(III) voltammogram.

200 Hz, ΔE = 20 mV, B = 0.6, 0.04V/sec, A = $6.65 \times 10^{-2} cm^2$, 1.0M potassium chloride,

pH = 2.7, Cr(III) = $9.66 \times 10^{-5} M$

a is the deaerated voltammogram

b is the air-saturated voltammogram

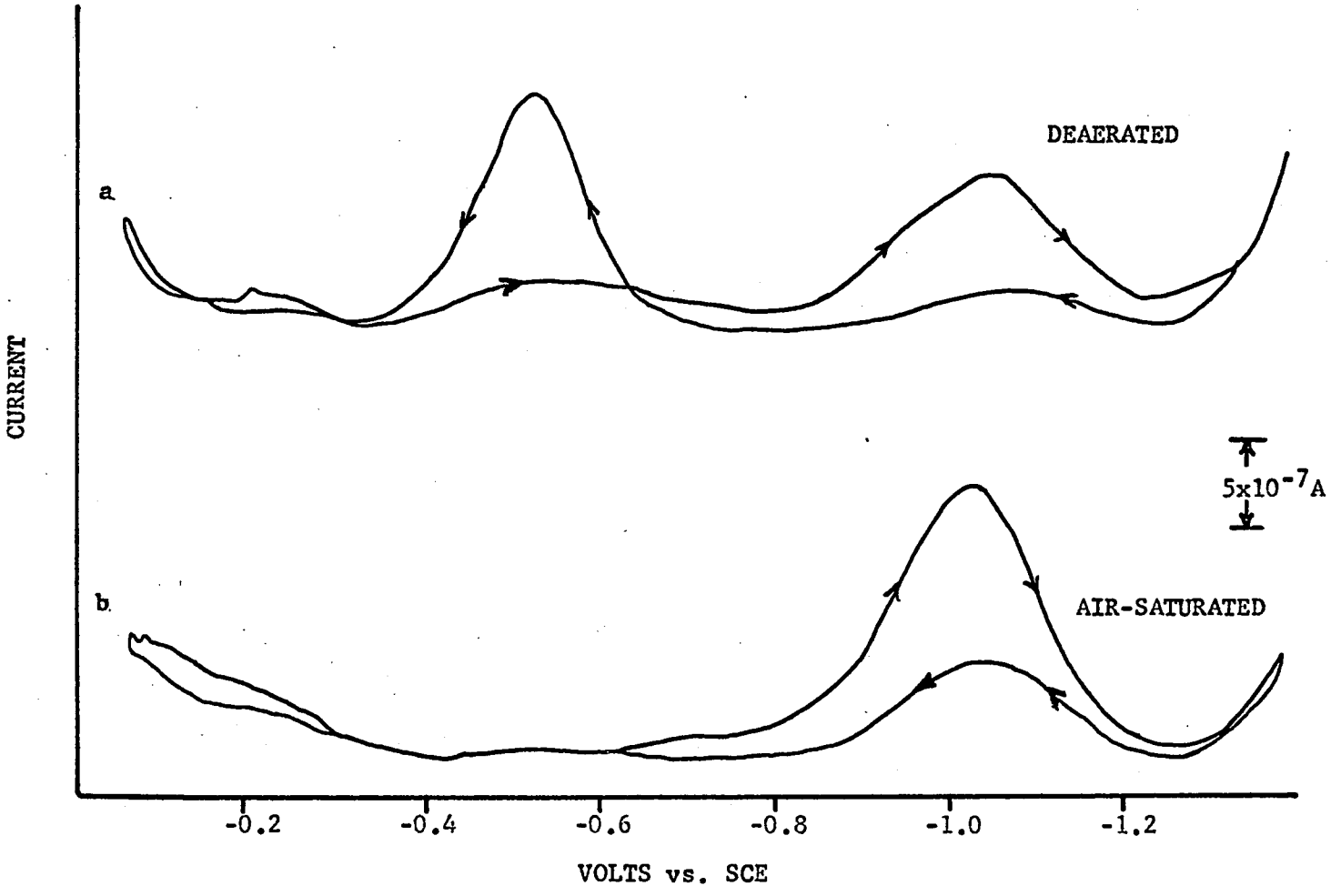

Figure 15. Chromium(III) voltammogram.

A value of α can also be obtained from a plot of E versus log i/i_d-i. The slope of this plot (1, p. 240) $\frac{\Delta E}{\Delta \log i/i_d-i}$ is 0.0542/n and for this chromium solution this plot yielded a slope of 0.125 and therefore an α of 0.44.

The two α obtained are in reasonable agreement and therefore show that an estimate of α can be obtained from the $W_{\frac{1}{2}}$ in square wave voltammetry.

Due to the reasonably low pH necessary to control the hydrolysis of the chromium(III) in solution, depolarization of the electrode by hydrogen ion started at potential -1.1V (SCE) near the chromium peak. This interfered with an accurate measurement of the chromium current near the limit of detection. The results obtained are therefore an extrapolation of the data on a plot of current versus concentration and are intended only as a guideline for this type of reduction. For 10 mV, 200 Hz, B = 0.6, 0.04V/sec, A = $6.65\times10^{-2}cm^2$, 1M potassium chloride, pH = 2.8, the results are as follows:

Concentration [Cr(III)]	i_p (amp)	i_{corr} (amp)
2.4×10^{-5}	4×10^{-8}	2.5×10^{-8}
4.8×10^{-5}	6.7×10^{-8}	5.2×10^{-8}
9.7×10^{-5}	1.2×10^{-7}	1.05×10^{-7}
2.4×10^{-4}	2.75×10^{-7}	2.50×10^{-7}
4.8×10^{-4}	5.02×10^{-7}	4.87×10^{-7}

A plot of current versus concentration is linear in this range. It exhibits a nonzero intercept and the currents are corrected for this.

The detection limits obtained were:

	Noise	S/N = 2	Detection Limit Concentration
High	7.2×10^{-9}A	1.44×10^{-8}A	1.4×10^{-5}M
Low	2.8×10^{-9}A	5.6×10^{-9}A	5.4×10^{-6}M

During the work with chromium(III) a lack of reproducibility of this reduction peak was observed. Cyclic voltammetry indicated a relationship between the reproducibility of this peak and the current measured for the chromium(II) oxidation. Careful control of the amount of deaeration indicated that any residual oxygen in solution would suppress the chromium(II) oxidation currents and enhance the chromium(III) reduction currents. Therefore, for reproducible work involving this couple, extensive deaeration is necessary.

Figure 15 represents the currents observed in an air-saturated and extensively deaerated solution after a large number of voltage cycles.

Attempts were made to utilize this enhancement of the chromium-(III) reduction by oxygen or hydrogen peroxide to extend the chromium-(III) detection limits. However, the currents observed for the hydrogen peroxide reduction overlap those for the chromium(III) reduction and therefore this enhancement is of little analytical use.

An anomalous behavior was observed for this enhancement by oxygen versus hydrogen peroxide when this solution was unbuffered. The oxygen catalysis currents were greater than those of hydrogen peroxide for equal concentration of oxidant. However, when the solution was

buffered at 2.8 by 0.01M formate buffer, an approximately equal two-fold enhancement was observed for the chromium(III) reduction either by oxygen or hydrogen peroxide. The anomalous behavior in the unbuffered air-saturated solution was therefore attributed to a hydrogen ion depletion of the diffusion layer caused by the reduction of oxygen in solution (about 2.1×10^{-4}M) which produced a 4×10^{-4}M concentration of hydroxide ion. The exact nature of this behavior in an unbuffered solution was not established, but it may be caused by either the adsorption of a neutral chromium(III) hydroxide species on the electrode or a more rapid electron exchange between a chromium(II) hydroxide species and the hydrogen peroxide in the diffusion layer.

Iron(III) Oxalate Detection Limit

In order to obtain a complete comparison of the currents obtained for a one-electron reduction, the results previously obtained for iron oxalate must be considered.

Before this couple was abandoned for linearity studies because of a bad background current, data were obtained which yielded a current divided by concentration constant having 4% deviation in the concentration range 10^{-3} to 10^{-6}M iron. This constant can be used to obtain an estimate of the detection limit for this couple. The actual current measured for this couple deviated by only 20% from the calculated value at a concentration of 5×10^{-7}M despite the poor background.

The constant obtained was 2.86×10^{-2} amp mole^{-1} for a 200 Hz, B = 0.6, 0.02V/sec, 10 mV square wave, and A = 6.06×10^{-2}cm^2. From this constant, the calculated detection limits are:

	Noise	S/N = 2	Detection Limit Concentration
High	7.2×10^{-9}A	1.44×10^{-8}A	5.0×10^{-7}M
Low	2.8×10^{-9}A	5.6×10^{-9}A	1.96×10^{-7}M

Detection Limit Summary

It is now possible to compare the detection limits obtained for the various electrochemical systems studied and thereby obtain an indication of how reversibility and n affect these limits.

Since only the results for a 10 mV square wave are complete, it alone shall be considered. All of the limits are normalized to the same electrode area, that is, $6.70\times10^{-2}cm^2$, and the following parameters: 200 Hz, 10 mV, B = 0.6, and 0.02V/sec (except chromium where v = 0.04V/sec). Only the low noise level detection limits are considered.

In example 1, both reduced and oxidized forms are soluble in solution.

	Fe(III)	Ti(IV)	Cr(III)
Supporting electrolyte	0.5M potassium oxalate	1M tartaric acid	1M potassium chloride
Rate constant	K = 1	$K = 9\times10^{-3}$	$K = 1\times10^{-5}$
Peak potentials	$E_{pc} = E_{pa} = -0.244$	$E_{pc} = -0.510$ $E_{pa} = -0.495$	$E_{pc} = -1.05$ $E_{pa} = -0.51$
Detection limit concentration	1.77×10^{-7}M	1.46×10^{-6}M	5.4×10^{-6}M

The detection limit for a reduction where n = 1 is seen to be ten times higher in a case where a slight degree of irreversibility exists. In

the case of total irreversibility, the detection limit is further raised and is about 25 times higher than for the reversible case.

The peak current for a totally irreversible reduction has been shown by Barker et al. (26) to be proportional to the transfer coefficient. In the example used, α was 0.4; if it had been higher or if the oxidation peak had been used, the detection limit would have been lower. However, despite the relatively poor detection limit for chromium, this limit is still competitive with dc polarography. The results in example 2 are for the cases where reduction is followed by solution of the reduced form into the electrode.

	Tl(I)	Cd(II)	In(III)
Supporting electrolyte	1M ammonium acetate	0.5M potassium nitrate	0.5M ammonium acetate 0.5M ammonium nitrate
Detection limit concentration	1.1×10^{-7}M	4.1×10^{-8}M	2.8×10^{-8}M

The detection limits in the case of amalgam formation are comparable to those stated for square wave polarography. These limits could be improved by using the oxidation peak, and thereby take advantage of a slight amount of anodic stripping. The results thus obtained would be affected by both the cathodic sweep direction switching potential and the sweep rate and would complicate the required number of parameters which must be stated to determine the detection limits.

Figure 16 represents a typical analytical signal near the detection limit of lead and cadmium. The lead peak is higher than the

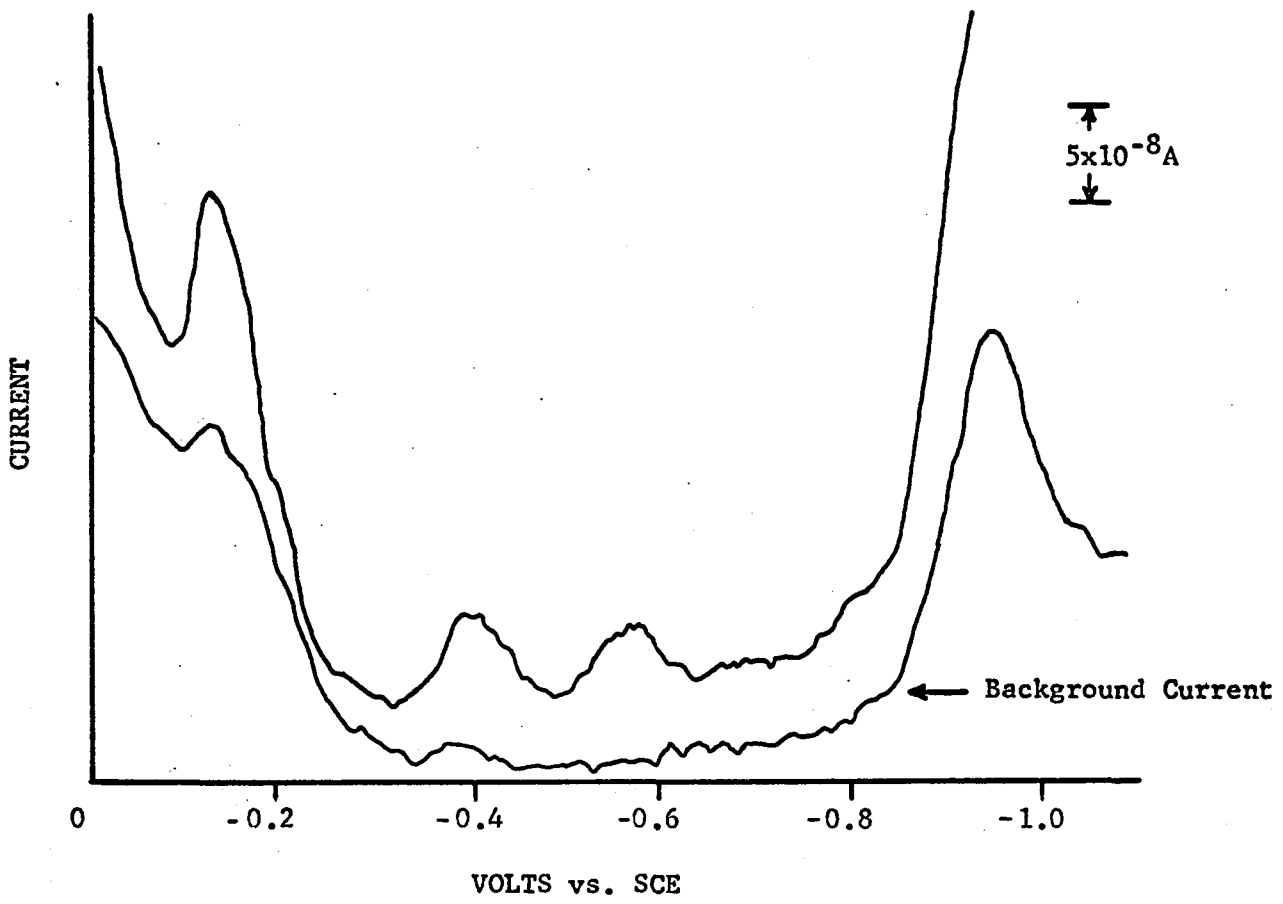

Figure 16. Detection limit voltammogram of lead(II) and cadmium(II).

cadmium due to a lead impurity in the 0.5M potassium nitrate. Data for Figure 16 are for a 200 Hz, B = 0.6, 0.02V/sec, 50 mV, A = $6.43 \times 10^{-2} cm^2$ and

$$[Cd(II)] = 5.24 \times 10^{-8} M$$

$$[Pb(II)] = 5.03 \times 10^{-8} M$$

While these signals are almost at the limits of detection, the reduction peaks are clearly observed above the background current.

Tensammetry

It has long been known that the adsorption of a nonelectroactive species (surface active) on an electrode alters the electrocapillary curves and also the differential capacity of an electrode. Some of these surface active species undergo desorption at potentials on either side of the potential of the electrocapillary maximum (ecm). The measurement of adsorption phenomena by ac methods is called tensammetry. In the case when a sine or square wave voltage is applied to the electrode and the average potential is swept as a function of time, two peaks will be observed on either side of the ecm corresponding to the current required by the adsorption and desorption phenomenon (Figure 17). An investigation was made in an attempt to determine the utility of square wave voltammetry to the analysis of trace quantities of surface active agents.

N-heptyl alcohol was chosen as a representative surface active agent. The deaeration of the solution was held to a minimum to avoid alteration of surfactant concentration. The electrode drops were collected, hung, and immediately used. The rate of attainment of surface

Figure 17. Surfactant voltammogram.

n-heptanol, 3.44×10^{-4}M, 0.5M potassium nitrate, ΔE = 20 mV, 200 Hz, B = 0.6, 0.02V/sec, A = $6.72 \times 10^{-2} cm^2$

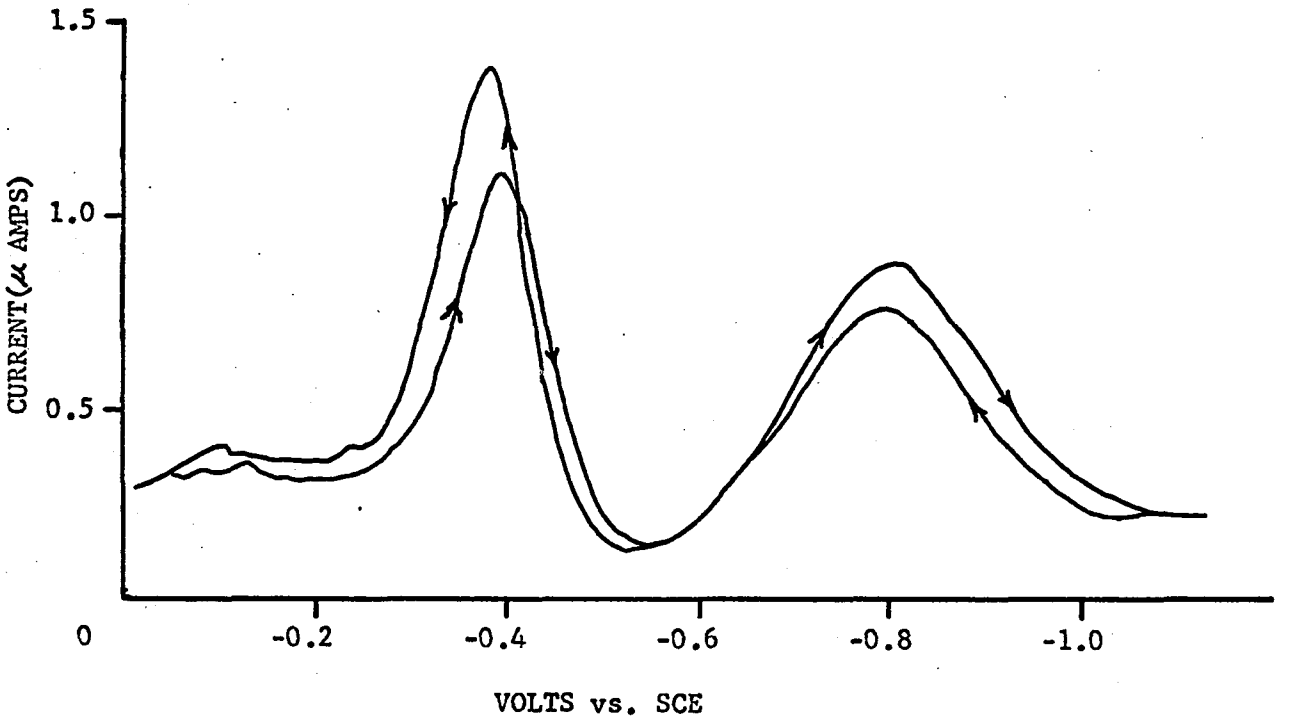

Figure 17. Surfactant voltammogram.

coverage equilibrium appeared very rapid for this surfactant and the signal for the adsorption did not depend upon age of the mercury drop used. The results obtained for B = 0.6, ΔE = 50 mV, 200 Hz, 0.02V/sec, A = $6.72 \times 10^{-2} cm^2$, 0.5M potassium nitrate were:

Concentration, M	E_p (SCE)	i_p (amp)	i_p/concentration
8.61×10^{-4}	-0.282	2.3×10^{-5}	2.7×10^{-2}
3.44×10^{-4}	-0.38	2.3×10^{-6}	6.7×10^{-3}
6.88×10^{-5}	-0.43	3.8×10^{-7}	5.5×10^{-3}
3.44×10^{-5}	-0.44	1.7×10^{-7}	4.9×10^{-3}
1.72×10^{-5}	-0.43	7.3×10^{-8}	4.3×10^{-3}
3.44×10^{-6}	-0.40	1.7×10^{-8}	4.9×10^{-3}

The results were very disappointing; only at low surfactant coverage did there appear any linearity between concentration and peak current. As the concentration increased, the current constant (amp $mole^{-1}$) did also. This is consistent with the work of Delahay and Trachtenberg (39) who showed that the adsorption equilibria are more rapid at higher surfactant concentration, and therefore the ac current should also rise in response to this more rapidly achieved surface coverage.

In the region of a reasonably linear current constant, E_p maintains a value of about -0.43V (SCE). However, with increasing concentration, the adsorption peak moved to more positive potentials as it could now better compete with the nitrate ions for the electrode surface.

From a plot of concentration versus current, a detection limit for n-heptanol in 0.5M potassium nitrate can be obtained:

		Noise	S/N = 2	Detection Limit Concentration
50 mV	High	2.5×10^{-8}A	5×10^{-8}A	1×10^{-5}M
	Low	1.2×10^{-8}A	2.4×10^{-8}A	5×10^{-6}M

Although the detection limit obtained is respectable, the non-linearity of the current over a reasonable range and the dependency of peak potential upon both concentration and type of surfactant will strongly diminish the utility of square wave tensammetry as a method of analysis.

Peak Resolution

Figure 18 represents the results of the analysis of a multi-component system observed under the conditions: 10 mV, 200 Hz square wave, with B = 0.6, 0.02V/sec, A = 6.30×10^{-2}cm^2, 1.0M potassium chloride, pH = 2, DME biased to 0.0V (SCE). The results are:

Ion	Concentration, M	$E_{p\ obs}$ (SCE)	$E_{\frac{1}{2}}$ (1, p. 629)
Bi(III)	1.00×10^{-5}	-0.085	-0.09
Cu(II)	2.11×10^{-5}	-0.225	-0.22
Pb(II)	2.01×10^{-5}	-0.435	-0.44
Tl(I)	5.00×10^{-5}	unresolved	-0.48
In(III)	1.57×10^{-5}	-0.595	-0.60
Cd(II)	2.09×10^{-5}	-0.637	-0.64
Zn(II)	2.02×10^{-4}	-1.000	-1.00

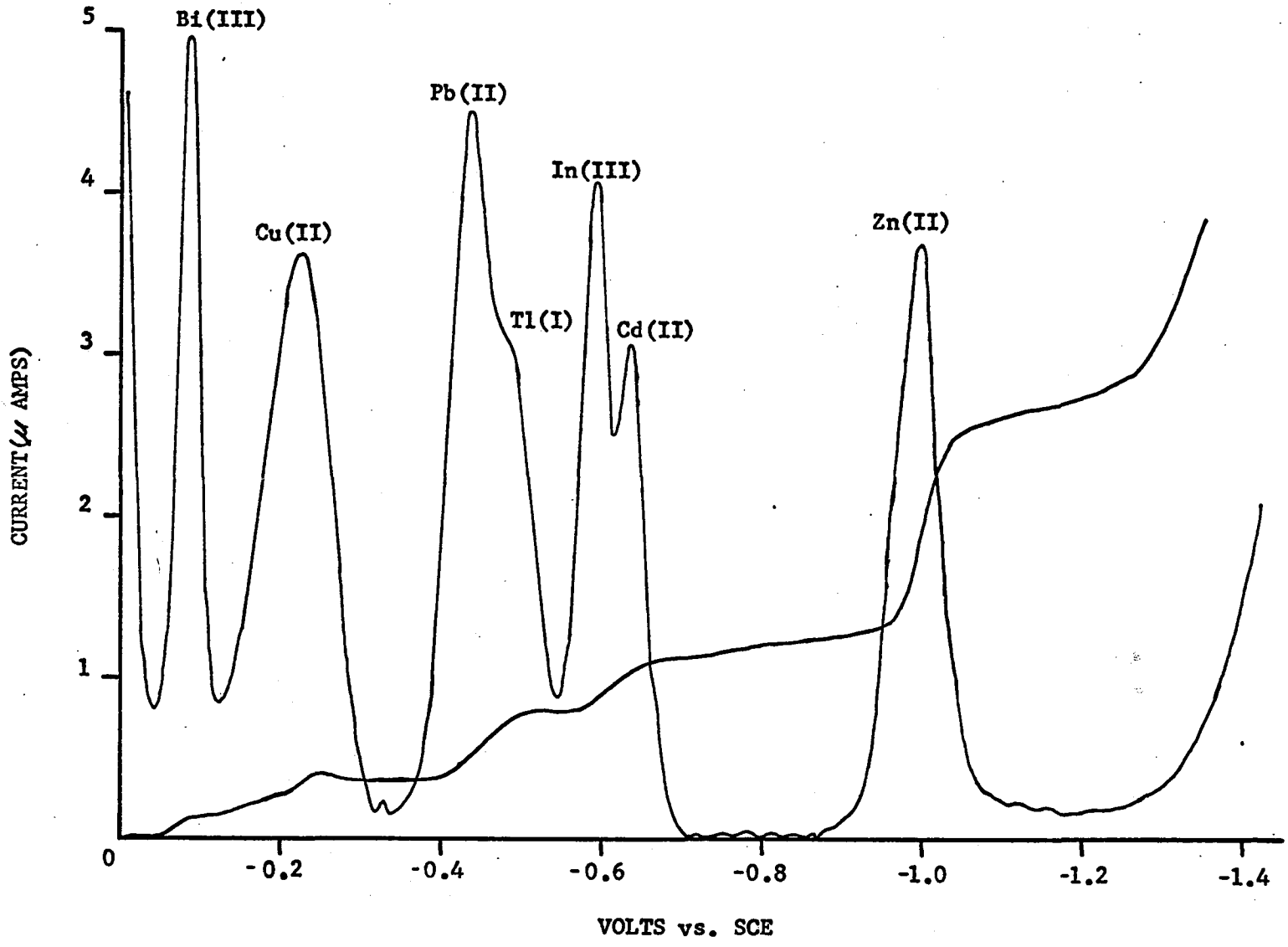

Figure 18. Multicomponent analysis voltammogram.

Superimposed across the square wave result is a normal dc polarogram.

A number of interesting facts may be observed from this analysis. Although the indium(III) concentration is greater than that of bismuth(III), more current is observed for the bismuth reduction, probably due to a more reversible reduction for the bismuth. The current observed for the zinc(II) is nowhere near the current expected when compared to that of cadmium(II). The $W_{\frac{1}{2}}$ for the zinc peak (62 mV) confirms that the low current is due to irreversibility.

These results indicate that square wave voltammetry offers resolution of successive reduction peaks equal to or better than any other electrochemical technique.

Another form of peak resolution that is important concerns the analysis of a trace component in the presence of a large excess of another reducible species. In the case where the trace component is the more easily reduced, almost any electrochemical method is excellent. However, in the case where the more easily reduced component is the one in excess, then difficulty exists in the accurate determination of the trace component. For example, dc polarography becomes of little use if the first reducible substance is 100 times the concentration of the second. A pre-electrolysis may often be performed to remove the more easily reduced species; however, this is both time consuming and only effective if the two reduction potentials are sufficiently separated.

In order to test the concentration resolution of square wave voltammetry, a series of cadmium(II), E_p =-0.568, concentrations were

run in the presence of a high background of lead(II), E_p =-0.380, concentrations under the following conditions: ΔE = 20 mV, 200 Hz, B = 0.6, 0.04V/sec, A = $6.43 \times 10^{-2} cm^2$, pH = 3, 0.5M potassium nitrate. The results were:

[Pb(II)]	[Cd(II)]	i_p Cd(II) (amp)
5×10^{-4}	5.2×10^{-5}	1.35×10^{-5}
5×10^{-4}	1.0×10^{-5}	2.75×10^{-6}
5×10^{-4}	4.2×10^{-6}	1.10×10^{-6}
5×10^{-4}	2.1×10^{-6}	5.57×10^{-7}
5×10^{-4}	1.0×10^{-6}	2.90×10^{-7}
5×10^{-4}	4.2×10^{-7}	1.15×10^{-7}
5×10^{-4}	2.1×10^{-7}	5.98×10^{-8}
0	2.1×10^{-7}	5.76×10^{-8}

Figure 19 is the current observed for the 5×10^{-4}M lead(II) and 2×10^{-7}M Cd(II) solution. The currents as tabulated above are linear with concentration. The current measured at 2.1×10^{-7}M cadmium with the lead background is within 4% of the value obtained in a solution containing no lead. This represents an accurate measurement of cadmium in the presence of a 2500-fold excess of lead.

Resolution of Overlapping Peaks

An attempt has been made to resolve two overlapping peaks in order to determine accurately the concentrations of the two depolarizers.

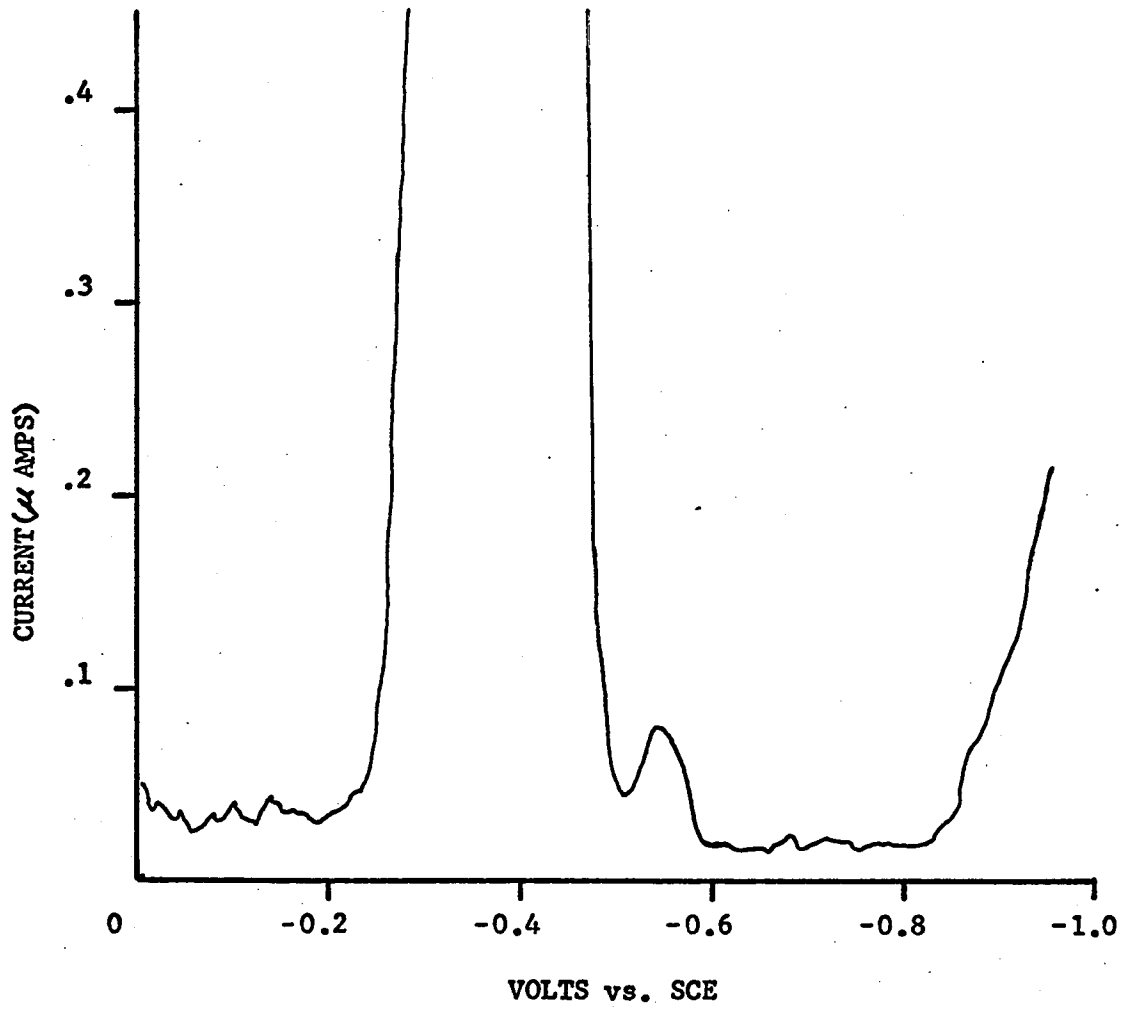

Figure 19. Concentration resolution voltammogram.

Figure 20 represents the currents measured for 1.05×10^{-4}M cadmium(II) and 7.86×10^{-5}M indium(III) in 1.0M potassium chloride, pH = 2, at 10 mV, 200 Hz square wave, with B = 0.6, 0.02V/sec, and A = $6.14 \times 10^{-2} cm^2$. The currents are shown both individually and as the composite wave. Breyer et al. (40) applied a method using the ratio of peak heights to resolve overlapping peaks in ac polarography with reasonable success. More recently, Israel (41) has applied matrix algebra to the resolution of overlapping peaks in first derivative dc polarography. In the case of a two component system, his results are basically the same as those below.

If the current i_1^* measured at a given E_1 is sufficiently below the region of IR drop problems, it may be considered to be composed of two linearly added components of current, i_1 and i_1'. Each of these currents is proportional to a concentration of depolarizer, that is, $i_1 = k_1(C)$ and $i_1' = k_1'(C')$. By measuring the current at the two peak reduction potentials for both of the systems in question when totally resolved, it is possible to obtain values for the four current constants (amp $mole^{-1}$), that is,

At E_{p1} (E_p for C)	and at E_{p2} (E_p for C')
k_1 for C	k_2 for C
k_1' for C'	k_2' for C'

Since

$$i_1^* = i_1 + i_1'$$

then

$$i_1^* = k_1C + k_1'C'$$

$$i_2^* = k_2C + k_2'C'$$

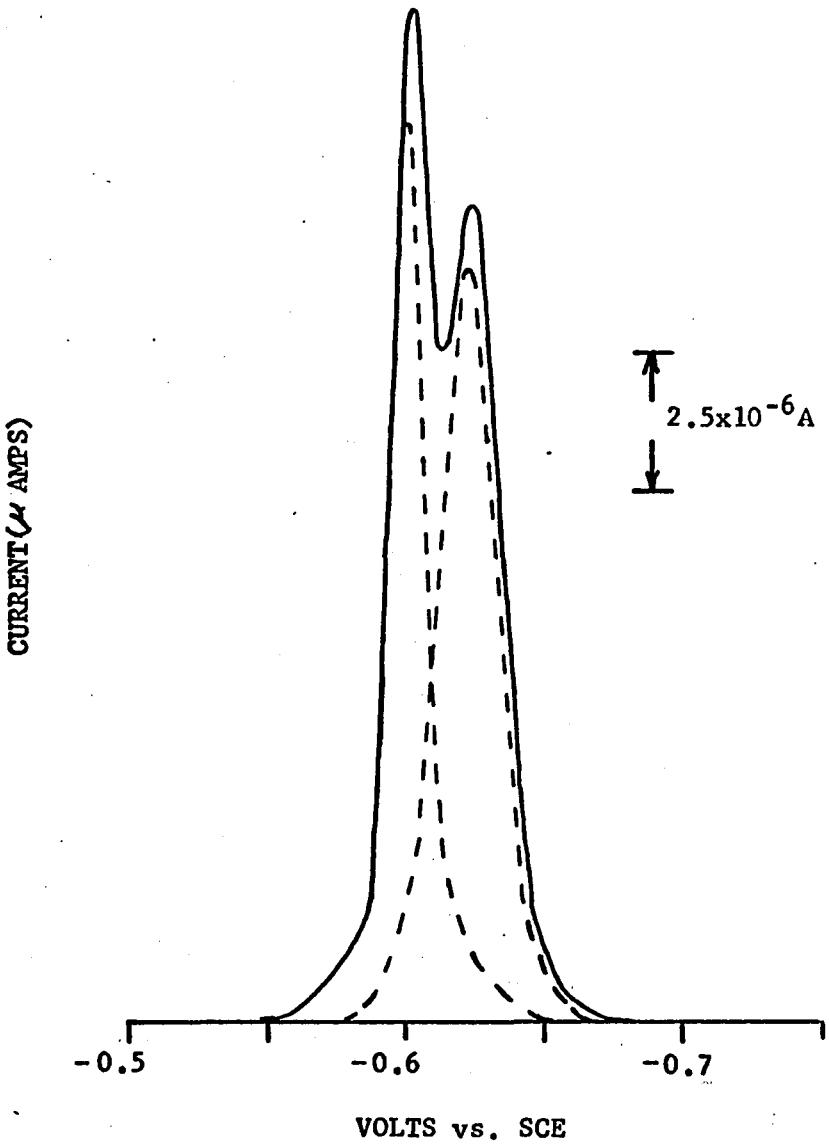

Figure 20. Resolution of overlapping voltammetric peaks.

These may be combined and solved for one concentration

$$C' = \frac{i_2^* k_1 - i_1^* k_2}{k_1 k_2' - k_1' k_2}$$

This result may then be applied to the data.

First, it must be noted that when the two peaks are close together, the resultant signal will exhibit its E_p's at different potentials from the resolved peaks; for example,

Ion		$E_{p\ resolved}$ (SCE)	$E_{p\ mixed}$
In(III)	7.86×10^{-5} M	-0.606	-0.602
Cd(II)	1.05×10^{-4} M	-0.646	-0.647

Thus, care must then be taken to measure the currents for the mixture at the values of $E_{p\ resolved}$.

For the system in question, the currents are:

In(III) 7.86×10^{-5} M E = -0.606 i = 1.64×10^{-5} A E = -0.646 i = 0.13×10^{-5} A

Cd(II) 1.05×10^{-4} M E = -0.606 i = 0.27×10^{-5} A E = -0.646 i = 1.37×10^{-5} A

The currents measured for the mixture are:

E = -0.606 (SCE) i = 1.83×10^{-5} A

E = -0.646 (SCE) i = 1.49×10^{-5} A

From these data we may calculate the concentrations of depolarizers and compare the results to the actual values. The concentrations thus calculated are:

In(III)	= 7.48×10^{-5}M	within 5% of actual value
Cd(II)	= 1.047×10^{-4}M	within 1% of actual value.

The inaccuracy in the calculated indium concentration is merely a result of an error in the cadmium background at this point. There is no doubt that the method is valid and only that the contributions of the non-major current element must be determined to a higher degree of accuracy than has been done.

CHAPTER VII

SQUARE WAVE ANODIC STRIPPING ANALYSIS

In the case where reduction of a depolarizer was accompanied by amalgam formation, an enhancement of the current in the anodic sweep direction versus the first cathodic sweep current was noticed. This enhancement of current suggested the possibility of applying square wave voltammetry to anodic stripping analysis.

Anodic stripping analysis at an HMDE was first performed by DeMars and Shain (42). In this method of analysis the depolarizer is concentrated in the mercury electrode by reduction at a potential of at least 0.4V cathodic to $E_{\frac{1}{2}}$. This preconcentration is performed in a stirred solution for a fixed amount of time. The stirring is discontinued and the solution is allowed to quiet. The potential is then swept anodically and the current due to the oxidation of the depolarizer which had been deposited in the electrode is measured. By this method of preconcentration the detection limit is enhanced by two orders of magnitude for most electroanalytical methods.

Kemula and Kublik (23) extended the method by coupling it with oscilloscopic voltammetry and gave consideration to the formation of intermetallic compounds in the mercury. Von Sturm and Ressel (43) applied the technique of square wave polarography to the anodic stripping in order to take advantage of the improved sensitivity and resolution

of peak currents afforded by this technique. However, the sweep rates used were still those of polarography (v = 0.1V/min) and no attempts were made at analyses below 10^{-8}M. A comprehensive review of the method is presented by Barendrecht (44).

The anodic stripping analysis was performed in a 150-ml Nalgene polyethylene weighing bottle. This vessel was washed with alcoholic potassium hydroxide to remove residual surface-active organics. Use of polyethylene was dictated by a tendency of trace metals to ion exchange into glass. A magnetic stirrer was used for solution stirring, and an on-off switch was used on the stirrer so that the motor speed control could remain unchanged. The cell top was made of Teflon with holes bored to admit the various electrodes. The reference electrode used was a Beckman fiber junction calomel electrode. It was isolated from the main cell compartment by an ultra-fine frit. Identical supporting electrolyte was placed in the cell and isolation compartment. Attempts to use the reference electrode directly in the cell failed due to potassium chloride from the reference electrode leaking into the cell. The "AR" potassium chloride used in this reference electrode contained so much lead and zinc that despite the low leak rate of the fiber junction the lead background continually rose. The same HMDE, spoon, and bias arrangement previously described were used. The counter electrode was a thick platinum coil remotely located in the cell. Deaeration was performed through the use of a small glass frit sealed onto 4-mm o.d. pyrex tubing. Nitrogen continually flowed through this frit so that solution contact with the frit was minimized. The problem resulting

from the previously mentioned ion exchange into the glass of the frit was probably minimal as this frit was only in the solution during the short (five minutes) deaeration time. After deaeration, the frit was arranged so that it could be raised out of solution while continuing to pass nitrogen over the solution during the cathodic plating and the subsequent stripping analysis.

The supporting electrolyte, 0.5M potassium nitrate, adjusted to a pH of 2, was pre-electrolyzed with vigorous stirring at a mercury cathode with its potential controlled at -1.2V (SCE) for several hours to remove trace metals which might undergo stripping analysis.

The cell and reference electrode compartments were filled with supporting electrolyte several times allowing 15 minutes equilibrium time with stirring for each filling. The cell was then filled with 100.0 ml of supporting electrolyte. The solution was extensively deaerated, then the frit was removed from solution, and the nitrogen was allowed to flow over the top of the solution. Three drops were collected, and the solution was stirred, plated, and analyzed. This run was discarded. A second set of three drops was collected and hung, and the stirring commenced. When the solution had achieved a steady stirring velocity, 30 sec, the test electrode was connected and the plating continued for five minutes. At the end of this accurately timed electrolysis period, the stirring was stopped. The solution was allowed to stand for 30 seconds both to allow the solution motion to stop and to permit the amalgam drop to achieve uniform concentration. The potential was then swept anodically at 0.02V/sec to strip the drop.

To obtain the data presented in Table 14, known volumes of a $5x10^{-7}$M lead and cadmium solution were added to the cell containing 100.0 ml of supporting electrolyte. The concentration of the solution after each analysis was then calculated. The solution was deaerated after each addition. Figure 21 presents a plot of these data for both the lead and cadmium currents. The results obtained are reasonably linear with concentration, with deviation toward lower currents at higher concentrations. This deviation in the measured currents has also been observed by Von Sturm and Ressel (43) but is not observed in the work of Underkofler and Shain (45) who achieved linearity over four orders of magnitude in concentration using ac polarography for the stripping voltage.

An observation of i_p/Ct where t is stripping time reveals that lead was reasonably constant over the interval studied (20 minutes). However, the signal for the cadmium deviated badly to lower values in the interval between eight and twenty minutes. This deviation is tentatively assigned to either intermetallic complex formation of the part of cadmium while in the electrode or the adherence of some surfactant to the drop surface, an effect which is known to influence cadmium more than lead (44). While due caution was observed in avoiding solution contamination by surfactant in this work, Kaplan and Sorokovskaya (46) have pointed out that square wave stripping is more hindered by surfactants than normal linear sweep stripping. They observed that while the value of i_p/Ct showed pronounced deviation at times greater than twenty minutes the comparable constant for linear sweep stripping was

Table 14. Peak Currents in Square Wave Stripping Voltammetry.

200 Hz B = 0.6 ΔE = 50 mV .02V/sec Strip 5 min at -1.00V (SCE) A = $6.31 \times 10^{-2} cm^2$

Standard addition of 5×10^{-7}M cadmium and lead to 100 ml cell volume

Total volume added (λ)	Concentration, M	i_p Lead (amp)	i_p Cadmium (amp)
0	0	2.8×10^{-8}	9.4×10^{-8}
100	5.0×10^{-10}	35.1×10^{-8}	19.4×10^{-8}
200	1.0×10^{-9}	38.9×10^{-8}	25.0×10^{-8}
500	2.5×10^{-9}	55.3×10^{-8}	38.0×10^{-8}
1000	5.0×10^{-9}	77.2×10^{-8}	61.0×10^{-8}
5000	2.4×10^{-8}	21.3×10^{-7}	20.0×10^{-7}
10000	4.6×10^{-8}	35.8×10^{-7}	34.0×10^{-7}

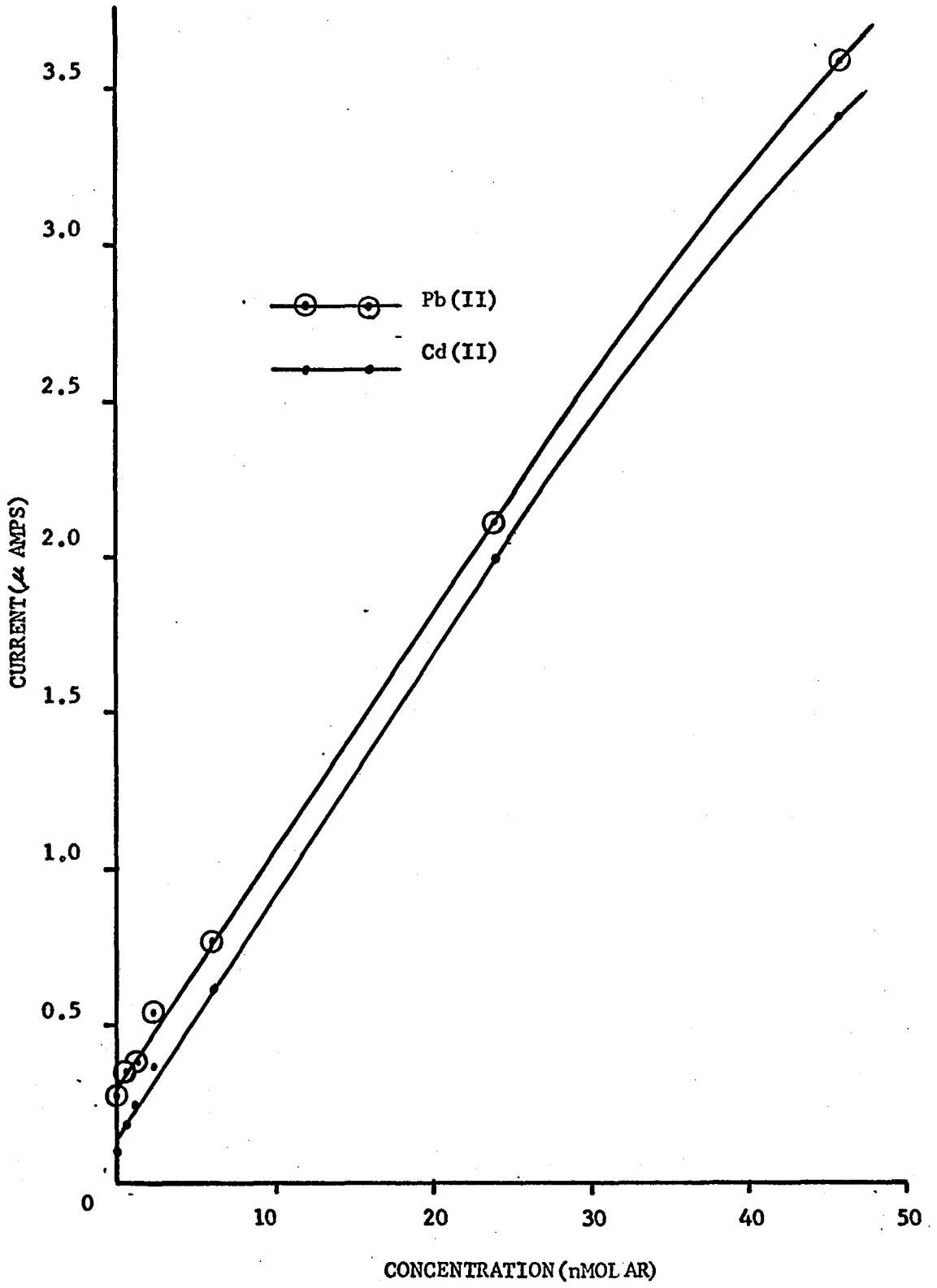

Figure 21. Current dependence on concentration in square wave anodic stripping voltammetry.

still unaffected at times of one hour and more. They also observed that the first analysis upon a given solution differs from those obtained in subsequent runs with new drops. This behavior was also noted in this laboratory for all work involving the HMDE when analyzing a new solution and is tentatively assigned to an oxygen related phenomenon.

The results presented here are far from the best attainable. Von Sturm recommends an accurately controlled stirring speed of between 800 and 1000 rpm, placement of the electrode 8 mm above the stirrer, temperature control of $\pm$ 0.1°C, and extensive deaeration. Due to available equipment many of these conditions were not attainable. However, despite these inadequacies, the current measured at 5×10^{-10} M was obtained in half the time as that of Underkofler and Shain (45). Utilization of better conditions as suggested would probably improve precision and reduce the required plating time for the same value of i_p/Ct.

While square wave voltammetry may not be able to extend significantly the detection limits obtainable by conventional linear anodic stripping voltammetry due to previously mentioned difficulties, it will be able to complete the analysis more rapidly and better resolve the resultant signal peaks.

CHAPTER VIII

TRACE FLUORIDE ANALYSIS

Trace fluoride analysis has for many years been a subject of much experimental work. Attempts have been made to apply the fluoride specific electrode to the direct determination of fluoride at trace levels. Durst (47) has recently applied the technique of null point potentiometry to this problem and achieved successful results in the range of 10^{-3} to 2×10^{-6}M. However, at this lower level, problems concerning the natural solubility of the electrode's lanthanum fluoride crystal are encountered (48) and therefore precision must suffer. Bond and O'Donnell (49) have reported a method for fluoride analysis based upon the shift in $E_{\frac{1}{2}}$ for the uranium(V) / uranium(III) reduction. Reasonable results were claimed in the range of 10^{-6} to 10^{-4}M; however, the method is dependent upon accurate measurement of the $E_{\frac{1}{2}}$, and the resultant calibration curve is not very linear for high fluoride concentrations.

Spectrophotometric methods have long been used. These methods, including the so-called bleaching methods, depend upon the displacement of a coordinated metal from a chelate by fluoride ion and the measurement of the color subsequently produced or the reduction in the color from the metal chelate. Of these methods, the most common is the zirconium with alizarin red-S (ARS), zirconium with Eriocyanine-R (50), lanthanum with alizarin complexone (51), and thorium with chloranilic

acid (52). All of these methods suffer from about the same interferences, for example, aluminum, chloride, and phosphate, and being spectrophotometric methods, the useful concentration range for high accuracy is limited. Since electrochemical methods are frequently accurately usable over several orders of magnitude of concentration change, attempts were made to detect fluoride by an electrochemical method.

Since fluoride ion is non-electroactive, it is necessary that the fluoride present in some way change the equilibrium of an electroactive species in solution. Among the spectrophotometric (equilibrium) methods stated, the chelate ARS was known to be reversibly reduced, the ZrARS complex is reduced cathodically to the free ligand, and the zirconium(IV) is not reduced in the potential range of interest. Since fluoride is quite effective in displacing the zirconium from the ARS complex, and in view of the well established electrochemistry of this system (53), it was the one chosen for this study.

The preliminary work performed upon this system confirmed the findings of Zittel and Florence (53); at a pH of 1.5 the ARS produces a sharp reduction peak at -0.20V (SCE), $W_{\frac{1}{2}}$ is about 50 mV, while the complex appears as a broad irreversible peak having a summit potential at about -0.26V (SCE). However, the resolution of peaks afforded by square wave voltammetry allows an accurate measurement of the current due to the ARS reduction.

The ARS used was recrystallized essentially as suggested by Zittel and Florence, with the only modification being the addition of some concentrated perchloric acid (1 ml/400 ml) to the mother liquor

before crystallization commenced. This modification yielded crystals of a uniform orange color. The molecular weight of this product after washing with anhydrous ethyl ether and drying at 100°C, as determined by potentiometric titration with sodium hydroxide, was 347.8g, a value intermediate between the anhydrous and monohydrated salt (sodium alizarin 3-sulfonate). This is comparable to the results of Zittel and Florence. The zirconium was obtained by fuming zirconyl nitrate in 5M perchloric acid. The zirconium(IV) nitrate was combined with a known quantity of ARS to produce a stoichiometric solution of complex, heeding the recommendation of Zittel whereby the zirconium(IV) is never added to a more acidic solution. When properly prepared, the solution achieved its equilibrium color in a few hours. It was then allowed to stand overnight and was found to be stable in the laboratory for days. The fluoride solutions were prepared from dried "AR" sodium fluoride, made slightly basic, and stored in polyethylene bottles.

The solution of the complex prepared was $4x10^{-5}$M in complex and about 0.1M in perchloric acid. It was then diluted to $4x10^{-6}$M with 0.5M sodium perchlorate. Preliminary runs upon this solution lacked precision in the peak currents measured. This problem was attributed to the slow adsorption equilibrium kinetics for the ARS adsorption (54).

Attempts were made to vary the potential at which the drops were collected and also to vary the aging of the electrode before analysis. These efforts proved ineffective in reducing this problem. In all previous work the currents measured were for the first cathodic sweep. A study was made of the currents observed for other than the

first cathodic sweep, hoping to improve reproducibility. This study was not successful because the complex appears to dissociate upon reduction of the ARS, and since the kinetics of formation of the complex are slow, the currents measured after the first cathodic sweep do not represent an equilibrium condition and are of no value.

In the previous electrochemical work on the zirconium-ARS complex (53), the pyrolytic graphite electrodes used did not appear as sensitive to adsorption as the HMDE used here. Therefore, attempts were made to use solid electrodes in square wave voltammetry.

The first solid electrode used was a platinum ball (radius about 0.5 mm). After cleaning in hot hydrochloric acid, it was used to observe the oxidation of the ARS. However, the only currents observed were attributable to the formation and dissolution of platinum oxides on this electrode in the potential range covered. The results obtained on a glassy carbon electrode (GC-30S, Tokai Electrode Mfg. Co., Tokyo, Japan) were reasonable; however, the background currents were too great for trace analysis.

Two types of pyrolytic graphite electrodes were tried. One consisted of a cylinder of polished pyrolytic graphite. This rod was then sealed in an appropriate diameter glass tube with Shell Epon 828 cement so that only the polished end was exposed to solution. This electrode exhibited a high background current greater than that of the glassy carbon electrode even after adjustment for electrode area. A second pyrolytic graphite electrode was tried. This was a rod of graphite upon which a thin coating of high-density pyrolytic graphite is deposited.

One end of the rod was sealed in a glass tube of appropriate diameter. The resultant cylindrical electrode offered currents for both the oxidation and background similar to that of the glassy carbon electrode. Since these electrodes were on loan from Dr. George Wilson, extreme care had to be exercised in their handling and use. A thorough study of the currents observed after various pretreatments of the electrode to reduce the background currents could not be pursued for fear of damaging the electrodes. The extremely high background for the polished pyrolytic graphite electrode could have resulted from a poor seal. The generally high background encountered with the carbon electrode may be the result of numerous microscopic pores on the electrode surface. Each pore will be of different size and have a different resistive component to the tip of the reference electrode. The sum of these effects will be an electrode consisting of many RC time constants yielding an electrode with a high frequency dispersion (55), and therefore a slow double layer charging rate and a high background current.

Due to the limited success with solid electrodes, it was decided to return to the HMDE and attempt to control as well as possible the collection and aging of the mercury drops prior to solution analysis. By biasing the electrode to -0.1V (SCE) and immediately analyzing the solution upon attaching the electrode, a reasonable degree of precision is attainable. The currents measured for five successive runs had deviations varying from $\pm$ 10% to $\pm$ 2% and the results tabulated are for the average current read.

In order to test this electrochemical method of fluoride analysis, a series of solutions were prepared, each 4.03×10^{-6}M in zirconium-ARS, 0.5M in sodium perchlorate, at a pH of 1.50, containing fluoride varying in concentration from 1×10^{-6} to 6×10^{-5}M. The solutions were prepared, agitated, and allowed to equilibrate overnight (eight hours). They were then deaerated, and the current due to the reduction of free ARS at -0.20V (SCE) was measured as a function of concentration. The results are presented in Table 15.

The resultant currents were reasonably linear with concentration. As is to be expected, the color of the solution went from red to yellow as the concentration of fluoride ion increased. The nonzero current intercept was probably due to dissociation of the zirconium-ARS complex at this concentration and pH. Attempts at analysis of fluoride at lower concentrations (10^{-7}M) by further diluting the zirconium-ARS complex to 4.03×10^{-7}M produced a much higher (relative to concentration) zero fluoride current and a smaller variation in current as a function of fluoride ion concentration.

Another analysis of fluoride performed at a different pH provided essentially the same result; however, the value of current as a function of fluoride concentration was different. This is not too surprising as both the stability of the zirconium-ARS complex and that of the zirconium fluoride complex are functions of pH.

It is therefore possible to analyze for fluoride by measuring the current for the reduction of the liberated ARS and to determine its concentration to about a 10% accuracy; however, careful pH control is

Table 15. Current Dependence on Fluoride Concentration.

200 Hz 10 mV 0.04V/sec B = 0.6 4.03×10^{-6} zirconium ARS pH = 1.5 A = $5.92 \times 10^{-2} cm^2$

$[F^-] \times 10^{-6}$	i (μA)	$i - i_o$ (μA)	$\frac{i - i_o}{[F^-]}$
0	1.32	0	-
1	1.68	.36	.36
3	1.98	.66	.22
5	2.58	1.26	.25
7	3.27	1.95	.28
10	3.80	2.48	.25
20	8.36	7.04	.35
30	12.3	11.0	.37
40	15.0	13.7	.34
60	20.2	18.9	.31

necessary and the problem of adsorption of ARS tends to seriously reduce the accuracy of this determination when compared to a spectrophotometric method.

CHAPTER IX

OXYGEN-RELATED ADSORPTION AT THE HMDE

All previously discussed electrochemistry involving redox couples had one common interference. This interference was manifest in that the first analysis performed after deaeration of a new solution differed in the faradaic current measured by about 2% from subsequent analyses with new electrodes. In the case of such depolarizers as lead(II), this effect might have been a suppression of current due to the formation of lead(II) hydroxide species at the electrode, whose reduction was not as reversible as the lead-aquo species. For the chromium(III) reduction, a slight enhancement of the current for the first analysis is observed, possibly due to hydrogen peroxide or some other oxidant still on the electrode surface.

Observations were made upon a single electrode, collected and hung in an air-saturated solution. Cyclic voltammetry between zero and -1.4V (SCE) produced the expected oxygen related peaks. If the solution was then purged with nitrogen for five minutes while the electrode remained at about -0.7V, the cyclic voltammetry then produced the same oxygen peaks at a diminished level. A fresh electrode, however, hung in this same solution produced an oxygen-free background current.

These observations tended to imply the possibility of the adsorption on the mercury electrode of some reduction product of oxygen. Since square wave voltammetry has been shown to be useful in analysis

of trace surfactant species, an attempt was made to obtain data to verify this possible adsorption phenomenon.

In 1936, Ilkovic (56) postulated that some polarographic maxima may be attributed to the adsorption of a reactant or product upon the electrode surface. This postulate remained reasonably ignored in favor of hydrodynamic theories which later flourished. In 1962, Smith and Stark (57), in their measurement of the surface tension of pendant mercury drops, noticed that in air-free solutions their results agreed with the parabolic curves for surface tension as a function of potential obtained by other methods. However, in air-saturated solutions a flattening of the parabola occurred, beginning at the potential where oxygen is reduced and extending to the potential for the reduction of hydrogen peroxide where the two curves again coincided. Furthermore, they observed that this flattening was more pronounced in the case where the electrode drop was allowed a long equilibrium time along this plateau. This distortion of the surface tension curve of mercury in water is characteristic of the adsorption of a surfactant upon this surface, and the authors (57) concluded that it may have been caused by the adsorption of hydrogen peroxide or some product from the reduction of oxygen. In 1965, DeLevie (58) again considered the possibility of adsorption as a cause of maxima and developed an approach whereby this adsorption affects the surface tension of the drop in a non-uniform manner. This produces the solution streaming at the drop and therefore the maxima. Under this approach the adsorption and hydrodynamic maxima

of the "first" kind are now reconciled. DeLevie further contends that this adsorption effect is what produces the oxygen maxima.

Barker and Bolzan (59) also advanced an adsorption-hydrodynamic mechanism for maxima and demonstrated the appearance of a maxima for 10^{-4}M lead(II) in 1.5M perchloric acid upon the addition of small amounts of bromide ion which produced an adsorbable lead(II) bromide complex. Barker also stated that the oxygen maxima are a result of adsorption, but the details of this work remain unpublished.

A series of air-saturated solutions at various pH's were run to determine if any observable behavior could be attributed to an adsorption phenomenon. The only interesting pattern noticed occurred on the second oxygen wave, $H_2O_2 + 2e^- \longrightarrow 2OH^-$. Upon increasing the pH, the summit potential of this wave moves to more cathodic potentials as is expected. There also appears, however, a small "prepeak" upon this broad irreversible peak. This peak is observed on both the anodic and cathodic sweep direction currents, and it maintains a reasonably constant peak potential varying slightly around -0.97V (SCE) in 0.5M potassium nitrate. Figure 22 exhibits the equilibrium currents observed for air-saturated solutions at a pH of 10.9 and 12.5. Similar prepeaks are also observed in fresh deaerated alkaline hydrogen peroxide solutions of 10^{-3}M and less, but they seem to diminish with solution aging probably due to decomposition of the peroxide.

Studies of this prepeak with respect to B, v, ΔE, etc., proved inconclusive. The peak did not shift its peak potential noticeably with concentration as would have been expected for adsorption; however,

Figure 22. Voltammograms of air-saturated buffered solutions.

200 Hz ΔE = 10 mV B = 0.8 0.04V/sec A = $6.73 \times 10^{-2} cm^2$

0.5M potassium nitrate A = pH of 12.5 B = pH of 10.9

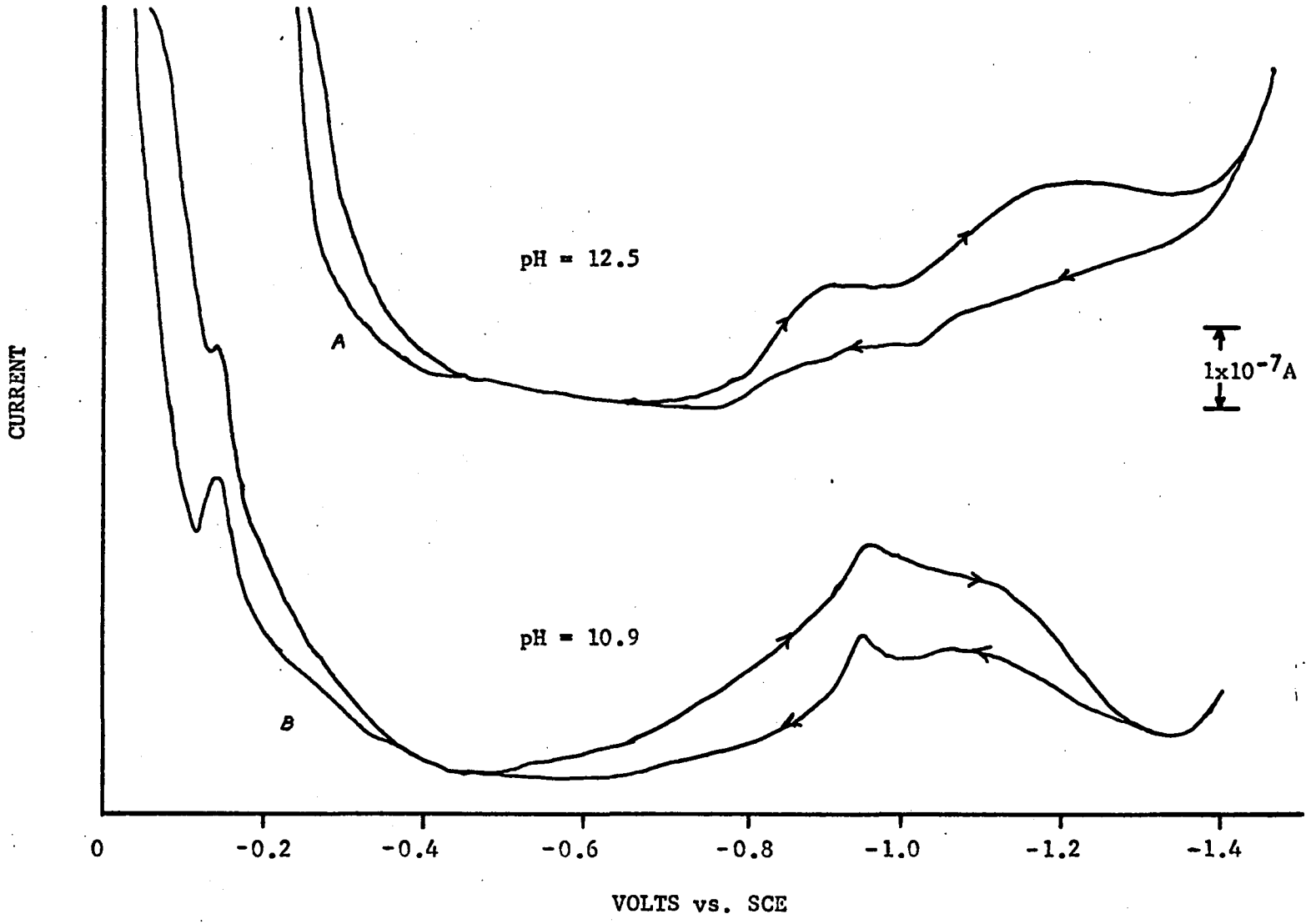

Figure 22. Voltammograms of air-saturated buffered solutions.

its shape appeared to be influenced by the age of the electrode. If the electrodes were hung and biased to a potential near the potential of zero charge (-0.6V for 0.5M potassium nitrate), the prepeak and the major peak appear to perfect their shapes and thereby become better resolved. The same result is obtained in deaerated hydrogen peroxide solutions and air-saturated solutions; thus it cannot be merely attributed to an increase in solution hydrogen peroxide concentration as a result of oxygen reduction. The only peak which may be attributed to adsorption or electrode surface reaction is this prepeak; however, there is a possibility that this peak may also be due to either a two step hydrogen peroxide reduction mechanism or another electroactive species in solution. Although the electrolytes used were electrolyzed at -1.4V (SCE) over a mercury cathode, the possibility does exist that a non-amalgam forming metal capable of oxygen catalysis, for example, chromium(III), may have remained in solution and therefore have produced this prepeak behavior.

CHAPTER X

INVESTIGATION OF N,N,N-TRIMETHYLETHYLENEDIAMMONIUM NITRATE

Good et al. (60) have suggested the use of N,N,N-trimethylethylenediammonium chloride, $(CH_3)_3\overset{+}{N}CH_2CH_2\overset{+}{N}H_3(Cl^-)_2$, as a buffer with a pK of 7.1, having a generally weak interaction with metals. An attempt was made to observe the utility of this buffer as a noninteracting supporting electrolyte. The synthesis was essentially that recommended by the authors. One mole of anhydrous trimethylamine was combined with four moles of 1,2-dibromoethane, in a two-neck round-bottomed flask fitted with a dropping funnel and a Dry Ice condenser. Stirring was accomplished by a magnetic stirring bar. The product, (2-bromoethyl)trimethylammonium bromide, was collected and recrystallized from 95% ethanol. One equivalent of this product was combined with ten equivalents of aqueous concentrated ammonium hydroxide. After standing for a week, the solvent was removed by vacuum at room temperature and the product was recrystallized from ethanol. The resultant N,N,N-trimethylethylenediammonium·bromide was dissolved in water and combined with a stoichiometric quantity of either silver nitrate or silver perchlorate for conversion to the appropriate salts. The silver bromide was filtered off, the water removed at reduced pressure, and the product recrystallized in ethanol. The equivalent weight of the products was determined by potentiometric titration with sodium hydroxide. The results were:

N,N,N-trimethylethylenediammonium nitrate

Calculated 228 Observed 229

N,N,N-trimethylethylenediammonium perchlorate

Calculated 303 Observed 302

The dc polarographic decomposition potential observed for a half-neutralized 0.1M solution of this salt, pH = 7, was -1.25V (SCE).

To test the utility of this salt as a supporting electrolyte, a solution of 0.1M of the N,N,N-trimethylethylenediammonium nitrate adjusted to a pH of 7.0 containing $1x10^{-5}$M lead(II) and cadmium(II) nitrate was analyzed with the square wave polarograph. Since in polarography half wave potentials may be used to obtain information about the coordination sphere of an ion, the measure of $E_{\frac{1}{2}}$ or E_p will demonstrate if this is indeed a noninteracting medium. The lead(II) reduction results failed, probably due to a formation of lead hydroxide species in solution whose reduction is not reversible. The results obtained for the cadmium(II) ion are:

Supporting Electrolyte	E_pV (SCE)
0.1M buffer	-0.584
0.5M KNO_3	-0.583
0.5M NH_4OH, NH_4NO_3 pH= 9.2	-0.764
0.5M NH_4NO_3 pH = 6	-0.584
0.5M KCl	-0.636

The results obtained indicate that for the cadmium(II) reduction the buffer yields results comparable to those obtained in the presence of nitrate alone and may therefore be considered a reasonably

noninteracting supporting electrolyte. Not enough of the perchlorate was available to complete a study with this salt.

APPENDIX A

SOLUTIONS AND REAGENTS

All solutions used in this work were prepared in redistilled water. This water was obtained by equilibrating the distilled water obtained from the building taps with activated charcoal. The charcoal was filtered off and the resultant water distilled at a basic pH in an all-borosilicate glass still.

The supporting electrolyte salts were all "AR" grade and used without further purification unless otherwise stated. The potassium oxalate used in this work was obtained from the crystals collected from cooling a saturated solution of recrystallized oxalic acid neutralized with "AR" potassium hydroxide. The stock iron(III) nitrate solutions were "fumed" with hydrochloric acid to destroy the nitrate, reduced with stannous chloride in the usual fashion, and titrated with dichromate. The other metal ion solutions of indium(III), chromium(III), copper(II), zinc(II), and bismuth(III) were prepared by acid dissolution of the appropriate pure metals and were used without further standardization as only 1% accuracy was desired. The solutions of thallium(I), zirconium(IV), cadmium(II), and lead(II) were standardized by EDTA titration using appropriate conditions (61). The hydrogen peroxide used was standardized by potentiometric titration in sulfuric acid with ceric sulfate as recommended by Furman and Wallace (62).

The mercury used was Bethlehem Instrument triple vacuum distilled. The nitrogen for deaeration was usually used without treatment other than presaturation with supporting electrolyte of interest (usually water). In the cases where higher purity nitrogen was desired, the tank nitrogen was passed over copper wire in a vicor tube (Sargent #S-36518) heated to 400°C in an appropriate Sargent #S-36517 heater. This reductor was regenerated with hydrogen in the usual manner. The salt bridge used in the reference electrode contained a polyacrylamide gel.

APPENDIX B

SCHEMATIC WIRING DIAGRAMS AND LIST OF PARTS

All resistors 1%

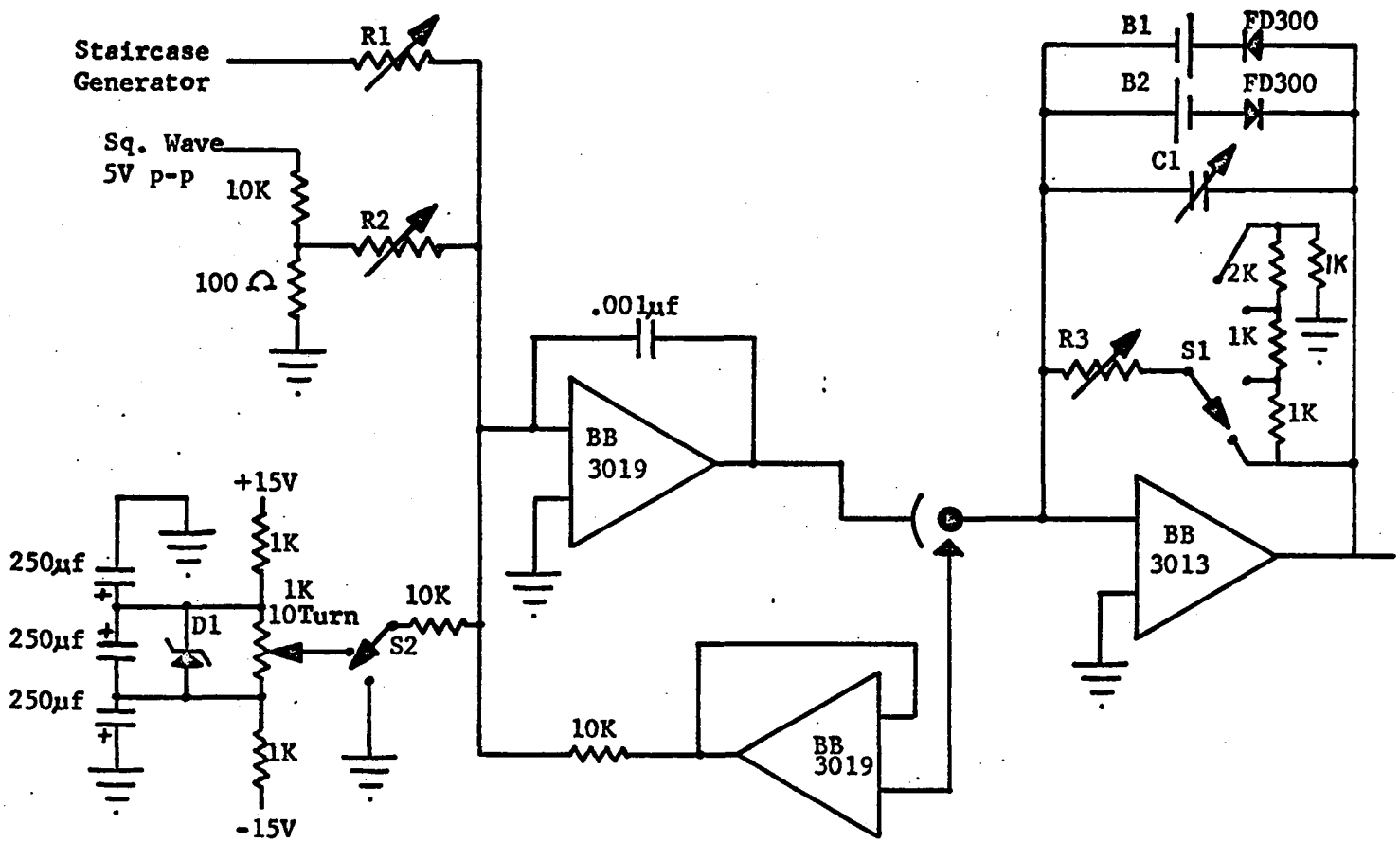

Figure B-1. Three-electrode potentiostat.

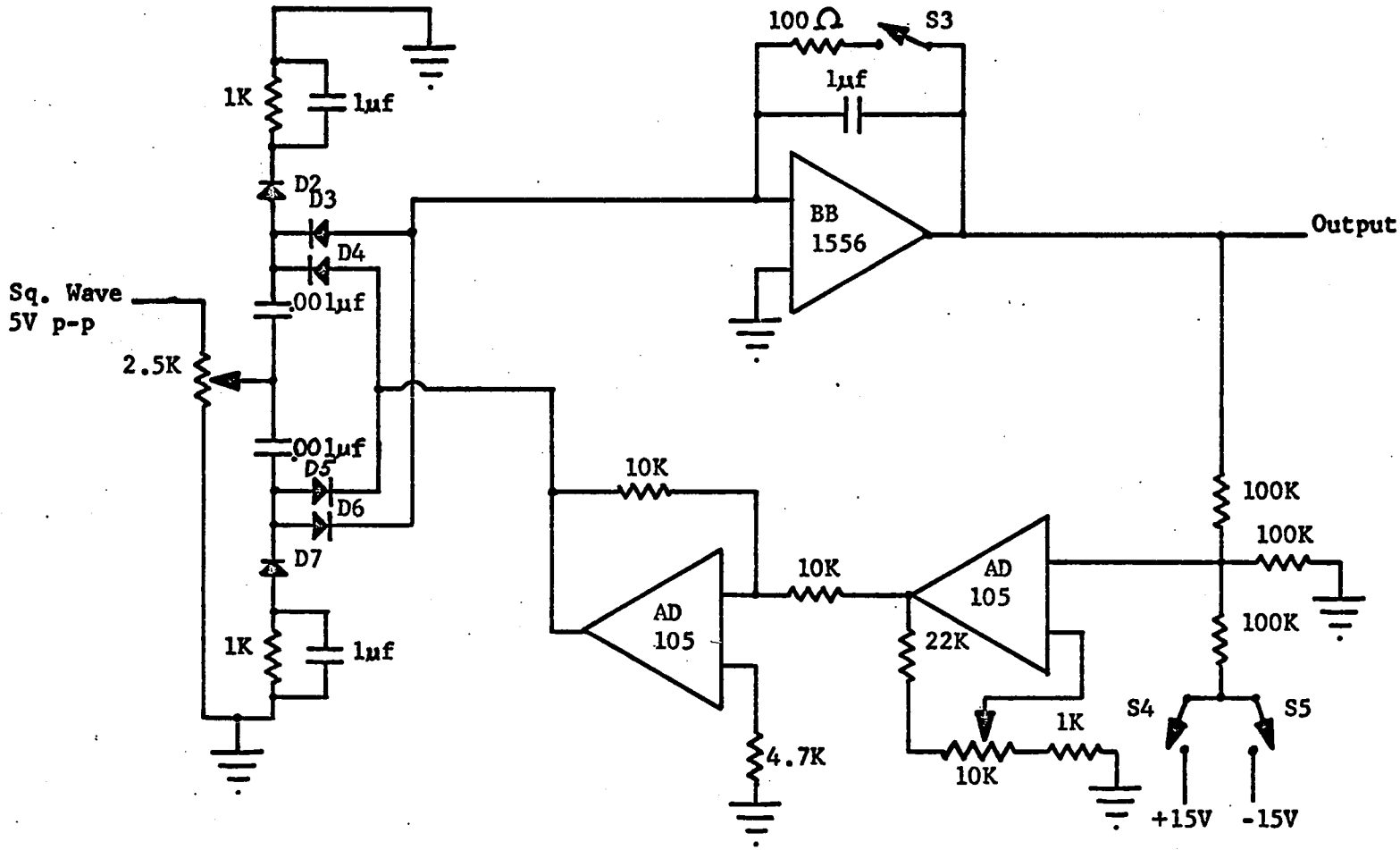

Figure B-2. Staircase sweep generator.

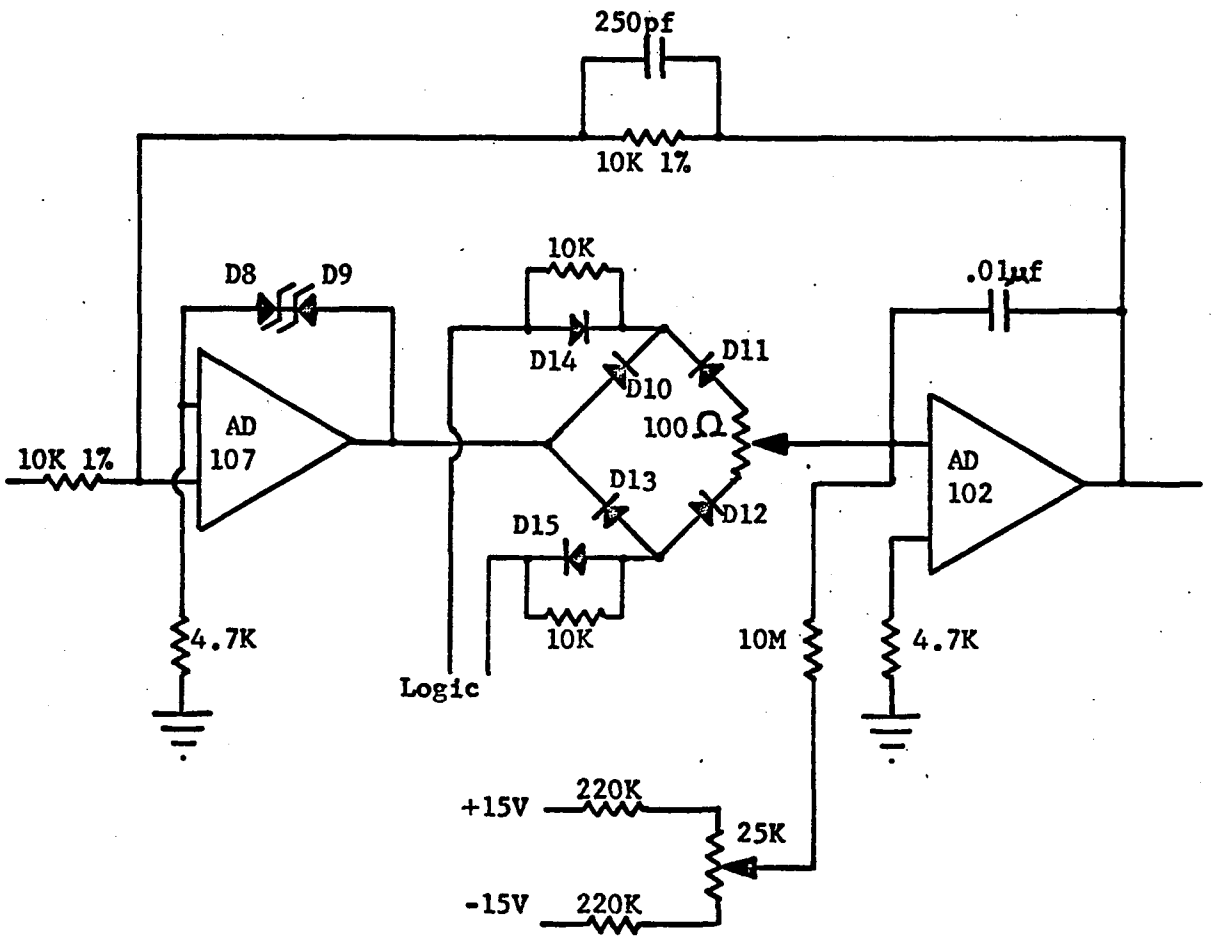

Figure B-3. Sample and hold circuit.

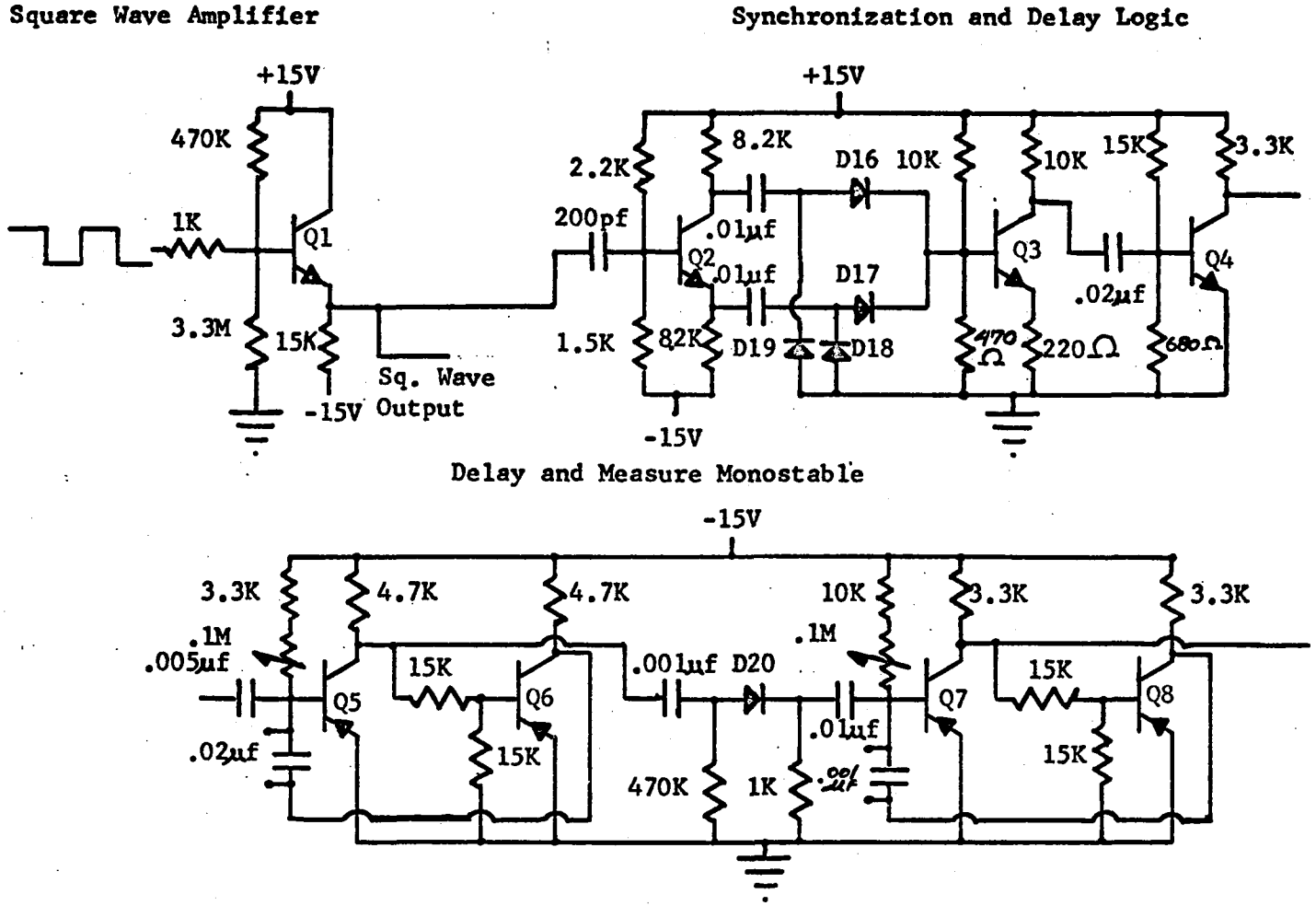

Figure B-4. Synchronization and timing circuits.

Track and Hold Logic

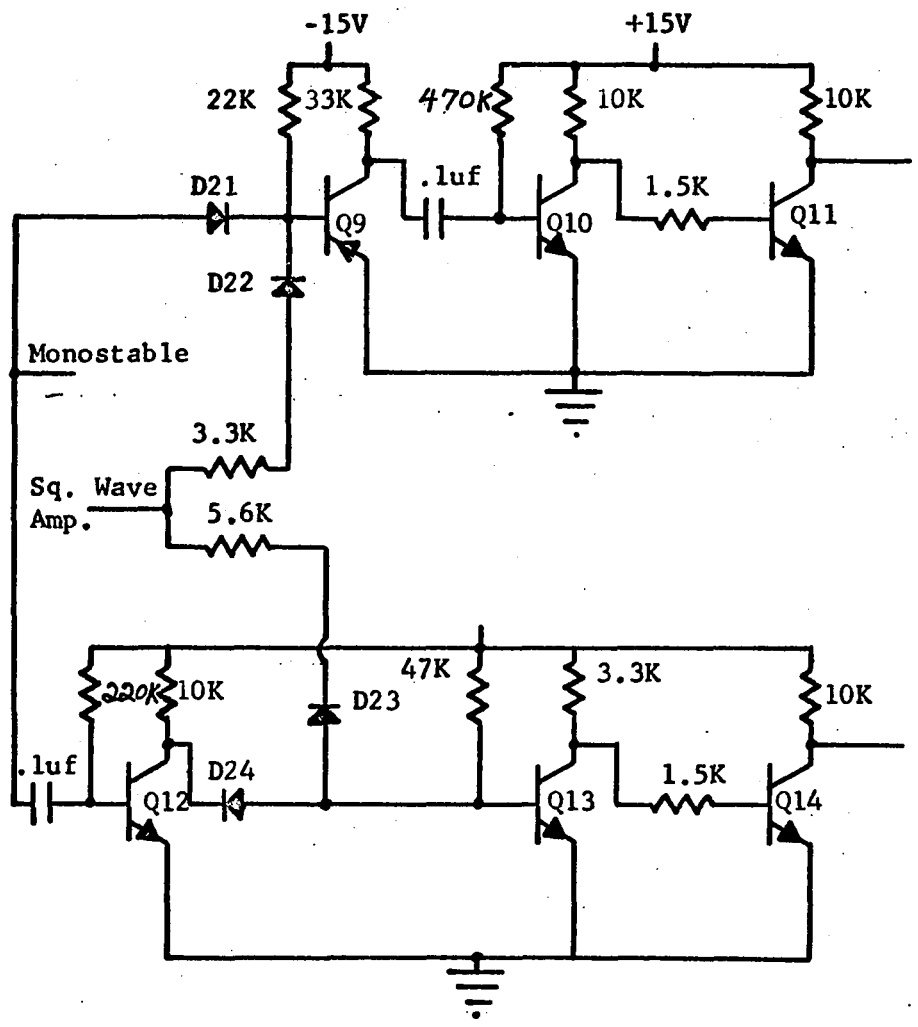

Figure B-5. Logic circuits.

Wave Shaping A or B

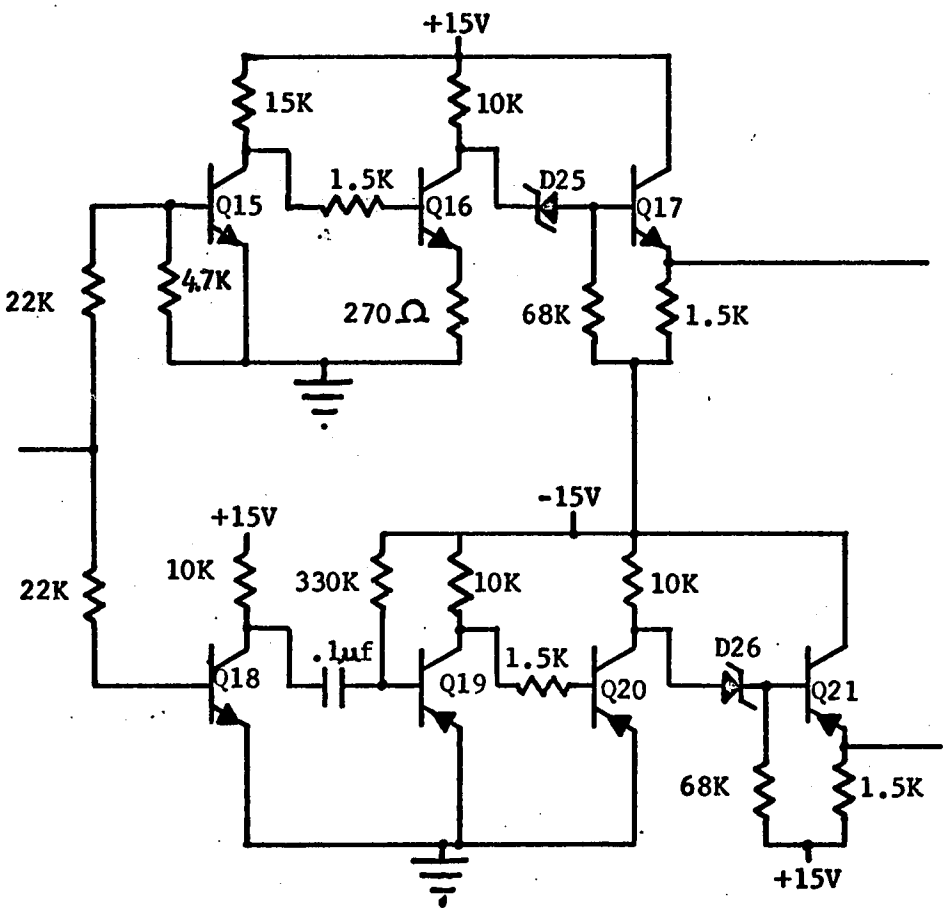

Figure B-6. Wave shaping circuits.

LIST OF PARTS FOR SCHEMATIC DIAGRAMS

B1- NEDA #1604, 8.40V

B2- NEDA #1604, 8.40V

C1- 0.05 µf, 0.02 µf, 0.01 µf, 500 pf, 270 pf, 100 pf, 68 pf, STEATITE ROTARY SWITCH

D1- Z4XL6.2	D10- FD300	D19- 1N3731
D2- 1N34A	D11- FD300	D20- 1N914
D3- 1N914	D12- FD300	D21- 1N121
D4- 1N914	D13- FD300	D22- 1N121
D5- 1N914	D14- 1N121	D23- 1N121
D6- 1N914	D15- 1N121	D24- 1N121
D7- 1N34A	D16- 1N3731	D25- 1N749
D8- 1N749	D17- 1N3731	D26- 1N749
D9- 1N749	D18- 1N3731	

Q1- 2N1711	Q8- 2N3638	Q15- 2N3568
Q2- 2N2923	Q9- 2N3638	Q16- 2N3568
Q3- 2N2923	Q10- 2N3568	Q17- 2N1711
Q4- 2N3415	Q11- 2N3568	Q18- 2N3568
Q5- 2N3638	Q12- 2N3568	Q19- 2N3638
Q6- 2N3638	Q13- 2N3568	Q20- 2N3638
Q7- 2N3638	Q14- 2N3568	Q21- 2N257

R1- 10K, 24.9K, 49.9K, 100K, 200K, 1% STEATITE ROTARY SWITCH

R2- 10K, 24.9K, 49.9K, 100K, 200K, 1% STEATITE ROTARY SWITCH

R3- 10K, 24.9K, 49.9K, 100K, 200K, 500K, 1M, 1% STEATITE ROTARY SWITCH

S1- Steatite Rotary Switch

S2- SPDT

S3- Lever Action Switch, Centralab #1467

S4- Momentary Contact Switch

S5- Momentary Contact Switch

LIST OF REFERENCES

1. Meites, L., "Polarographic Techniques," 2nd ed., Interscience, New York (1965).

2. Delahay, P., "New Instrumental Methods in Electrochemistry," Interscience, New York (1954).

3. Ishibashi, M., and Fujinaga, T., Bull. Chem. Soc. Japan, 23, 261 (1950).

4. Barker, G. C., and Jenkins, I. L., Analyst, 77, 685 (1952).

5. Cooke, W. D., Kelley, M. T., and Fisher, D. J., Anal. Chem., 33, 1209 (1961).

6. DeLevie, R., J. Electroanal. Chem., 9, 117 (1965).

7. Barker, G. C., Anal. Chim. Acta, 18, 118 (1958).

8. Mann, C. K., Anal. Chem., 33, 1484 (1961).

9. Mann, C. K., Anal. Chem., 37, 326 (1965).

10. Saito, Y., and Okamoto, K., Rev. Polarography, 10, 227 (1962).

11. Okamoto, K., "Modern Aspects of Polarography," T. Kambara, ed., Plenum Press, New York (1966), p. 225.

12. Kelley, M. T., Fisher, D. J., and Jones, H. C., Anal. Chem., 31, 1475 (1959).

13. Buchanan, E. B., Jr., and McCarten, J. B., Anal. Chem., 37, 29 (1965).

14. Philbrick Researches, Inc., "Application Manual for Computing Amplifiers," 2nd ed., Dedham, Mass. (1966).

15. General Electric Transistor Manual, 7th ed., Figure 108 (1961), p. 232.

16. Vyaselev, M. R., Zavod. Lab., 31, 21 (1965).

17. Booman, G. L., and Brown, W. B., Anal. Chem., 37, 795 (1965).

18. Brown, E. R., McCord, T. G., Smith, D. E., and DeFord, D. D., Anal. Chem., 38, 1119 (1966).

19. Lauer, G., and Osteryoung, R. A., Anal. Chem., 38, 1106 (1966).

20. Brown, E. R., Smith, D. E., and Booman, G. L., Anal. Chem., 40, 1411 (1968).

21. Gerischer, H., Z. Phyzik. Chem. (Leipzig), 202, 302 (1953).

22. Berzins, T., and Delahay, P., J. Amer. Chem. Soc., 77, 6448 (1955).

23. Kemula, W., and Kublik, Z., Anal. Chim. Acta, 18, 104 (1958).

24. Ramaley, L., Brubaker, R. L., and Enke, C. G., Anal. Chem., 35, 1088 (1963).

25. Grahame, D. C., J. Amer. Chem. Soc., 71, 2975 (1949).

26. Barker, G. C., Faircloth, R. L., and Gardner, A. W., A.E.R.E. C/R 1786, Harwell, Berkshire (1958).

27. Kambara, T., Bull. Chem. Soc. Japan, 27, 527 (1954).

28. Carslaw, H. S., and Jaegers, J. C., "Conduction of Heat and Solids," 2nd ed., Oxford, Clarendon Press (1959), p. 63.

29. Crank, J., "The Mathematics of Diffusion," Oxford, Clarendon Press (1956), p. 9.

30. Kambara, T., Bull. Chem. Soc. Japan, 27, 523 (1954).

31. Lingane, J. J., J. Amer. Chem. Soc., 68, 2448 (1946).

32. Schaap, W. B., Laitinen, H. A., and Bailar, J. C., Jr., J. Amer. Chem. Soc., 76, 5868 (1954).

33. Ramaley, L., Ph. D. Dissertation, Princeton University, Princeton, New Jersey (1963).

34. Kaplan, B. Ya., and Sorokovskaya, I. A., Zavod. Lab., 38, 1053 (1963).

35. Olmstead, M. L., and Nicholson, R. S., Anal. Chem., 38, 150 (1966).

36. Breyer, B., and Bauer, H. H., "AC Polarography and Tensammetry," Interscience, New York (1963), p. 165.

37. Markovac, V., and Lovrecek, B., J. Electrochem. Soc., 113, 838 (1966).

38. Randles, J. E. B., and Somerton, K. W., Trans. Faraday Soc., 48, 937 (1952).

39. Delahay, P., and Trachtenberg, I., J. Amer. Chem. Soc., 79, 2355 (1957).

40. Breyer, B., Gutman, F., and Hacobian, S., Aust. J. Sci. Res., A3, 567 (1950).

41. Israel, Y., Talanta, 13, 1113 (1966).

42. DeMars, R. D., and Shain, I., Anal. Chem., 29, 1825 (1957).

43. Von Sturm, F., and Ressel, M., Z. Anal. Chem., 186, 63 (1962).

44. Barendrecht, E., "Electroanalytical Chemistry," Vol. 2, A. Bard, ed., Dekker Press, New York (1967), p. 53.

45. Underkofler, W. L., and Shain, I., Anal. Chem., 37, 218 (1965).

46. Kaplan, B. Ya., and Sorokovskaya, I. A., Zavod. Lab., 30, 1177 (1964).

47. Durst, R. A., Anal. Chem., 40, 931 (1968).

48. Lingane, J. J., Anal. Chem., 40, 935 (1968).

49. Bond, A. M., and O'Donnell, T. A., Anal. Chem., 40, 1405 (1968).

50. Rainwater, F. H., and Thatcher, L. L., "Methods for Collection and Analysis of Water Samples," Geological Survey Water Supply Paper, 1454, U. S. Government Printing Office, Washington, D. C. (1960), p. 163.

51. Greenhalgh, R., and Riley, J. P., Anal. Chim. Acta, 25, 179 (1961).

52. Hensley, A. L., and Barney II, J. F., Anal. Chem., 32, 828 (1960).

53. Zittel, H. E., and Florence, T. M., Anal. Chem., 39, 320 (1967).

54. Laitinen, H. A., and Chambers, L. M., Anal. Chem., 36, 5 (1964).

55. Bauer, H. H., Spritzer, M. S., and Elving, P. J., J. Electroanal. Chem., 17, 299 (1968).

56. Ilkovic, D., Collect. Czech. Chem. Commun., 18, 13 (1936).

57. Smith, G. W., and Stark, V., J. Phys. Chem., 62, 195 (1958).

58. DeLevie, R., J. Electroanal. Chem., 9, 311 (1965).

59. Barker, G. C., and Bolzan, J. A., Z. Anal. Chem., 216, 215 (1966).

60. Good, N. E., Winget, G. D., Winter, W., Connolly, T. N., Izawa, S., and Singh, R. M. M., Biochemistry, 5, 467 (1966).

61. Handbook of Analytical Chemistry, L. Meites, ed., McGraw-Hill, New York, 3 (1963), p. 166.

62. Furman, N. H., and Wallace, J. H., Jr., J. Amer. Chem. Soc., 51, 1449 (1929).